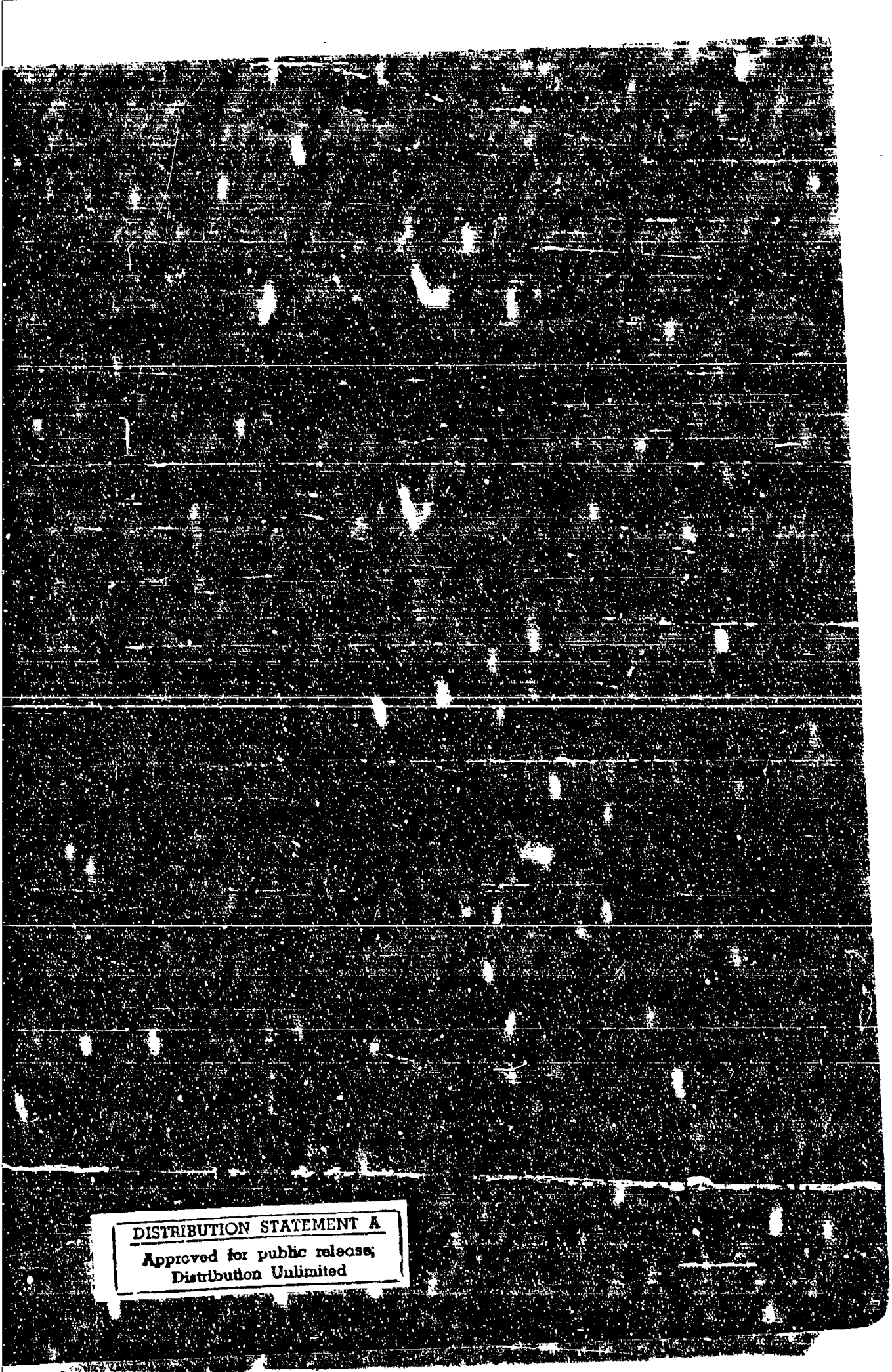

SECURITY CLASSIFICATION OF THIS PAGE (When Data Entered)

REPORT DOCUMENTATION PAGE

READ INSTRUCTIONS BEFORE COMPLETING FORM

1. REPORT NUMBER	2. GOVT ACCESSION NO. AD-A119 397
3. RECIPIENT'S CATALOG NUMBER	
4. TITLE (and Subtitle) NUMERICAL CALCULATIONS OF TURBULENT HEAT TRANSFER BEYOND TWO-DIMENSIONAL BACK-STEPS AND SUDDEN PIPE EXPANSIONS (RECIRCULATING)	5. TYPE OF REPORT & PERIOD COVERED Final 6. PERFORMING ORG. REPORT NUMBER 1 May 80 - 31 July 82
7. AUTHOR(s) Charles B. Watkins, Arthur M. Gooray	8. CONTRACT OR GRANT NUMBER(s) ~~N0014~~-80-C-0545 (N00014)
9. PERFORMING ORGANIZATION NAME AND ADDRESS Department of Mechanical Engineering, Howard University, Washington, D.C. 20059	10. PROGRAM ELEMENT, PROJECT, TASK AREA & WORK UNIT NUMBERS NR 097-444
11. CONTROLLING OFFICE NAME AND ADDRESS Office of Naval Research, Power Program, Arlington, Va. 22217	12. REPORT DATE August 1982 13. NUMBER OF PAGES Unclassified
14. MONITORING AGENCY NAME & ADDRESS(if different from Controlling Office)	15. SECURITY CLASS. (of this report) Unclassified 15a. DECLASSIFICATION/DOWNGRADING SCHEDULE

16. DISTRIBUTION STATEMENT (of this Report)

Approved for public release; distribution unlimited

17. DISTRIBUTION STATEMENT (of the abstract entered in Block 20, if different from Report)

18. SUPPLEMENTARY NOTES

19. KEY WORDS (Continue on reverse side if necessary and identify by block number)

turbulent flow, heat transfer, numerical solution

(EPSILON)

20. ABSTRACT (Continue on reverse side if necessary and identify by block number)

Results of an investigation of numerical modeling techniques for turbulent heat transfer in the recirculating and reattached flow downstream of two-dimensional reqard-facing steps and sudden pipe expansions are presented. The computations were performed using an improved k-ε two-equation model of turbulence in a modified version of the Teach-T code.

DD FORM 1 JAN 73 1473 EDITION OF 1 NOV 65 IS OBSOLETE S/N 0102-014-6601

UNCLASSIFIED

SECURITY CLASSIFICATION OF THIS PAGE (When Data Entered)

NUMERICAL CALCULATIONS OF TURBULENT RECIRCULATING HEAT TRANSFER BEYOND TWO-DIMENSIONAL BACK-STEPS AND SUDDEN PIPE EXPANSIONS

by

Charles B. Watkins

and

Arthur M. Gooray
Department of Mechanical Engineering
Howard University
Washington, D.C. 20059

Final Report
ONR Contract Number N0014-80C-0545
Work Unit Number NR 097-444

August 1982

ARSTRACT

Extensive results of numerical calculations for turbulent recirculating flow with heat transfer are presented. The geometries studied were two-dimensional flows over rearward (backward) - facing steps and sudden pipe expansions. The computations described were performed using the k-ε, two equation model of turbulence. To yield better predictions of heat transfer, the standard model was improved, by developing algebraic approximations for Reynolds stresses and scalar fluxes, so as to account for the effects of streamline curvature, pressure-strain and variation of turbulent Prandtl number in the flow field. In addition, the low-Reynolds-number version of the standard k-ε model was employed in the redeveloping region. In order to apply the low-Reynolds-number model to the redeveloping region, a two pass procedure was developed to partition the flow field into separated and reattached regions. This procedure consists of: a first pass utilizing the standard k-ε model to establish the reattachment length, and a second computational pass, in which all variables are recomputed. During the second pass, the standard k-ε model is maintained up to reattachment but the low-Reynolds-number version is employed beyond reattachment. The numerical scheme incorporates the basic solution algorithm of the TEACH-T code. However, this algorithm was extended to include heat transfer and was improved by using quadratic differencing for the convective terms.

Results of calculations for mean velocity, mean temperature and, turbulent intensity fields, together with heat transfer coefficients for both the side and base walls are presented. Also described are the effects of the turbulent approach boundary layer on heat transfer, the characteristics of the redeveloping turbulent thermal boundary layer after reattachment and correlations of heat transfer coefficients.

Comparisons are made with other numerical calculations and with available experimental data. The results indicate that reliable predictions of reattachment lengths can be obtained by the present improved standard k-ε model. Also, fairly accurate overall heat transfer coefficients are obtained by incorporating both the improved standard k-ε model and the low-Reynolds number form of the model in a two-pass procedure.

ACKNOWLEDGEMENTS

The contribution of Dr. Win Aung, who made many helpful suggestions and comments during the course of this investigation, is gratefully acknowledged.

TABLE OF CONTENTS

LIST OF FIGURES

LIST OF TABLES

NOMENCLATURE

A_m ... A_r	empirical constants in low-turbulence-Reynolds number model
c_p	specific heat at constant pressure
C_p	pressure coefficient
$C_{\varepsilon 1}$, $C_{\varepsilon 2}$, C_μ	empirical constants appearing in k-ε turbulence model
C_{s1}, C_{s1w}, C_{s2w}, $C_{\theta 1}$, $C_{\theta 1w}$, C_w	empirical constants appearing in the closure approximations for the pressure-strain (scalar) terms
D	diameter downstream of pipe

D_{ij}	a production like term in Reynolds stress equation
H	step or expansion height
$f(\ell/x_2)$	near-wall function appearing in closure approximations of pressure-strain (scalar) terms
f_1, f_2	empirical functions of turbulent Reynolds number appearing in low Reynolds number k-ε model
j	exponent set = 0 for two-dimensional flow or set = 1 for axisymmetric flow
J	Convective plus diffusive terms in discretized equations
k	turbulent kinetic energy (= $(\overline{u'^2 + v'^2 + w'^2})/2$)
k_t	thermal conductivity
K_1, K_2	constants in streamline curvature formulation of C_μ
ℓ_o	length scale in turbulent viscosity model
n	coordinate normal to streamline
Nu	Nusselt number based on step height for back step and down-stream diameter for pipe expansion
p	time mean-pressure
p'	fluctuating pressure
P	$\frac{1}{2} P_{ii}$
P_{ij}	production term in Reynolds stress equation

Pr	laminar Prandtl number
Pr_t	turbulent Prandtl number
$\dot{q}''_w$	wall heat flux
R_c	radius of curvature for streamline
R_t	turbulent Reynolds number ($= k^2/\varepsilon\nu$)
R_e	Reynolds number based on mean inlet velocity and step height for back step or downstream pipe diameter for pipe expansion
r	in cylindrical co-ordinates, $y = r$
s	coordinate parallel to streamline
S_ϕ	source term in discretized equations
T	mean temperature
T^+	mean dimensionless temperature ($=(T_w - T)/T_\tau$)
T	turbulent temperature parameter ($= \dot{q}''_w/\rho\, c_p u_\tau$)
u	mean velocity in the streamwise or x direction
u	friction velocity ($= (\tau_w/\rho)^{\frac{1}{2}} = (C_\mu^{\frac{1}{4}} k_p)^{\frac{1}{2}}$)
u^+	dimensionless value of u ($= u/u_\tau$)
u'	fluctuating velocity in the streamwise or x direction
$\overline{u'_i u'_j}$	Reynolds stresses
U_o	free-stream mean velocity
$\overline{u'_j \theta'}$	scalar fluxes
v	mean velocity in the normal or y direction
v_o	velocity scale in turbulent viscosity model
v'	fluctuating velocity in the normal or y direction

x	distance along the main flow direction
x^+	dimensionless value of x ($= u_\tau x/\nu$)
x_R	reattachment distance
$\bar{x}$	distance from reattachment ($= x-x_R$)
y	distance normal to x direction
y^+	dimensionless value of y ($= u_\tau y/\nu$)

Greek Symbols

Γ	dynamic thermal diffusivity
Γ_{eff}	laminar plus turbulent dynamic thermal diffusivity
δ_T	thermal boundary layer thickness
δ_u	momentum boundary layer thickness
ε	dissipation rate of turbulent energy
ξ	unheated starting length
θ	angle between streamline and x - direction
θ'	fluctuating temperature
κ	Von Karman constant (= 0.42)
μ	dynamic viscosity of fluid
μ_{eff}	turbulent plus laminar viscosities
μ_t	turbulent viscosity
ν	kinematic viscosity
ρ	density
σ_k, σ_ε	turbulent "Prandtl numbers" for diffusion of k and ε

τ_w	wall shear stress
ϕ	any dependent variable
ψ	stream function

Subscripts

eff	effective value of diffusion coefficient; i.e., sum of molecular and turbulent quantities
H	value of quantity just upstream of step
n	value of quantity normal to streamline
P	values at the first near-wall grid in standard k-ε model
s	value of quantity tangential to streamline
w	wall values
$\overline{x}$	value of parameter based on distance measured from reattachment

CHAPTER 1

INTRODUCTION

1.1 General Remarks

In recent years, the energy crisis has motivated heat transfer engineers to develop high performance heat exchangers and other advanced thermal devices. In developing the new technology needed to accomplish this task, a great deal of attention has been given to the various heat transfer enhancement techniques. Some of these augmentation schemes include: surface promoters, vortex flows, and additives [1]. With surface promoters, the heat transfer for flows over rough surfaces can be as much as 15 percent larger than for flows over smooth surfaces [2,3]. In vortex flows, the heat transfer is significantly increased (by swirling the flow), in some cases as much as 80 percent [4,5]. The present research is focused on effects due to sudden changes of the surface geometry. Such abrupt changes can enhance the heat transfer by as much as 50 percent over that of the corresponding attached flow [6].

The heat transfer augmentation which occurs as a result of alterations of the flow caused by sudden changes in body geometry is a very important aspect of engineering heat transfer. Such flow alteration, consisting of separation, reattachment and subsequent redevelopment may accidentally occur in some systems, and in others, may be deliberately induced, primarily to enhance the wall convective heat transfer rates at the expense of an increase in the

friction factor. While there have been significant contributions in this field, current understanding of the reattachment process is still relatively poor, essentially because of its complexity. Thus, a designer is still somewhat at a loss in predicting heat transfer in separated flows. The geometries chosen for the present calculations are the simple, yet vitally important, two-dimensional back-step and sudden expansion in a pipe. A considerable amount of the needed information for validating turbulence models and numerical schemes can be obtained by studying these fundamental engineering geometries.

Among two-dimensional flows, the back-step is the simplest reattaching flow of practical significance. The separation point is fixed at the edge of the step, and there is only one separated zone, unlike flow over a fence or obstacle. It should be noted that, although the overall gross features of the turbulent flow are two-dimensional, the fluctuating components are actually three-dimensional. Even in this "simplest" reattaching flow, the flow field for the back-step is still very complex.

The qualitative nature of separated flow fields has been known for a long time as discussed by Prandtl and Tietjens [7]. Figure (1) shows a typical abrupt expansion geometry. The inception of separation occurs at the point of geometrical discontinuity. The 'dividing streamline' is the hypothetical streamline that separates

the reversing fluid from that continuing in the main flow direction. Reattachment is the point where the separated layer rejoins a boundary surface (or another layer as in free shear flows). Thus, at reattachment two flows of opposing directions exist; and the shear stress vanishes. Figure (1) depicts some of the qualitative flow characteristics. Immediately after the boundary layer separates at the step, a new free-shear layer develops inside the original shear layer. In the separated zone the flow is highly turbulent and is reversed towards the step in the near-wall region and re-enters into the new shear layer. This results in a recirculating zone that is separated from the main stream flow. Also, in the separated region the shear layer curves sharply downwards and is influenced by the effects of curvature, adverse pressure gradient, and wall interaction. Immediately downstream of reattachment, a new sub-boundary layer is formed; this layer interacts with the original (incoming) shear layer. Further downstream, the flow tends to a more reestablished turbulent boundary layer (or fully-developed flow in a pipe or channel) [8,9].

In the recirculation region, the early studies of Abbott and Kline [10] clearly identify the presence of three dissimilar zones. Immediately downstream of the step is a three-dimensional zone, characterized by one or more vortices rotating about an axis normal

to the plane of the flow. Adjacent vortices are counter-rotating, and they may not all be of the same size. Downstream of the first zone is a two-dimensional zone that contains the classical recirculation pattern, i.e., flow near the wall moving upstream and near the dividing streamline moving downstream. Beyond the second zone exists a transient tail region (close to the wall and upstream of reattachment) that eventually disappears with the second zone.

The separation mechanism is somewhat different for a body with a sudden geometric change as opposed to one with a gradual geometric change. For a body with a slowly varying geometric change the curvature of the velocity profile at the wall is directly affected by the impressed pressure gradient. For instance, for a negative (favorable) pressure gradient, the velocity profile has a negative curvature all the way to the edge of the layer, and no separation occurs. For a zero pressure gradient, the velocity profile has zero curvature at the wall and negative curvature near the edge of the layer, and no separation occurs. For a positive (unfavorable or adverse) pressure gradient, the velocity profile has a positive curvature at the wall and negative curvature at the outer edge, and separation occurs. For a sudden expansion geometry due to the interaction there is no impressed pressure gradient as such, and the wall (surface) static

pressure, expressed in terms of pressure coefficients, is characterized as follows. At separation the pressure coefficient is negative and decreases gradually to a minimum value just beyond the step. In the reattachment zone it increases sharply to a positive value, reaching a maximum just beyond reattachment. Further downstream of reattachment it decreases gradually to the value of the local free stream pressure [9]. The static pressure variation across the expansion (perpendicular to the flow direction) is nearly constant throughout, except for sharp peaks across the dividing streamline.

The presence of a recirculating wall layer greatly influences the process of energy transfer. It has been demonstrated experimentally, cf [6,8], that within the recirculating region the heat transfer coefficient is many times larger than that of an attached flow. This increase in heat transfer, in principle, can be attributed to the increase in streamwise turbulent kinetic energy in the mixing layer (region remote from the wall). Recent measurements of Moss and Baker [9] and Fraser and Siddig [11] illustrate this effect. They showed that the streamwise turbulent intensity $(\overline{u'^2}/U_o^2)$ is small within the buffer zone and then increases quite sharply to a maximum in the mixing layer, before falling off again to a low value in the main flow. Furthermore, the peak value of the turbulent kinetic energy increases initially

with the downstream distance from the sudden change in body geometry, reaching a maximum just before the reattachment point, and then decreasing after attachment. In the redevelopment region where the flow tends toward a reestablished boundary layer (or fully developed flow in a pipe or channel), the turbulent kinetic energy takes on boundary layer type profiles. The high values of the turbulent kinetic energy in the mixing layer, particularly around reattachment, is associated with spreading of the layer or an increase in turbulent diffusion coefficient in the main flow. This then results in a 'shrinking' of the near-wall viscous sub-layer, thus allowing greater passage of heat by molecular diffusion. The increase in heat transfer due to recirculation can also be viewed as a manifestation of streamline curvature. For instance, the fluid particle near the wall follows a longer curved streamline (as opposed to the rectilinear path present in attached flows), thereby transferring more energy along the curved path.

From the above discussion it is evident that the separating, reattaching, and redeveloping shear layers are characterized by active coupling between the external flow and the separated shear layers. It is for this reason that the flow field is complex. In attached flows, active coupling between the free stream and boundary layer need not be considered, and so inviscid and boundary

layer theories can usually be applied in an uncoupled manner to yield fairly reasonable predictions. With separation, boundary layer approximations are not valid, and with the inclusion of heat transfer, the problem of coupling becomes even more complex.

1.2 General Form of the Governing Equations

It is accepted that the Navier-Stokes equations, comprising a closed set of equations for instantaneous velocity and pressure fields, are valid for both laminar and turbulent flows. For laminar flows, with well defined initial and boundary conditions, numerical solutions can be obtained fairly easily. For turbulent flows, the important components of the turbulence phenomena take place in small eddies of the order of 1 mm. in size while the entire flow field may extend over meters. Reliable numerical results can only be expected if the numerical discretization is smaller than the smallest scales of turbulence. Such a procedure would require a large and impractical number of nodes; and as such, demand computer storage and time far beyond the capabilities of present systems. As an example, an eddy size of 1 mm. and a value of 10 percent of the average velocity for the turbulent fluctuations, will result in turbulence frequencies of 10^{-5} sec $^{-1}$. Cebecci and Smith [12] explored the possibility of obtaining a computer solution to reveal the fine scale structures. They showed that boundary layer flow calculations over an airfoil, with about ten grid points per eddy-size, will need about 35,000 years of computing time with a present-day computer. By requiring less physical detail, so as to obtain solutions of practical engineering problems, restrictions can be made regarding the fine scale

structures. The problem can be effectively side-stepped by considering the time-averaged equations of turbulence. Time - averaging 'smears out' the fine scale structures, and the resulting gross properties of turbulence (such as mean velocities and temperatures) are much more gradual in space; as a consequence excessively fine grids are not required. However, time-averaging the governing equations results in terms involving statistical correlations of fluctuations in velocities, temperature, pressure, etc. There is no direct way of knowing these correlations, so they have to be modeled in terms of quantities that can be determined. Hence, turbulent modeling involves developing a set of equations for the correlations, which when solved with the mean flow equations, simulate the behavior of the actual flow. The details of modeling procedures are discussed in a later chapter.

Rather than using the time-averaging procedure, there are less restrictive formulations in the literature. A group of theoreticians, such as Kraichnan, Edwards and Orszag (these studies are discussed in the book of Orszag [13]), have developed sophisticated statistical theories of turbulence. The mathematical formulation takes into account the dynamics of the turbulent motion through the interaction of eddies of different sizes. The procedure is often referred to as the "direct interaction" method and is discussed by Orszag [13]. The mathematical complexity of

the procedure is overwhelming; thus the understanding and applications to basic engineering calculations of turbulent flow are almost non-existent. Another scheme is the "subgrid-scale" procedure of Deardorff [14] in which averaging is taken over small time intervals. In the final procedure all the energy-containing turbulent motions are treated as though they are unsteady three-dimensional flows. However, applying this procedure to study atmospheric turbulence, Deardorff [15] reported central processor time on a CDC 7600 of about 350 hours; thereby, implying the impracticality of the procedure for rudimentary engineering calculations.

In the present work the generalized steady equations of fluid motion in the Cartesian tensor notation are employed. Details of the foregoing analysis are given in Hinze [16].

For an incompressible fluid, the continuity equation takes the form,

$$\frac{\partial u_i}{\partial x_j} = 0 \qquad (1.2.1)$$

where u_i is the i'th component of velocity. For a Newtonian fluid of uniform density, ρ, and kinematic viscosity, ν, the instantaneous Navier-Stokes equations in the absence of body forces are,

$$u_j \frac{\partial u_i}{\partial x_j} = -\frac{1}{\rho}\frac{\partial p}{\partial x_i} + \nu \frac{\partial}{\partial x_j}\left(\frac{\partial u_i}{\partial x_j}\right) \qquad (1.2.2)$$

The Navier-Stokes equations for turbulent flow is obtained by employing the Reynolds procedure, namely

$$u_i = \bar{u}_i + u_i'$$
$$p = \bar{p} + p'$$

where the primed and overbar superscripts indicate fluctuating and mean quantities, respectively. Before substituting the Reynolds procedure into the above equations to obtain the Navier-Stokes equations for turbulent flow, a brief discussion of time-averaging with respect to "steady" turbulence is presented.

A turbulent flow is referred to as steady, if for all dependent variable, $\phi(x_i,t)$,

$$\phi(x_i) = \frac{1}{t_0} \int_0^{t_0} \phi(x_i,t)\, dt$$

as time t_o becomes large compared with the time scales of turbulence motions, ϕ'. The average value is independent of the origin of t of the averaging procedure, provided $t < t_o$.

Substituting the above Reynolds relations into Eqn. (1.2.2), making use of Eqn. (1.2.1), and time - averaging the results yield the corresponding Navier-Stokes equations for turbulent flow,

$$\rho \bar{u}_j \frac{\partial \bar{u}_i}{\partial x_j} = - \frac{\partial \bar{p}}{\partial x_i} + \frac{\partial}{\partial x_j} \left[\mu \frac{\partial \bar{u}_i}{\partial x_j} - \rho \overline{u_i' u_j'} \right] \qquad (1.2.3)$$

The equation governing the transport of thermal energy (Temperature, T), is,

$$u_j \frac{\partial T}{\partial x_j} = S_T + \Gamma \frac{\partial}{\partial x_j} \left(\frac{\partial T}{\partial x_j} \right) \qquad (1.2.4)$$

where S_T is the generation of T per unit volume and Γ is the kinematic diffusivity of T.

Using the same Reynolds procedure, i.e.,

$$T = \bar{T} + \theta'$$

where θ' is the fluctuating part of the temperature. Substituting into Eqn. (1.2.4) and time averaging, results in,

$$\bar{u}_j \frac{\partial \bar{T}}{\partial x_j} = \bar{S}_T + \Gamma \frac{\partial}{\partial x_j} \left(\frac{\partial \bar{T}}{\partial x_j} \right) - \frac{\partial}{\partial x_j} \left(\overline{u_j' \theta'} \right) \qquad (1.2.5.)$$

The turbulent results, Eqns. (1.2.3) and (1.2.5) are identical to their laminar counterpart, Eqns. (1.2.2) and (1.2.5), except for the unknown correlations, $\overline{u_i' u_j'}$ and $\overline{u_j' \theta'}$. These are commonly referred to as Reynolds stresses and scalar fluxes, respectively. Solving for these unknown stresses and fluxes is referred to as turbulence closure or turbulent modeling. For general information Appendix (A) discusses the mathematics and physics involved in some of the most common turbulence closure techniques.

Presently, it is possible to predict velocity profiles in an incompressible turbulent boundary layer with a reasonable degree of success by using a wide variety of eddy viscosity models [12,17]. In these models the turbulent stresses in the mean momentum

equation are written in terms of a turbulent (eddy) viscosity and mean velocity gradients. This level of success has led many investigators to consider a similar approach for the prediction of heat transfer in thermal boundary layers by employing the Reynolds analogy [18,19]. The hypothesis is that the same complex processes govern the transport of both momentum and thermal energy in a turbulent boundary layer. It follows then that the turbulent heat flux (e.g. $\overline{v'\theta'}$) in the above thermal energy equation can be written as an eddy conductivity times mean temperature gradients with the turbulent Prandtl number defined as the ratio of turbulent viscosity to turbulent conductivity. The turbulent viscosity can be approximated by using a single length scale (Prandtl's mixing length) or by using length and velocity scales (k-ε model). Then, according to the Reynolds analogy, the turbulent Prandtl number is O(1).

The focus of the present analysis is on numerical calculation of the flow and temperature fields, turbulent variables, and side and bottom wall heat transfer coefficients, for both rearward-facing steps and pipe expansions, for the entire turbulent flow regime. The range of Reynolds numbers emphasized are in the low to moderate range. The upstream wall is heated and the momentum and thermal boundary layers are turbulent at both separation and reattachment (often referred to as

turbulent-turbulent interaction). Emphasis in this study is on exploring turbulent viscosity models for heat transfer flows with recirculation and subsequent redevelopment. In the present closure scheme the turbulent viscosity and thermal diffusivity are approximated by less restrictive formulations than are usually employed. Generalized functional relationships for critical parameters are algebraically derived to better represent the physics in both the recirculating and redeveloping regions. This improved modeling procedure is incorporated into an improved computational algorithm for the entire flow field, yielding an improved modeling and computational technique that is unique to the present research. The modeling and computational technique is validated by comparison of computed results with available experimental data. Based on the comparisons a favorable assessment can be made as to the feasability of the present computational procedure for routine engineering calculations. Also, it is expected that the calculated heat transfer coefficients presented may in themselves be useful to the designer.

1.3 Brief Description of Contents

The discussion of the present research proceeds as follows. In Chapter II the state of the art of investigation of turbulent recirculating flow is reviewed, with emphasis on heat transfer. Relevant experimental work is mentioned and attention is brought to some of the most common closure techniques for modeling. Appendix A discusses the mathematical formulations of some of these closure techniques. In Chapter III the mathematical equations actually used for the present computations are presented with the detailed derivation of the k-ε viscosity model, and a discussion of the present improvements, detailed derivation of the improvements given in Appendix (B). Chapter III also includes a discussion of the less successful modeling procedures attempted in the initial stages of this study. In Chapter IV the computational procedures including the treatment of the near-wall conditions are discussed. In Chapter V, the results of calculations for both the back-step and pipe expansion geometries are presented. Comparison is made with available experimental data and another numerical calculation (for the pipe expansion). Heat transfer coefficient correlations are also presented. Finally, in Chapter VI conclusions are discussed concerning the calculation procedures and their general applicability, and finally, suggestions for further studies are presented.

CHAPTER II

REVIEW OF LITERATURE

2.1 Review of Recirculating Flow Measurements

Reliable experimental data are essential for the development and testing of turbulence models. This is simply, because the models are not wholly analytic; for instance, they contain some unknown empirical coefficients (constants) which can only be estimated by comparison to experimental data. Hence, availability of accurate measurements means that the turbulence models can be adjusted to yield reliable predictions. In this survey of recirculating flow measurements it is convenient to divide the review into two categories: hydrodynamic and scalar (temperature) flow field measurements.

2.1.1 Hydrodynamic Flow Field Measurements

Measurements of hydrodynamic flow fields for recirculating shear flows are much more extensive than those of scalar flow fields. Until recently measurement of turbulent flow quantities (even the time-averaged quantities) for simple recirculating flows, such as the back-step was very difficult [20]. The flow is highly turbulent and the flow reversals make hot - wire anemometers generally unsuitable. Since the implementation of laser-Doppler and pulsed-wire anemometries, the quality of available data has begun to improve. The following literature

survey represents the major reported research on reattaching flows, with emphasis on the back-step geometry. A similar survey was recently compiled by Eaton and Johnston [20].

The measurements of Hsu (1950) [21] are apparently the first experiments to study both mean flow and turbulent profiles for low speed flows over a large step. However, his turbulence data, obtained from hot-wire anemometers, differs significantly from many of the more recent experiments. Another early study is that of Abbott and Kline [10] in 1961. They studied both single and double backward-facing steps of various heights. By using water as the working fluid and employing flow visualization techniques, they obtained detailed measurements of mean velocity profiles and reattachment lengths. This work includes only a few turbulent quantity measurements by hot-film anemometry. Also in 1961 Tani [22] used hot-wires to measure mean velocity, turbulence intensity and turbulent shear stress for various step heights for both laminar and turbulent incident boundary layers. These measurements apparently represent the first reliable turbulence data for the back-step.

In some of the more recent literature, Bradshaw and Wong [23] obtained turbulence measurements in the entire flow region downstream of the step. These data were then used to obtain some

indirect information about the turbulence structure by "numerical experiments", i.e., by forcing empirical calculations to match the experiments. This then enabled them to study in more detail the shear-layer mass flow recirculating zone. They also studied the redeveloping boundary layer and noticed that for at least 52 step heights downstream the attached boundary layer characteristics ("law of the wall" behavior) were not fully recovered.

In 1975 Bradshaw [24] reviewed and identified some complex turbulent flows. One of the complex flows identified was separated flow. To contribute to the understanding of the separation and redevelopment phenomena, recently Chandrsuda and Bradshaw [25] continued the experiments of Bradshaw and Wong [23]. Their back-step experiments utilized a thin laminar approach boundary layer, mainly bacause in the reattached region full development is reached much faster for a laminar approach boundary layer than for a turbulent one [26]. Measurements reported include mean velocity and Reynolds stresses (including higher order correlations). They concluded because of the importance of the triple products, any successful modeling procedure should reflect these effects together with the 'wall-effects' in the pressure - strain term. The modeling procedure in the present research, to be discussed later, does include some of these effects.

Narayanan et al. [27] have measured the wall static pressure behind steps (of varying heights) in a wind tunnel. Their results indicate reasonably well defined similarity patterns in the pressure distributions of the separated flow regions, from these distributions they were able to estimate reattachment lengths.

Kim et al. [28] measured mean velocity, Reynolds stresses and intermittency (fraction of time for which the flow at a given point is turbulent) in the entire flow field of the back-step. They noticed that downstream of rattachment the flow very slowly returns to the structure of the attached boundary layer.

For the double facing back-step geometry, Mehta [29] presented hot-wire anemometer results of mean pressure and velocity fields, turbulence intensities and Reynolds shear stresses.

Recently, Moss and Baker [9] presented very detailed measurements by using the plused-wire anemometer for flows over a rearward-facing step, over a front-facing step and over a rectangular block. They presented pressure field, velocity profiles and turbulence intensities.

Laser anemometry has also been employed in the study of recirculating flows. Denham and Patrick [30] verified the use of this technique by presenting detailed velocity profiles for laminar flows beyond a back-step in a plane duct. Etheridge and Kemp [31] used a frequency-shifted laser to study the flow behind the

back-step in a water channel. They presented mean velocities, turbulent intensities and Reynolds stresses. By also using the laser, Smyth [32] studied flows over a double backward-facing step. Streamwise, transverse and cross-stream components of velocity fluctuations, turbulent kinetic energy and Reynolds shear stresses were presented. Armaly et al. [33] also presented laser—Doppler measurements of velocity distributions and reattachment lengths for the back-step. Results were for laminar, transitional and turbulent flow of air. For a related geometry, Fraser and Siddig [11] also applied laser anemometry to study recirculation due to air flow over a normal plane wall in a duct. They presented mean and fluctuating velocities.

For the pipe expansion Back and Roschke [34] measured velocity profiles for laminar, transitional and turbulent approach boundary layers, the fluid being water.

All of the above studies reported reattachment lengths varying from about 5.5 to 8.0 st_ heights downstream of separation. Reattachment length is a very significant quantity in recirculating flows and it is worthwhile to give some attention to the factors that affect it. For example, changes in pressure gradient can cause large changes in the reattachment length. Recently, Kuehn [35] studied this effect. He measured the influence of adverse pressure gradient on reattachment length. The results are shown in

Figure (2), which indicates an increase in streamwise pressure gradient causes an increase in reattachment length. Narayanan et al. [27] examined the effects of approach momentum boundary layer thickness on reattachment length. Figure (3) summarizes their experimental results. As can be seen the effects are slight, particularly in the range $\delta_u/H < 1.5$ (δ_u is the approach boundary layer thickness and H the step height). Finally, the effects of approach free - stream turbulence have been examined by Etheridge and Kemp [31]. They noticed that increasing the level of free stream turbulence results in a decrease in reattachment.

2.1.2 Scalar Flow Field Measurements

Mean scalar field measurements are extremely important in understanding the fluid mechanics and are directly applicable to practical situations. Yet, as mentioned earlier, turbulence measurements of scalar fields are very rare in the literature. Often only the mean scalar field is reported; usually no study is made of the heat transfer coefficients, scalar fluxes or scalar fluctuations. Conversely, quite a few heat transfer measurements are concerned only with scalar measurments; no hydrodynamic field measurements are included.

Convective recirculating heat transfer flows have been reviewed earlier by Hansen and Richardson [36], Fletcher et al. [37] and by Aung and Watkins [38]. Aung and Goldstein [8] reported

what is apparently the only existing low speed turbulent heat transfer data for the back-step. The measurements were obtained by using a Mach-Zehnder interferometer. Temperature profiles and heat transfer coefficients are presented for the entire flow field. Much earlier than Aung and Goldstein's [8] study, Seban et al. [6] studied the heat transfer over the back step for high speed flows, with the upstream plate unheated. For the pipe expansion Zemanick and Dougall [39] reported what are also the most complete heat transfer measurements for the entire flow field. Also in related work, much earlier than this study, were the measurements of Ede et al. [40]. In their study they did not emphasize heat transfer in the redeveloping region. Recently, Sparrow and O'Brien [41] presented heat transfer data for the heated side wall in a pipe expansion geometry. The heat transfer coefficients were determined by a napthalene sublimation technique. It should be reemphasised that it is unfortunate than none of the above studies measured the hydrodynamic flow field in conjunction with the heat transfer.

Some heat transfer measurements for related geometries are: a double step by Seki et al. [42,43], a blockage in a pipe by Koram and Sparrow [44], flow over a disc by Smyth [45], high speed flow over a cavity by Haugen and Dhanak [46] and flow over blunt plate by Ota and Kon [47,48].

All of the recirculating flow heat transfer measurements

confirm a peak in the surface heat transfer coefficient near the reattachment point, the peak value being many times larger than the fully developed (or attached) value. Correlations of experimental heat transfer data are very rare in the literature, probably because of the wide range of discrepancies between the measurements. However, for the back-step and for supersonic flows, a correlation procedure was attempted by Lamb [49].

2.2 Turbulent Modeling For Recirculating Flows

A great deal of modeling success has been achieved for turbulent boundary layer flow, with and without heat transfer. For these flows empirical relations such as the 'law of the wall' were adequate. Such approaches fail for turbulent separated flows. This then led to the development of other theoretical models, both simple and complex. The advantages of the simple models are that they enable the development of very versatile and useful numerical codes. Employing these codes furnished and emphasized the need for more realistic and advanced turbulent models.

As seen in Chapter I, in order to solve the mean momentum and mean scalar equations, Eqns. (1.2.3) and (1.2.5), one needs information on the correlations, $\overline{u_i' u_j'}$ and $\overline{u_i' \theta'}$. Before reviewing the modeling procedures employed by researchers for these terms in heat transfer recirculating flows, a generalized discussion of some of the proposals for turbulent closures is presented.

2.2.1 Some Closure Techniques

There are a few extensive reviews in the literature that examine the various closure techniques. For example, four such reviews are: Bradshaw [50], Rodi [51], Reynolds [52] and Mellor and Herring [53]. Modeling is better accomplished with an insight into the physics of turbulence. Such an insight is given by Bradshaw [50]. In this section modeling of both hydrodynamic and scalar

flow fields is discussed. Appendix A contains the mathematical expressions of the models discussed below.

(a) Eddy Viscosity Models

This closure procedure is based on Boussinesq's (1877) [54] idea of a "turbulent visocity". He suggested that the local turbulent shear stress be related to the eddy viscosity and the local mean velocity gradient, i.e., analagous to laminar stresses. The turbulent (eddy) viscosity is assumed a property of the flow field and not a fluid property. For scalar fluxes use is made of the ratio of eddy viscosity to eddy diffusivity, denoted by the turbulent Prandtl number. Closure is accomplished by specifying the eddy viscosity.

Two common procedures are in use, one expresses the eddy viscosity algebraically in terms of mean quantities and the other by differential equations. The simplest algebraic expression is the mixing length hypothesis of Prandtl [55]. An improvement of this length scale was suggested by Van Driest [56].

The first level of improvement of the algebraic viscosity model is the so called one-equation model. In this model, in approximating the turbulent viscosity, a differential equation for a velocity scale (in terms of the turbulent kinetic energy, k) is introduced together with the mixing length scale. For boundary layer flows this procedure was tested by Bradshaw et

al.[57]. The turbulent kinetic energy is an important parameter, for it distinguishes turbulent from laminar flow and is well documented by experiments.

A major problem in turbulent modeling techniques is the choice of necessary and adequate equations. Most work features the diffusion of kinetic energy, ε, as a key quantity. An improved modeling procedure involves approximating the viscosity in terms of differential equations for the velocity and length scales (done in terms of k and ε). This procedure is commonly referred to as the two - equation model of turbulence or simply the k-ε model. The standard k-ε model (high Reynolds number) requires specification of 'wall-functions' [58]. Some improvements of the standard 'wall-functions' are given by Chieng and Launder [59]. Jones and Launder [60] extended the standard k- ε model to include near-wall effects; no specification of the 'wall-functions' outside the viscous sublayer is needed. Because of the simplicity and success of the k- ε model many recent studies were focused on improving the deficiencies of the model. The formulation of the ε differential equation has been the topic of much controversy. Re-examining the equation, Hanjalic and Launder [61,62] 'sensitized' the diffusion of energy effects by considering the importance of near-wall turbulence and the influence of normal strains. Another drawback of the model is that it uses an empirical constant in the

formulation of the turbulent viscosity. Recently, Ljuboja and Rodi [63], Leschziner and Rodi [64], Humphrey and Pourahmadi [65] and Gooray, Watkins and Aung [66] replaced these constants by a function derived from an algebraic stress model. The improvement procedure is outlined in a later chapter. In the present study an analagous calculation was performed for the turbulent Prandtl number and is discussed in a later section. An earlier study by So [67], attempted a similar procedure, but by using the curvature modifications of Bradshaw [68].

(b) Stress and Flux Transport Models

Rather than assume a direct relation between the shear stress and mean strain field (Boussinesq's idea), transport equations for the Reynolds stresses and scalar fluxes are developed. The advantages of this procedure are that solutions start at the wall itself, thus no specification of 'wall-functions', or assumptions as to the turbulent Prandtl number are required, and it automatically includes such effects as streamline curvatures and pressure-strain (scalar) interactions. However, it does require solving some 5 to 7 transport equations of turbulence.

This modeling procedure is much more reliable for predicting non-equilibruim flow (which include recirculating and mixing flows), i.e., when using the turbulent viscosity procedure,

the forcing of the shear stress to instantaneously respond to changes in the mean strain field is not conceptually valid in such flows.

Thus, the closure of the approximate differential equations for the Reynolds stresses ($\overline{u_i'u_j'}$) and scalar fluxes ($\overline{u_i'\theta'}$) offers a very promising class of turbulence models for the solution of complicated turbulent flows. The development of the closure procedures, including procedures for scalar fluxes, can be found in many references, e.g. Launder, Reece and Rodi [17], Launder [69], Hanjalic and Launder [71] (extension of the model to include near-wall effects). Closure of the stresses and fluxes requires approximations for the pressure - strain/scalar and triple correlation terms. The various approximations suggested for these terms differ significantly; for this reason much present research is still directed in this area. For example, Cormack et al. [72] developed an improvement of the Hanjalic and Launder [71] triple velocity correlation closure. However, because of the model's complexity Cormack et al. [72] recommended the one-parameter model of Hanjalic and Launder [71] for most basic flow situations. This conclusion was arrived at after making comparisons with various other models and experiments for axisymmetric channel flow, pipe flow, wall-jets and mixing layers. Recently, both So [73] and Speziale [74] independently further studied the pressure-strain

modeling of Hanjalic and Launder [71]. In his work, So [73] included terms which account for rapid distortion of the shear stress and the return to isotropy process. However, the improvements were found to be minor when compared to the Rotta return to isotropy model used by Hanjalic and Launder [71]. This indicated that much improvement of the pressure-strain term is not possible by just refining the simple Rotta model, a procedure suggested by Launder [69]. With this in mind Speziale [74] redefined the pressure - strain term. Proving this term to be invariant, he developed a representation for it that is dependent on the Reynolds stresses, mean velocity gradients and a master length scale. However, this improvement still has to be tested to determine its usefulness and range of validity. The above modeling procedures do not correctly predict the complex turbulent scales that are present in corner flows. Recently, Gessner and Emery and Gessner [75,76] improved the Launder, Recce and Rodi's model [71] to better simulate corner flows.

Modeling of the scalar fuxes have been carried out by Launder [69]. Gibson and Launder [77] extended the models to include buoyancy effects for thin shear flows remote from walls. Recently, Samaraweera [78] performed extensive testing of the various scalar flux models for boundary-layer type flows.

Analogous to the pressure-strain modeling is the

pressure- scalar modeling. This procedure is outlined in Gibson [79]. The empirical constants appearing in the pressure-scalar model can be obtained from the data of Antonia and Danh [80].

In an effort to reduce the number of transport equations to be solved, simpler versions of the Reynolds stresses and scalar fluxes closure schemes have been derived. One such simplification is the so called algebraic stress closure. The mathematics of the procedure is given in the next chapter, and is similar to that formulated by Launder [69]. Gessner and Emery [77] and Gessner and Po [81] applied this model to flow in a rectangular duct, and found that the model is very accurate when only two empirical constants and a generalized mixing length are specified. Also, So [82] showed that this model can be used to predict the behavior of different kinds of shear flows, i.e., flows over curved surfaces. Algebraic modeling of the scalar flux equation has been done by Gibson [79] and Gibson and Launder [77].

As previously mentioned, algebraic modeling has been used to estimate the constant in the eddy viscosity model, thereby simultaneously accounting for streamline curvature and pressure - strain effects. Bradshaw [68] reported an early study on the importance of these effects. Irwin and Smith [83] used the algebraic stress model to also demonstrate these effects. However, because of the difficulties involved in specifying length scales

and an empirical constant in Bradshaw's [68] model, the algebraic stress modeling seems more adaptable to improving the k-ε model.

2.2.2 Application to Recirculating Flows

The mixing length models can be used for satisfactory prediction of two-dimensional boundary layer flows. Since these flows are self preserving and have local equilibruim regions, the single length scale, with correctly chosen empirical constants can yield satisfactory results. However, applications to recirculating flows have only met moderate success at best [91].

Use of the two-equation (k-ε) model is an obvious improvement, since it incorporates the transport effects of the length scale into the turbulence model. A review of the applicability and validity of this model is demonstrated by Launder and Spalding [58] for many flow situations. Included is flow recirculation, i.e., a film cooling application and flow in a cavity.

After the inception of the present study, a few researchers have attempted modeling recirculating flows for the back-step and pipe expansion. In all cases known to the author, the k-ε model was used. For momentum transfer studies, Taylor et al. [84] incorporated this model with a finite element solution procedure to yield velocity profiles, turbulent intensity and reattachment lengths. Oliver [85] studied heat transfer over the

back-step and compared his results with the experiments of Seban [6] for high speed flows. His predictions overestimate the heat transfer data in the entire flow field, particularly in the reattachment region. Chieng and Launder [59] studied the pipe expansion geometry, by using both the standard k-ε model and the low Reynolds number version of the model. They compared heat transfer coefficients with the data of Zemamick and Dougall [39]. A more detailed discussion of the Chieng and Launder [59] calculations is presented later.

An early analytic analysis of heat transfer for turbulent separated flows was performed by Spalding [86]. He considered a one dimensional analysis near the wall and postulated relationships for the generation, diffusion and dissipation of turbulent energy in terms of the turbulent kinetic energy and empirical constants. Solving the differential equation for k, the Stanton number dependence was obtained. However, as Spalding [86] suggested a two-dimensional analysis with a more realistic turbulent model is needed so as to quantitatively determine velocity and temperature profiles and turbulent intensities.

Modeling procedures for recirculating free shear flows (such as jets) have also been studied. Such flows have been reviewed by Durst and Rastogi [87] and by Leschziner and Rodi [64].

2.3 Review of Computational Methods for Recirculating Flows

Computation of recirculating flows has been a major problem for decades now. For laminar flows the hydrodynamic flow field for the back-step was reliably predicted by the vorticity/stream function formulation of Roache and Mueller [88]. Turbulent flow field simulations of recirculating flow by solving the complete Navier-Stokes equations have increased with the advent of high speed computers. As discussed in the previous section great difficulties exist in the formulation of a set of differential equations to model the flow; and as expected, numerical computations of these equations are also very tedious. For this reason many investigators have concentrated their efforts at looking at the numerical schemes. A review of some of this research is discussed below.

Recently, Atkins et al. [89] examined various numerical schemes for separated flows and compared the different results obtained for the back-step geometry. They concluded that for low Reynolds number by using pure upwind differencing to approximate the convective terms yields reattachment lengths about 8 percent lower than that obtained by a corresponding central differencing approximation procedure. At high Reynolds number, the upwind difference prediction agrees well with experimental results, but the numerical specification of the inlet condition is very

critical. Also, Minh and Chassaing [90] recently studied turbulent numerical calculations for both boundary layer and recirculating type flows. Emphasis was not placed on turbulent modeling, but on choice of unknown variables (vorticity/stream function, ω ,ψ, or pressure/velocity, u, v, p) and the influence of inlet conditions. They found that the (u v p) primitive variable formulation was better than the ($\omega\psi$) method for yielding pressure fields and turbulent quantities (k, $\overline{u'v'}$). Castro [91] also noted that the accuracy of the common differencing schemes is often suspect. He showed that upwind differencing is not accurate near the sharp edges at which the flow separates, and found that skew differencing schemes seem to be better. However, skew differencing techniques have not been fully tested and verified for recirculating flows. Richards and Crane [92] developed a new central differencing scheme and found it to be more accurate than the conventional upwind differencing scheme. However, the scheme will only yield convergence if there is an upper limit on a quantity defined as the grid Reynolds number. Unfortunately, to satisfy this condition requires an excessively fine mesh system and restricts the Reynolds number to extremely low values. Biringen [93] solved the partial differential equations by a time explicit finite differencing scheme, a modified Lax-Wendroff method. He found that values of the turbulent kinetic energy were very sensitive to the empirical

input; whereas, mean velocities and stresses were not so sensitive.

A recent review by Barrett and Demunshi [94] examined finite element, finite difference and finite integral methods for recirculating flows. They concluded that finite difference procedures seem to more reliably predict the recirculating flow field.

Initially many calculation procedures utilized the hybrid central/upwind scheme for the convective terms and central differencing for the diffusive terms. This procedure was developed by Patankar [95]. Very recently, Patankar [96] reviewed the procedure. The procedure suffers from inaccuracies due to truncation error and false diffusion. In light of this, many recent studies have focused on improving the hybrid scheme. Two improvement procedures were studied recently, namely, the hybrid central/skew-upwind differencing scheme of Raithby [97] and the quadratic differencing scheme of Leonard [98]. The quadratic scheme is incorporated in this research and will be discussed in a later chapter. Practical evaluation of these schemes, very recently, were reported by Leschziner [99], Leschziner and Rodi [64] and Han, Humphrey and Launder [100]. The numerical procedure employed in this study employs the improvement of Leonard [98] on the Patankar procedure [95], as developed by Gosman [101].

2.4 SUMMARY

Presently, the information on the complex turbulent flows of the backward step and the sudden pipe expansion is sufficient enough for qualitative discussion of these flows. However, engineering applications require quantitative predictions of some of these complex flows. In the foregoing sections such prediction possibilities were explored by looking at the existing experimental measurements and modeling procedures for turbulent recirculating heat transfer, with emphasis on the back-step and pipe expansion geometries. The existing numerical procedures were also examined with the conclusion being that they are well tested and quite adequate for use in studying recirculating flows. So with confidence in the numerical procedure, the validity and applicability of the turbulence models can be tested to some degree. However, for such modeling to be more meaningful there is a need for more extensive heat transfer measurements for these basic engineering geometries.

As a final remark, the turbulent modeling procedures do not take into account the intermittent nature of turbulence that simple experiments can detail. This is due to the fact that in seeking a model for tractable computer solution, resorting to the averaging of the equations of motion smears out this time dependency. Such effects, however, are probably more dominating in free shear flows than in wall bounded flows and moreover, the time scales involved

are probably not significant when considering application to heat exchange equipment.

CHAPTER III

MATHEMATICAL AND PHYSICAL MODEL FOR GEOMETRIES CONSIDERED

3.1 General Remarks

As discussed previously in Chapter I, solution of the Navier-Stokes and energy equations for turbulent flows, Eqns. (1.2.3) and (1.2.5), requires closure of the Reynolds stresses and scalar fluxes. In Chapter II the various closure schemes were described. In the present study, variations of one such closure scheme, turbulent viscosity modeling (modeling based on the Boussinesq [54] approximation), were applied to two recirculating flow geometries where consistent experimental data exists: air flow at moderate Reynolds numbers over two-dimensional rearward-facing steps and sudden pipe expansions. Successful predictions of the turbulent flow over the two-dimensional rearward-facing steps and axisymmetric pipe expansions were eventually obtained by solving numerically the governing partial differential equations as formulated for the k-ε turbulent viscosity model by Launder and co-workers, cf [19,58,61]. Although the present study focuses on the so called turbulent viscosity models, details of other turbulence closure schemes as well as details of the turbulent viscosity models are presented in Appendix (A) for convenient reference purposes.

3.2 The Boussinesq Approximation

As mentioned before, the closure procedure used in the present study incorporates the Boussinesq [54] turbulent viscosity hypothesis, which relates the Reynolds stresses to mean rates of strains by a turbulent viscosity concept. According to this formulation, the various components of the Reynolds stresses are,

$$-\rho \overline{u'v'} = \mu_t \left(\frac{\partial u}{\partial y} + \frac{\partial v}{\partial x} \right) \qquad (3.2.1)$$

$$-\rho \overline{u'^2} = \mu_t \left(2 \frac{\partial u}{\partial x} \right) - \frac{2}{3} \rho k \qquad (3.2.2)$$

$$-\rho \overline{v'^2} = \mu_t \left(2 \frac{\partial v}{\partial y} \right) - \frac{2}{3} \rho k \qquad (3.2.3)$$

As before, μ_t is the turbulent viscosity. Assuming similar relationships for the heat fluxes,

$$-\rho \overline{u'\theta'} = \Gamma_t \left(\frac{\partial T}{\partial x} \right) \qquad (3.2.4)$$

$$-\rho \overline{v'\theta'} = \Gamma_t \left(\frac{\partial T}{\partial y} \right) \qquad (3.2.5)$$

where Γ_t ($= \mu_t/Pr_t$) is the turbulent diffusivity of temperature. The turbulent viscosity has to be modeled and Γ_t is approximated by using the turbulent Prandtl number, Pr_t, i.e., the ratio of turbulent viscosity to turbulent diffusivity (μ_t/Γ_t).

$$Pr_t = \mu_t/\Gamma_t$$

3.3 Fluid and Thermal Transport Equations

By employing the Boussinesq [54] approximations of the previous section, the time independent mean momentum and energy equations, Eqns. (1.2.1), (1.2.3) and (1.2.4), for an incompressible fluid (for each component) become:

$$\frac{\partial u}{\partial x} + \frac{1}{y^j}\frac{\partial}{\partial y}(y^j v) = 0 \tag{3.3.1}$$

$$\rho u\frac{\partial u}{\partial x} + \rho v\frac{\partial u}{\partial y} = -\frac{\partial p}{\partial x} + \frac{1}{y^j}\left[\frac{\partial}{\partial x}\left(y^j\mu_{eff}\frac{\partial u}{\partial x}\right) + \frac{\partial}{\partial y}\left(y^j\mu_{eff}\frac{\partial u}{\partial y}\right)\right] - \frac{2}{3}\rho\frac{\partial k}{\partial x} + S_u \tag{3.3.2}$$

$$S_u \equiv \frac{\partial}{\partial x}\left(\mu_{eff}\frac{\partial u}{\partial x}\right) + \frac{1}{y^j}\frac{\partial}{\partial y}\left(y^j\mu_{eff}\frac{\partial v}{\partial x}\right)$$

$$\rho u\frac{\partial v}{\partial x} + \rho v\frac{\partial v}{\partial y} = -\frac{\partial p}{\partial y} + \frac{1}{y^j}\left[\frac{\partial}{\partial x}\left(y^j\mu_{eff}\frac{\partial v}{\partial x}\right) + \frac{\partial}{\partial y}\left(y^j\mu_{eff}\frac{\partial v}{\partial y}\right)\right] - j\mu_{eff}\frac{v}{y^{2j}} - \frac{2}{3}\rho\frac{\partial k}{\partial y} + S_v \tag{3.3.3}$$

$$S_v \equiv \frac{\partial}{\partial x}\left(\mu_{eff}\frac{\partial u}{\partial y}\right) + \frac{1}{y^j}\frac{\partial}{\partial y}\left(y^j\mu_{eff}\frac{\partial v}{\partial y}\right) - j\mu_{eff}\frac{v}{y^{2j}}$$

$$\rho u\frac{\partial T}{\partial x} + \rho v\frac{\partial T}{\partial y} = \frac{1}{y^j}\left[\frac{\partial}{\partial x}\left(y^j\Gamma_{eff}\frac{\partial T}{\partial x}\right) + \frac{\partial}{\partial y}\left(y^j\Gamma_{eff}\frac{\partial T}{\partial y}\right)\right] \tag{3.3.4}$$

where, $j = 0$ applies to the back step and

j = 1 applies to the pipe expansion

In the above

$\mu_{eff} = \mu + \mu_t$, where μ_t is the turbulent viscosity

$\Gamma_{eff} = \frac{\mu}{Pr} + \frac{\mu_t}{Pr_t}$, where Pr_t is the turbulent Prandtl number

In the foregoing equations, for notational simplicity the usual overbars have been omitted for the mean fluid-dynamic and temperature variables. As shown in Figure (4), y is measured from the free stream of the back-step or the pipe centerline, and x is the distance along the plate or pipe axis from the vertical face.

Solution of the above equations requires solving a set of coupled non-linear elliptic partial differential equations, with a provision for determination of the pressure field. Initial conditions are discussed in a later section and boundary conditions, together with the solution algorithm are discussed in the next chapter.

Specification of μ_t and Pr_t, so as to solve the system of equations, constitutes a major part of this research. In the initial phase of this study, the simplest turbulent viscosity model (the mixing length model) together with a constant value for the turbulent Prandtl number was used. As will be discussed later, because of the presence of complexities in the turbulence associated with recirculating heat transfer flows, the mixing length model was replaced with a somewhat more sophisticated

turbulent viscosity the k-ε model which gave better results. As the study progressed, it became evident that in order to further improve overall predictions, modifications of the k-ε model were necessary. Numerical experiments were then performed to determine the most reliable form of the k-ε model that could be applied for engineering predictions of recirculating heat transfer. The final calculations in this study use the modified standard k-ε model, together with a variation of this model appropriate for wall shear flows. Functional relationships were derived for two coefficients appearing in the model, a coefficient that relates the viscosity to the turbulent length and velocity scales, and the turbulent Prandtl number.

The remainder of this chapter is devoted primarily to the formulations of the various viscosity models tested in this study.

3.4 Turbulent Prandtl Number and Viscosity Models

3.4.1 Turbulent Prandtl Number

In most previous numerical calculations Pr_t has been assumed to be a constant value, e.g., for air a value of 0.9. This value has been substantiated by experiments for regions outside the viscous sublayer [102]. However, in the viscous sublayer as shown by Blackwell [102] the value is significantly different. Crawford and Kays [103] developed an empirical expression which simulates the data very well,

$$Pr_t = \left\{ \frac{1}{2Pr_{t\infty}} + c\, Pe_t\, (Pr_{t\infty}) - \left(c\, Pe_t\right)^2 \left[1 - \exp\left(\frac{-1}{c\, Pe_t (Pr_{t\infty})^{1/2}}\right)\right] \right\}^{-1/2} \qquad (3.4.1)$$

where $Pr_{t\infty}$ is the free stream value of 0.9, $c = 0.2$ and

$$Pe_t = (\mu_t/\mu)\, Pr \quad , \qquad Pr \text{ (molecular)} = 0.7 \text{ (for air)}$$

In the above, the turbulent viscosity, μ_t, was approximated by using the mixing length model.

By using a Taylor series expansion procedure, Antonia [114] developed a simpler analytic approximation for the behavior of Pr_t in the Buffer zone ($5 < y^+ < 20$).

$$Pr_t = 0.61\, \frac{(1-0.045y^+)}{(1-0.05y^+)} \qquad (3.4.2)$$

where y^+ is the non-dimensional normal co-ordinate,

$y^+ = y\, u_\tau / \nu$, $u_\tau = (\tau_w/\rho)^{\frac{1}{2}}$, τ_w is the wall shear stress.

In the present st dy preliminary calculations used Eqn. (3.4.2) in the viscous sublayer and a value of 0.9 elsewhere. Such a procedure is somewhat inconsistent for the recirculating region, since Eqn. (3.4.2) was derived for a developed boundary layer. In subsequent calculations, the above approach was abandoned for a more generalized description of Pr_t based on algebraic stress modeling. Since the concept and derivation of this new expression is similar to that of the improved turbulent viscosity model, discussion of it is deferred to Section (3.4.4) where both are discussed concurrently.

3.4.2 Mixing Length Model

The mixing length hypothesis is the simplest closure procedure. In this model the viscosity is approximated by a single length scale. During the initial phase of the present study numerical experiments were performed with a modified Van Driest [105] length scale, where,

$$\mu_t = \rho \ell_o^2 \left| \frac{\partial u}{\partial y} \right| \tag{3.4.3}$$

in which

$$\ell_o = \kappa y \left[1-\exp\left(-y^+\tau_w/A^+\right)\right] \tag{3.4.4}$$

where A^+ is normally taken to be a constant value of 26, to conform with the fully turbulent profile remote from a wall. Initial calculations were performed incorporating the above length scale, but with A^+ given a functional behavior, as discussed by Crawford

and Kays [103.] Unfortunately, the heat transfer predictions by this simple model grossly underestimated the data, particularly in the recirculating region. Such a result however, is anticipated, for, in the recirculating (and redeveloping) region it should not be expected that a single length scale will accurately predict the complex turbulence phenomena that exist. After the unsuccessful initial numerical experiments, the mixing length approach was abandoned in favor of the k-ε model.

3.4.3 k-ε Model

The k- ε viscosity approximation procedure is one of the most successful and widely used closure techniques. The standard approximation for the viscosity by two scales is,

$$\mu_t = C_\mu \rho k^{1/2} \frac{k}{\varepsilon}^{3/2} \qquad (3.4.5)$$

where C_μ is normally assumed a constant, $k^{\frac{1}{2}}$ (k is the turbulent kinetic energy, i.e., $k = \overline{u_i' u_i'}/2$) is the vel scale and $k^{3/2}/\varepsilon$ is the length scale, ε being the dissipation rate of turbulence energy. Transport differential equations for k and ε are required and will be presented shortly with non-essential details given in Appendix A. However, first some remarks on C_μ are appropriate. Early calculations in the present research [106] used the established constant value of 0.09 for C_μ [58], but subsequent

studies indicated the need to improve this model through giving C_μ a functional value. The rationale for this improvement is that in recirculating flows the effects of streamline curvatures and pressure-strain interactions are significant factors that influence the recirculating process [63,64,65]. Neglecting these effects results in a shorter recirculating zone. In the k-ε model the most consistent manner in which both these effects can be included is through C_μ. As in the case of Pr_t a generalized expression based on algebraic stress modeling can be derived and further discussion is deferred to Section (3.4.4).

In this study two forms of the k-ε model are used, the standard or "high-Reynolds-number" version [58] and the low-Reynolds-number form proposed by Jones and Launder [106]. In the generalized equations presented below, terms appearing within the broken lines are omitted when using the standard version (Eqn. 3.4.5) of the model. The effective viscosity and diffusivity terms appearing in Eqns. (3.3.2) - (3.3.4) are given by (approximations for Pr_t were discussed previously),

$$\mu_{eff} = \mu + \mu_t \quad ; \quad \mu_t = C_\mu \left| f_1 \right| \rho \, k^2/\varepsilon$$

$$\Gamma_{eff} = \left(\frac{\mu}{Pr} + \frac{\mu_t}{Pr_t} \right) \qquad (3.4.6)$$

The transport of turbulent kinetic energy, k, is expressed by (Appendix A)

$$\rho \frac{\partial}{\partial x}(uk) + \rho \frac{\partial}{\partial y}(vk) = \frac{1}{y^j}\left\{ \frac{\partial}{\partial x}\left[y^j \left(\mu + \frac{\mu_t}{\sigma_k} \right) \frac{\partial k}{\partial x} \right] + \frac{\partial}{\partial y}\left[y^j \left(\mu + \frac{\mu_t}{\sigma_k} \right) \frac{\partial k}{\partial y} \right] \right\} + \mu_t G - \rho\varepsilon - \left| 2\mu \left(\frac{\partial k}{\partial y}^{1/2} \right)^2 \right| \quad (3.4.7)$$

The transport of the rate of dissipation of this energy, ε, can similarly be expressed by,

$$\rho \frac{\partial}{\partial x}(u\varepsilon) + \rho \frac{\partial}{\partial y}(v\varepsilon) = \frac{1}{y^j}\left\{ \frac{\partial}{\partial x}\left[y^j \left(\mu + \frac{\mu_t}{\sigma_\varepsilon} \right) \frac{\partial \varepsilon}{\partial x} \right] + \frac{\partial}{\partial y}\left[y^j \left(\mu + \frac{\mu_t}{\sigma_\varepsilon} \right) \frac{\partial \varepsilon}{\partial y} \right] \right\} + \frac{\varepsilon}{k} C_{\varepsilon 1} \mu_t G - C_{\varepsilon 2} \rho \frac{\varepsilon^2}{k} f_2 + 2 \frac{\mu \mu_t}{\rho} \left(\frac{\partial^2 u}{\partial y^2} \right)^2 \quad (3.4.8)$$

In the preceding equations,

$$G \equiv 2\left[\left(\frac{\partial u}{\partial x} \right)^2 + \left(\frac{\partial v}{\partial y} \right)^2 + j\left(\frac{v}{y^j} \right)^2 \right] + \left(\frac{\partial u}{\partial y} + \frac{\partial v}{\partial x} \right)^2$$

C_μ, $C_{\varepsilon 1}$, $C_{\varepsilon 2}$, σ_k and σ_ε are constants of the standard model and are presented in Table (3.1). The low-turbulent Reynolds number functions are taken as,

TABLE 3.1

VALUES OF EMPIRICAL COEFFICIENTS IN STANDARD k-ε

AND PRESSURE-STRAIN (SCALAR) MODELS

Coefficient	Equation Of First Appearance	Variable Modeled	Value	Reference(s) from which obtained
C_μ	3.4.5	Turbulent Viscosity	From Eqn. (3.4.36)	[58]
σ_k	3.4.7	Turbulent Kinetic energy	1.0	[58]
σ_ε	3.4.8	Dissipation	1.3	[58]
$C_{\varepsilon 1}$	3.4.8	Rate of Turbulence	1.44	[58]
$C_{\varepsilon 2}$	3.4.8	Energy	1.92	[58]
A_m	3.4.8	Low-Reynolds	3.4	[58,107]
A_ε	3.4.8	No. Effects	0.2	[58,107]
C_{s1}	A27	Pressure	2.6	[108]
C_{s2}	A27	Strain	0.2?	[108]
C_{s1w}	A27	Effects	0.75	[17]
C_{s2w}	A27		0.3	[109]
$C_{\theta 1}$	A31	Pressure	3.0	[18]
$C_{\theta 2}$	A31	Scalar Effects	0.33	[18]
$C_{\theta 1w}$	A31		0.5	[18]
C_w	B 22	Wall-effects in pressure strain (scalar)	2.44	[65]

$$f_1 = \exp\left[\frac{-A_m}{1+R_t A_r}\right] \quad , \quad R_t = \frac{\rho v_o \ell_o}{\mu} = \frac{\rho k^2}{\varepsilon\mu}$$

$$f_2 = 1.0 - 0.222 \exp\left[-R_t^2/36\right]$$

where values for A_m and A_r are also presented in Table (3.1).

The standard k-ε model as originally described by Launder and Spalding [19] does not have the capability of including details of flow processes involving the molecular viscous effects near a wall. Away from a wall (in the logarithmic region), where the influences of molecular viscosity are insignificant ($\mu < \mu_t$), the standard equations for k and ε are valid. Thus to account for the viscous diffusion of k and ε close to the wall, Launder and Jones [60] added the molecular viscosity dependent terms to the standard equations. The viscosity dependent functions are related to the turbulent Reynolds number $R_t(\rho k^2/\varepsilon\mu)$, which has a dominating influence near the wall. These additional terms are based on empirical relationships obtained from boundary layer type flows; as such, they are not based on exact mathematical formulations.

Apart from the low-Reynolds number form of the model other improvements of the standard model were also incorporated in this study. Need for improvements to the standard model have been recognized for some time now by several researchers [62,64,69]. As pointed out by Launder [69], the term that is most loosely

approximated in the k-ε model is ε . Primarily because none of the terms in the transport equation for ε can be measured experimentally, empirical approximations are difficult. To improve the modeling of the ε transport equation for accelerated shear flows. Hanjalic and Launder [62] "sensitized" the equation to the diffusion of energy effects by considering the importance of near-wall turbulence and the influence of normal strains. The term added to the ε differential equation is,

$$-C\,(0.33\varepsilon)\,\partial u/\partial x \qquad (3.4.9)$$

Direct application of the term represented by Eqn. (3.4.9) into the k-ε model, resulted in minimal improvement of the heat transfer results for the redeveloping region in the present study. Leschziner and Rodi [64] used the formulations of Hanjalic and Launder [62] in streamline co-ordinates to "sensitize" the ε equation to a recirculating flow by including the effects of streamline curvature. This procedure was also tested in this study. In streamline co-ordinates, the extra term appearing in the ε transport equation is,

$$-\frac{\varepsilon}{k}\,C_1''\,C_\mu\,\rho\,\frac{k^2}{\varepsilon}\,S_{ns}^2 \qquad (3.4.10)$$

in which,

$$C_1'' = 0.8$$

and $$S_{ns} = \frac{\partial u_s}{\partial n} - \frac{u_s}{R_c}$$

In the above u_s is the velocity normal to the streamline, n is the co-ordinate normal to the streamline and R_c is the radius of curvature (Fig. (B1)). Expressions for $\partial u_s/\partial n$ and R_c, developed in Appendix (B) are,

$$\frac{\partial u_s}{\partial n} = \sin(2\theta)\left[\frac{\partial v}{\partial y} - \frac{\partial u}{\partial x}\right] + \cos(2\theta)\left[\frac{\partial u}{\partial y} + \frac{\partial v}{\partial x}\right] + \frac{u_s}{R_c} \qquad (3.4.11)$$

and,

$$R_c = \frac{\left(u^2 + v^2\right)^{3/2}}{uv\left(\frac{\partial v}{\partial y} - \frac{\partial u}{\partial x}\right) + u^2\frac{\partial v}{\partial x} - v^2\frac{\partial u}{\partial y}} \qquad (3.4.12)$$

In Eqn. (3.4.11) θ is the angle between the velocity vector that is tangent to the streamline and the x-axis (Figure (B1)).

In the present research, including the term represented by Eqn. (3.4.10) resulted in some improvement in the results over the standard model for the recirculating zone. However, it was eventually discarded in favor of the more comprehensive approach of including curvature effects by modifying C_μ, as discussed in Section (3.4.4). Results of reattachment lengths and heat transfer calculated using Eqn. (3.4.10) in the standard k-ε model are presented in a later chapter and are compared with results from other modifications.

Solution of the equations of motion, energy and turbulence presented in this section require specification of inlet

and boundary conditions. Detailed discussions of these conditions are presented in a separate section.

3.4.4 Incorporation of Algebraic Reynolds Stress and Scalar Flux Closure

In this section functional relationships are derived for the coefficients C_μ and Pr_t that are presented in Eqn. (3.4.6). This procedure involves obtaining transport equations for the Reynolds stresses and scalar fluxes. These equations are then closed by the so called algebraic stress closure procedure. The algebraically closed equations are not directly employed in this study, but the interesting relationship between the shear stress and local rate of strain, as obtained from the model, is compared with the k-ε viscosity model of the preceding section to obtain new relationships for C_μ and Pr_t. As a result of this application of the algebraic Reynolds stress and scalar flux closure scheme, the new expressions for C_μ and Pr_t in Eqn. (3.4.5), and hence the k-ε viscosity model, is now sensitized to account for the effects of streamline curvatures and pressure-strain (scalar) interactions with the inclusion of 'wall-damping' contributions. The inclusion of these two effects are crucial for obtaining accurate solutions.

The importance of streamline curvature effects in turbulent flow has been demonstrated in experimental studies [110,111]. These studies indicate that curvature of the mean flow

gives rise to an appreciable change in the turbulent flow structure, which then results in a direct influence on turbulent transport of heat and momentum [79]. Attempts to include the effects of streamline curvature in numerical calculations have in the past been based on Brashaw's [68] modification of the mixing length theory. However, because of difficulties in specifying length scales and an empirical constant in Bradshaw's equation, Leschziner and Rodi [64], Ljuboja and Rodi [63] and Humphrey and Pourhmadi [65] found inclusion of streamline curvature effects in the k-ε model through C_μ to be more practical. In the present study a more generalized procedure of Leschziner and Rodi [64] is adopted for describing C_μ, in streamline co-ordinates, for the recirculating region. The expression for C_μ is generalized to include 'wall-damping' effects in the pressure-strain term and also the local equilibrium of turbulence energy is not assumed (i.e., $P/\varepsilon = 1$, where P is the production of turbulent kinetic energy). In the redeveloped region, a generalized expression for C_μ is also developed in cartesian coordinates, similar to the less restricted procedure of Ljuboja and Rodi [63]. In both regions, the turbulent Prandtl number, Pr_t, is similarly functionalized. This generalized procedure of improving the approximations of both C_μ and Pr_t in the entire flow field (recirculating and redeveloping) is unique to the present research.

The general outline of the derivation is presented below, tedious algebraic details are presented in Appendix (A). Proceeding from the Navier-Stokes and energy equations, the equations that represent the transport of Reynolds stresses, $\overline{u_i' u_j'}$, and scalar fluxes $\overline{u_i' \theta'}$, respectively, are:

$$\frac{D}{Dt}\left(\overline{u_i' u_j'}\right) = -\left\{ \overline{u_i' u_k'} \frac{\partial u_i}{\partial x_k} + \overline{u_j' u_k'} \frac{\partial u_i}{\partial x_k} \right\}$$

I

$$- 2\nu \overline{\frac{\partial u_i'}{\partial x_k} \frac{\partial u_j'}{\partial x_k}} - \overline{\frac{p'}{\rho}\left(\frac{\partial u_i'}{\partial x_j} + \frac{\partial u_j'}{\partial x_i}\right)} \qquad (3.4.13)$$

II III

$$- \frac{\partial}{\partial x_k}\left[\overline{\left(u_i' u_j' u_k'\right)} - \nu \frac{\partial}{\partial x_k} \overline{u_k' u_j'} + \overline{\frac{p'}{\rho}\left(\delta_{jk} u_i' + \delta_{ik} u_j'\right)} \right]$$

IV

$$\frac{D}{Dt}\left(\overline{u_i' \theta'}\right) = -\left(\overline{u_i' u_k'} \frac{\partial T}{\partial x_k} + \overline{\theta' u_k'} \frac{\partial u_i}{\partial x_k} \right)$$

I

$$+ (\Gamma+\nu) \overline{\frac{\partial \theta'}{\partial x_k} \frac{\partial u_i'}{\partial x_k}} + \overline{\frac{p'}{\rho} \frac{\partial \theta'}{\partial x_i}} \qquad (3.4.14)$$

II III

$$- \frac{\partial}{\partial x_k}\left[\overline{u_i' u_k' \theta'} - \Gamma \frac{\partial}{\partial x_k} \overline{u_i' \theta'} - \nu \frac{\partial}{\partial x_k} \overline{\theta' u_i'} + \overline{\frac{p' \theta'}{\rho}} \delta_{ik} \right]$$

IV

Terms I, II, III, and IV are often referred to as the generation (production), dissipation, pressure-strain (scalar) and diffusion terms, respectively.

For complete closure of Eqns. (3.4.13) and (3.4.14), terms II, III and IV need to be approximated. Launder [69] and Samaraweera [78] discuss in detail the mathematical procedures involved in closing these unknown gradient terms. This procedure is often referred to as the Reynolds stresses (scalar fluxes) closure scheme. Eqns. (3.4.13) and (3.4.14) with the closure approximations included are then solved with the transport equations for mass, momentum, energy, k and ε to obtain the turbulent flow field. A somewhat more restrictive closure scheme has been developed for approximating Eqns. (3.4.13) and (3.4.14) and for simplifying the unknown gradient terms in Eqns. (3.4.13) and (3.4.14) [51]. In this procedure the convective minus the diffusive transport terms are approximated by algebraic equations and terms II and III are approximated using the same procedure as that discussed by Launder [69] and Samaraweera [78]. It is this procedure, often referred to as the algebraic stress (scalar flux) closure scheme, that is incorporated in the present study so as to derive functional relationships for C_μ and Pr_t. The procedure to

eliminate the convective and diffusive terms was proposed by Rodi [51] and later Irwin and Smith [83] and Gibson [79] adopted the procedure to solve a variety of turbulent flow fields. The basic relations are derived as follows:

Rewriting Eqn (3.4.13) as,

$$\frac{D}{Dt}(\overline{u_i'u_j'}) = P_{ij} + \phi_{ij} - \varepsilon_{ij} + D(\overline{u_i'u_j'}) \qquad (3.4.15)$$

where,

$P_{ij} \equiv$ Term I (production)

$\phi_{ij} \equiv$ Term III (pressure-Strain)

$\varepsilon_{ij} \equiv$ Term II (dissipation)

$D(\overline{u_i'u_j'}) \equiv$ Term IV (diffusion)

Rodi [51] proposed that the convective and diffusive transport of Reynolds stresses are connected through the kinetic energy rates. Replacing the kinetic energy rates by using a balance between production and dissipation rates result in the following balance equation,

$$\frac{D}{Dt}(\overline{u_i'u_j'}) - D(\overline{u_i'u_j'}) = \frac{\overline{u_i'u_j'}}{k}(P-\varepsilon) \qquad (3.4.16)$$

where as defined previously P is the production of turbulent kinetic energy,

$$P = \tfrac{1}{2} P_{ij}$$

Substituting Eqn. (3.4.16) into (3.4.15) results in,

$$\frac{\overline{u_i'u_j'}}{k}(P-\varepsilon) = P_{ij} + \phi_{ij} - \varepsilon_{ij} \qquad (3.4.17)$$

Closure of ϕ_{ij} and ε_{ij} results in a set of algebraic equations for the stresses $\overline{u_i'u_j'}$. Closure of the pressure-strain term is as follows [69]:

$$\phi_{ij} = \phi_{ij(1)} + \phi_{ij(2)} + \phi_{ij(1w)} + \phi_{ij(2w)} \qquad (3.4.18)$$

where the w subscript terms are the 'wall-damping' corrections to the pressure due to turbulence and turbulence and mean rate of strain interactions. Each of the terms in Eqn. (3.4.18) are then approximated as [17,69],

$$\begin{aligned}
\phi_{ij(1)} &= -C_{s1}\frac{\varepsilon}{k}\left(\overline{u_i'u_j'} - \frac{2}{3}\delta_{ij}k\right) \\
\phi_{ij(2)} &= -C_{s2}\left(P_{ij} - \frac{2}{3}P\delta_{ij}\right) \\
\phi_{ij(1w)} &= -C_{s1w}\frac{\varepsilon}{k}\left(\overline{u_i'u_j'} - \frac{2}{3}k\delta_{ij}\right) f(\ell/x_2) \\
\phi_{ij(2w)} &= -C_{s2w}\left(P_{ij} - D_{ij}\right) f(\ell/x_2)
\end{aligned} \qquad (3.4.19)$$

In the above,

$$D_{ij} = -\left[\overline{u_i'u_j'}\frac{\partial u_k}{\partial x_j} + \overline{u_j'u_k'}\frac{\partial u_k}{\partial x_i}\right]$$

and C_{s1}, C_{s2}, C_{s1w} and C_{s2w} are empirical constants, their values are presented in Table (3.1). The near-wall function, $f(\ell/x_2)$,

takes on a value of unity near a wall and zero remote from a wall. Specification of $f(\ell/x_2)$ is as follows: For flows in the presence of a single wall [17],

$$f(\ell/x_2) \propto \ell_o/y \quad , \quad \ell_o = k^{3/2}/\varepsilon$$

$$f(\ell/x_2) = \frac{1}{C_w} \frac{k^{3/2}}{\varepsilon} \qquad (3.4.20)$$

where, C_w is obtained by imposing the following condition,

$f(\ell/x_2) \to 1$, as $y \to 0$ (Linear Sublayer)

For the 'log-law' Region (Inertial Sublayer),

$$\tau_w = C_\mu^{1/2} \rho k \qquad (3.4.21)$$

and,

$$\mu_t = \kappa y (\rho \tau_w)^{1/2} \qquad (3.4.22)$$

And from the k-ε viscosity model,

$$\mu_t = C_\mu \rho k^2/\varepsilon \qquad (3.4.23)$$

Subsituting Eqn. (3.4.21) into Eqn. (3.4.22), comparing with Eqn. (3.4.23) and imposing the limiting condition in the viscous sublayer, results in,

$$\frac{1}{C_w} = \frac{C_\mu^{3/4}}{\kappa} \quad ; \quad \kappa = 0.4$$

Using the local equilibruim assumption, $C_\mu = 0.09$ [58], the above becomes,

$1/C_w = 0.41$

In the present recirculating flow geometries the near-wall function should be modeled so as to reflect the importance of both side and bottom walls in the corner region of Fig. (4). Therefore, in the present study, a superposition relationship is assumed,

$$f(\ell/x_2) = \frac{1}{C_w}\frac{k}{\varepsilon}^{3/2}\left[\left(\frac{1}{x}\right)^{1/m} + \left(\frac{1}{y}\right)^{1/m}\right]^m, \quad m=2 \qquad (3.4.24)$$

Rewriting Eqn. (3.4.24) to correspond with the co-ordinate system of the present study, Fig. (4), results in

$$f(\ell/x_2) = \frac{1}{C_w}\frac{k}{\varepsilon}^{3/2}\left\{\left[\frac{1}{(D/2-y)}\right]^{1/m} + \left[\frac{1}{x}\right]^{1/m}\right\}^m \qquad (3.4.25)$$

where, $\frac{1}{x} = 0$, for $(\frac{D}{2} - y) < \frac{d}{2}$

The only term remaining to be closed is Eqn. (3.4.17) is the dissipation term. According to Launder, Reece and Rodi [17], this term is,

$$\varepsilon_{ij} = \frac{2}{3}\delta_{ij}\varepsilon \qquad (3.4.26)$$

Subsituting Eqns. (3.4.19) and (3.4.26) into Eqn. (3.4.17) results in,

$$\frac{\overline{u_i u_j}}{k} = \frac{A}{\varepsilon}\left[P_{ij} - \frac{2}{3}P\,\delta_{ij}\right]$$

$$+ \frac{\Lambda''}{\varepsilon} \left[P_{ij} - D_{ij} \right] + \frac{2}{3} \delta_{ij} \qquad (3.4.27)$$

where,

$$\Lambda' \equiv (1-C_{s2})/\left[\frac{P}{\varepsilon} - 1 + C_{s1} - C_{s1w}\, f(\ell/x_2) \right]$$

and

$$\Lambda'' \equiv C_{s2w}\, f(\ell/x_2)\, \Lambda'/(1-C_{s2})$$

Eqn. (3.4.27) gives the interesting relationship between the shear stress and the local rate of strain; as such, it is like the 'effective viscosity' relationship. In the analysis to follow, this concept is algebraically explored so as to derive the functional expression for C_μ, which, as pointed out earlier, is the principal objective of this section.

A similar analysis to the preceding can be performed for the scalar flux transport equation. Rewriting Eqn. (3.4.14),

$$\frac{D}{Dt} \overline{(u_i'\theta')} = P_{i\theta} + \phi_{i\theta} + D\overline{(u_i'\theta')} \qquad (3.4.28)$$

where, $P_{i\theta} \equiv$ Term I (production)

$$\phi_{i\theta} \equiv \phi_{i\theta(1)} + \phi_{i\theta(2)} + \phi_{i\theta(1w)} + \phi_{i\theta(2w)}$$

$\equiv$ Term III (pressure - scalar)

$\overline{D(u_i'\theta')} \equiv$ Term IV (diffusion)

Again, using the closure procedures discussed by Launder [69],

$$\phi_{i\theta(1)} = -C_{\theta 1} \frac{\varepsilon}{k} \overline{u_i'\theta'}$$

$$\phi_{i\theta(2)} = C_{\theta 2} \overline{u_k'\theta'} \frac{\partial u_i}{\partial x_k} \qquad (3.4.29)$$

$$\phi_{i\theta(1w)} = -C_{\theta 1w} \frac{\varepsilon}{k} \overline{u_i'\theta'} f(\ell/x_2)$$

$$\phi_{i\theta(2w)} = 0$$

Values of the empirical constants, $C_{\theta 1}$, $C_{\theta 2}$, and $C_{\theta 1w}$ are given in Table (3.1).

Analagous to Rodi's [51] proposal for the Reynolds stresses, the convective and diffusive balance of scalar fluxes can be written as,

$$\frac{D}{Dt}(\overline{u_i'\theta'}) - D(\overline{u_i'\theta'}) = \overline{u_i'\theta'}\left[\frac{P_\theta - \varepsilon_\theta}{\overline{\theta'^2}} + \frac{P-\varepsilon}{k}\right] \qquad (3.4.30)$$

where P_θ (production rate of $\overline{\theta'^2}$) $= -2\,[\overline{u_k'\theta'}\,\partial T/\partial x_k]$

ε_θ(dissipation rate of $\overline{\theta'^2}$) $= 2\,\Gamma\,\overline{(\partial\theta'/\partial x_k)^2}$

Substituting Eqn. (3.4.30) into Eqn. (3.4.28) and making use of Eqn. (3.4.29) results in,

$$-\overline{u_i'\theta'} = \phi_T \frac{k}{\varepsilon} \overline{u_i'u_k'} \frac{\partial T}{\partial x_k} + \phi_T' \frac{k}{\varepsilon} \overline{u_k'\theta'} \frac{\partial u_i}{\partial x_k} \qquad (3.4.31) \rightarrow$$

where

$$\phi_T = C_{\theta 1} + C_{\theta 1w} f(\ell/x_2) + \frac{1}{2}\left(\frac{P}{\varepsilon} - 1\right)$$

$$+ \frac{1}{2} \frac{k}{\varepsilon} \frac{\varepsilon_\theta}{\overline{\theta'^2}} (P_\theta/\varepsilon_\theta - 1)$$

and

$$\phi_T' = \phi_T(1-C_{\theta 2})$$

The expression for ϕ_T, Eqn. (3.4.31) can be simplified by assuming local equilibruim of turbulence, in which the production and dissipation rates of $\overline{\theta'^2}$ are assumed equal, i.e.,

$$P_\theta/\varepsilon_\theta = 1$$

Thus,

$$\phi_T = C_{\theta 1} + C_{\theta 1w} f(\ell/x_2) + \frac{1}{2} (P/\varepsilon - 1)$$

As a consequence of the local equilibruim assumption, the term containing ε_θ and $\overline{\theta'^2}$ in Eqn. (3.4.31) drops out. As such, transport equations for ε_θ and $\overline{\theta'^2}$ are not needed. Eqn. (3.4.31) will also be explored algebraically to yield a functional relationship for the turbulent Prandtl number, Pr_t, which as stated before is the objective of this section.

In the recirculating region, adopting the procedure of Leschziner and Rodi [64], Eqns. (3.4.27) and (3.4.31) are expressed in streamline coordinates (s,n). As pointed out previously Figure (B1) illustrates the coordinate system, where coordinate s is

along the streamline and n is normal to the streamline. Writing these equations for all the combinations of stresses and scalar fluxes results in a set of algebraic equations. By lengthy algebraic elimination procedures, unique expressions for the shear stress, $(\overline{u_s' u_n'})$, and the scalar flux, $(\overline{u_n' \theta'})$, can be obtained. Subscripts 's' and 'n' refer to velocities tangential and normal to streamlines, respectively. The final expressions are presented below, with the tedious algebraic elimination details presented in Appendix (B).

$$-\overline{u_s' u_n'} = \frac{2}{3}\frac{k^2}{\varepsilon}\left(\Lambda' \frac{P}{\varepsilon} - 1\right)\left(\frac{\partial u_s}{\partial n} - \frac{u_s}{R_c}\right)/S_4 \qquad (3.4.32)$$

$$-\overline{u_n' \theta'} = \phi_T \frac{k}{\varepsilon}\frac{\partial T}{\partial n}\left[\overline{u_n'^2} + 2\phi_T \frac{k}{\varepsilon}\frac{u_s}{R_c}\overline{u_s' u_n'}\right]/S_{T1} \qquad (3.4.33)$$

In the above S_4 and S_{T1} are lengthy algebraic expressions in terms of turbulent constants, u_s/R_c, and $\partial u_s/\partial n$. Expressions for R_c and $\partial u_s/\partial n$ were given previously in Eqns. (3.4.12) and (3.4.11), respectively. The algebraic expressions for S_4 and S_{T1} are,

$$S_4 = 1 + \frac{k^2}{\varepsilon^2}\left[8\Lambda'^2 \frac{u_s}{R_c} S_1 + 4\Lambda'' S_2 \left(3\Lambda' \frac{u_s}{R_c} + \Lambda'' \frac{\partial u_s}{\partial n} + \Lambda'' S_2\right)\right] \qquad (3.4.34)$$

in which,

$$S_1 = \partial u_s/\partial n + u_s/R_c$$

$$S_2 = \partial u_s/\partial n + 3 u_s/R_c$$

$$S_{T1} = 1 + 2\left(\phi_T' \frac{k}{\varepsilon}\right)^2 \frac{u_s}{R_c}\left(\frac{\partial u_s}{\partial n} + \frac{u_s}{R_c}\right) \qquad (3.4.35)$$

The expressions for C_μ and Pr_t are readily obtained by compairing Eqns. (3.4.32) and 3.4.33) with the Boussinesq approximations, Eqns. (3.2.1) and (3.2.5) expressed in streamline co-ordinates. The results are,

$$C_\mu = -\frac{2}{3}\Lambda'(\Lambda'\frac{P}{\varepsilon} - 1)/S_4 \qquad (3.4.36)$$

$$Pr_t = C_\mu S_{T1} S_{T2} \qquad (3.4.37)$$

where S_{T2} is also a lengthy algebraic expression given by,

$$S_{T2} = \left\{ -\frac{2\phi_T}{\varepsilon}\left[C_\mu \frac{k^2}{\varepsilon}\left(\frac{\partial u_s}{\partial n} - \frac{u_s}{R_c}\right)\left[\frac{u_s}{R_c}(2\Lambda' + \phi_T') + \Lambda'' S_2\right] + \frac{1}{3}\varepsilon(\Lambda'\frac{P}{\varepsilon} - 1)\right]\right\}^{-1}$$

Eqn. (3.4.36) reduces to the more restrictive formulation of Leschziner and Rodi [64] if equilibrium of turbulence energy is assumed, $P/\varepsilon = 1$, and if 'wall-damping' corrections in the pressure-strain terms are ignored, i.e., $\Lambda'' = 0$.

In the preceding analysis C_μ (and Pr_t) are modeled in streamline coordinates to reflect the sharp bending of the streamlines that dominate in the recirculating region. In the present study the expressions for C_μ and Pr_t, Eqns. (3.4.36) and

(3.4.37), are used with the standard k-ε model for predicting the flow field in the recirculating region. In the redeveloping region, where the bending of the streamlines are not so severe, expressions for C_μ (to account for curvature effects) and Pr_t are obtained in (x,y) coordinate system. The mathematical procedures involved in obtaining these expressions for the redeveloping region are analogous to the previous derivation. They however, result in even more tedious algebraic detail and lengthy algebraic expressions. Consequently, the mathematical details are presented in Appendix (B). The final expressions are:

$$C_\mu = \frac{\Lambda''}{Ak}\cdot\frac{1}{C_\ell}\left\{ F\left(\frac{A}{\beta}+\frac{C}{A}\right)+\frac{2}{3}\,k\,B\left(\frac{1}{\beta A}+\frac{C}{A}\right) + \frac{A}{\alpha}\left(F+\frac{2}{3}\,k\,B\right)\right\} \qquad (3.4.38)$$

$$Pr_t = \frac{C_\mu\left[\left(1+\frac{k}{\varepsilon}\,\phi_T'\,\frac{\partial v}{\partial y}\right)\left(1+\frac{k}{\varepsilon}\,\phi_T'\,\frac{\partial u}{\partial x}\right)+\frac{k}{\varepsilon}\,\phi_T'\,\frac{\partial u}{\partial y}\right]}{\phi_T\left(1+\frac{k}{\varepsilon}\,\phi_T'\,\frac{\partial u}{\partial x}\,\frac{\overline{v'^2}}{k}\right)} \qquad (3.4.39)$$

in which,

$$\frac{\overline{v'^2}}{k} = -\frac{1}{\beta k}\left[F+\beta C+\frac{2}{3}\,kB(1+\beta C)\right]$$

$A, B, C, C_{\ell}, E, F, \alpha$ and β are lengthy algebraic expressions involving turbulent constants and mean gradients and are presented in Appendix (B). The above expression for C_{μ}, Eqn. (3.4.38), reduces to the expression of Ljuboja and Rodi [63] if the convective/diffusive transport of $\overline{u'v'}$ and longitudinal gradients, $\partial v/\partial y/\partial u/\partial y$, are ignored.

The expressions given above for C_{μ} and Pr_t, valid for the redeveloping region, are used with the low-Reynolds number version of the k-ε model. When using the expression for C_{μ}, the near-wall function, f_1 (Eqn. 3.4.6), in the low-Reynolds number model is omitted. This is essentially because C_{μ} is already modeled to reflect the near-wall effects. The physical procedures involved in dividing the flow field beyond rearward steps and pipe expansions into two distinct regions, for application of either the standard or low-Reynolds number model, are described in the next section.

3.5 Two-Pass Procedure

Initial calculations made by simply employing the standard k- ε model formulation and the corresponding wall-function boundary conditions yielded unsatisfactory results for the heat transfer coefficients in the redeveloping region [106]. The predicted heat transfer coefficients in this region were significantly higher than the data. Using the low-Reynolds-number formulation results in a large and erroneous reduction in heat transfer coefficients in the recirculating region, but better agreement is obtained with the data in the redeveloped region. This behavior is understandable, because the extra terms appearing in the low-Reynolds-number model were a result of tests made on shear layers [60]. Thus, using the low-Reynolds number model in recirculating flows, upstream of reattachment will not be totally consistent.

Improvement of solutions for heat transfer in the entire flow field required a sequence of two calculations. In the first calculation, the reattachment point is estimated using the improved standard k- ε model. In general, as will be shown in a later chapter, this initial solution tends to deviate somewhat from the experimental results, particularly in the redeveloped region, but it does predict fairly accurately, with the appropriate modification to C_μ, the reattachment point. Once the reattachment point is determined, the calculation is repeated with the improved

standard k- ε model employed upstream of reattachment, and the improved low-Reynolds number version of the model applied downstream of reattachment. Figure (5) shows the solution domains for each model during the second calculation. In implementing this procedure during the second pass, the low-Reynolds number terms in Eqns. (3.4.6) - (3.4.8) are simply omittted upstream of reattachment. The boundary conditions for this procedure are discussed in the next chapter.

3.6 Treatment of Initial Conditions for Computed Flows

The upstream conditions for each test case computed in this study are summarized in Table 3.2. Unfortunately, the work of Aung and Goldstein [8] does not include complete measurements of upstream (approach) profiles since their focus was on heat-transfer coefficients. They do, however, include measurements of approach temperature boundary-layer profiles. Their experiment was performed utilizing a tripped approach boundary-layer with a fairly short, but not entirely insignificant, thermal entry length. The approximations of the inlet profiles for u, k and ε are described below. A similar procedure as that used to obtain the velocity profiles was used to determine the temperature profiles, which when compared with the data revealed no inconsistencies. Thus, serving as a check on the validity of the procedure for the velocity profiles. The simulation procedure is presented below, with algebraic details presented in Appendix (C). The various lengths that appear in the equations below (e.g., x_1 and ζ) are schematically presented in Figure (C1). From turbulent flat plate boundary-layer theory [103] the momentum boundary-layer thickness at the step is,

$$\delta_u(x_1) = 0.3814\, x_1 \left(\frac{\mu}{\rho U_o x_1} \right)^{0.2} \qquad (3.6.1)$$

The corresponding unheated starting length thermal boundary layer

TABLE 3.2

SUMMARY OF APPROACH CONDITIONS FOR TEST CASES

Geometry	Experimenters	δ_0/H	δ_T/H	k	ε	u and T
Back-Step	Aung and Goldstein [8]	Simulated	1.0	Klebanoff [112] fit	Klebanoff [112] fit	Abbott and Kline [10] fit
Back-Step	Moss and Baker [9]	0.7	Not Applicable (Non-Heat Transfer)	Measurements	From k Profile fit	Abbott and Kline [10] fit
Back-Step	Eaton and Johnston [20]	0.23	Not Applicable (Non-Heat Transfer)	Measurements	From k Profile	Measurements
Pipe Expansion	Semanick and Doysill [39]	Fully Developed	Fully Developed	Laufer [113] fit	Laufer [113] fit	Fully Developed Profiles
Pipe Expansion	Sparrow and O'Brien [41]	Fully Developed	Fully Developed	Laufer [113] fit	Laufer [113] fit	Fully Developed Profiles

thickness at the step is [103],

$$\delta_T(x_2) = \delta_u(x_1) \left\{ \frac{\left[1 - (\xi/x_1)^{9/10}\right]^{-1/9}}{0.169\ Re_{x_1}^{-0.1}\ (13.2\ Pr - 10.1)\ 0.9} \right\}^{-7} \qquad (3.6.2)$$

in which $\xi = x_1" - x_2"$, $x_1"$ and $x_2"$ are defined below. Eqns. (3.6.1) and (3.6.2) require that the effective starting length x_1 be known. The procedure to determine x_1 is as follows. (See Figure (C1) for the schematics.) The momentum boundary layer up to the trip is assumed laminar, given the starting length, as specified by the experiment [8], thus boundary layer thickness at the step is readily determined. Assuming that immediately at the step the boundary layer is turbulent, and equating the obtained laminar value to the turbulent growth law, results in an effective starting length for a turbulent boundary layer at the trip, $x_1"$. Thus the total effective starting length, x_1, is sum of $x_1"$ and the distance between the trip and the step, x_s. A similar procedure is applied to obtain the equivalent turbulent thermal starting length at the trip, $x_2"$. When this distance is used in Eqn.(3.6.2), the thermal boundary layer thickness compares favorably with the experimental values [8].

Once the momentum and thermal boundary layer thickness are determined, the velocity and temperature profiles at the step can

be determined by using the Abbott and Kline [10] fit for a tripped boundary layer.

$$\frac{u}{U_o} = \left[\frac{x_2}{\delta_u(x_1)} \right]^{1/5.6} \qquad (3.6.3)$$

Rewriting the above for the coordinate system used in this study, Figure (4),

$$\frac{u}{U_o} = \left[\frac{d/2-y}{\delta_u(x_1)} \right]^{1/5.6} \quad ; \left(\frac{d/2-y}{\delta_u(x_1)} \right) < 1$$

$$\frac{u}{U_o} = 1 \quad ; \left(\frac{d/2-y}{\delta_u(x_1)} \right) \geq 1 \qquad (3.6.4)$$

Assuming that temperature develops similarly as the velocity,

$$\frac{T_w-T}{T_w-T_\infty} = \left[\frac{d/2-y}{\delta_T(x_2)} \right]^{1/5.6} \quad ; \left(\frac{d/2-y}{\delta_T(x_2)} \right) < 1$$

$$\frac{T_w-T}{T_w-T_\infty} = 1 \quad ; \left(\frac{d/2-y}{\delta_T(x_2)} \right) \geq 1 \qquad (3.6.5)$$

In the above U_o and T_∞ are the free stream velocity and temperature, respectively, and T_w is the wall temperature. Inlet

profiles for k and ε are obtained by a piecewise linear fit of the flat plate boundary layer data of Klebanoff [112] as presented in Hinze [16]. In the free stream, k is assigned a value of 0.1 percent of the free stream velocity (i.e., $k=0.001U_o^2$). In initial calculations [106] it was discovered that the level of turbulence intensity in the mixing region of the fit led to unreasonable reattachment lengths when compared with the data. To eliminate this difficulty it was necessary to increase the level of turbulent kinetic energy in this region approximately three-fold. This higher level of turbulent energy is not completely arbitrary, since the presence of the trip in the experiments would seem likely to produce turbulence levels persisting downstream of the trip higher than those of the corresponding Klebanoff data for the same Reynolds number. Subsequent calculations studied the influences of the trip (which is situated approximately 11 trip-heights upstream of the step) on approach conditions at the step and on the net effect on reattachment lengths. The results indicate that in order to have reattachment length similar to the experiment, the turbulent intensity at the step must be equivalent to the intensity found at 11 step-heights downstream of a step, which is significantly much more enhanced than the Klebanoff [112] intensities. Results of these studies are presented in a later chapter.

In the data of Klebanoff [112] the turbulent kinetic energy (and ε) are normalized by relations containing the friction velocity, u_τ . For a turbulent flat plate u_τ is,

$$u_\tau^2 \approx 0.0066\ U_o^2\ Re_{\delta(x_1)}^{-1/6} \qquad (3.6.6)$$

The heat transfer results of Aung and Goldstein [8] are normalized by the Nusselt number just upstream of the step (Nu_H). This quantity is not provided, and so must be calculated. This quantity is readily obtained from turblent flat plate theory [103],

$$Nu_H \approx \frac{0.0287\ Re_H^{0.8}\ Pr \left[1 - (\xi/x)^{9/10}\right]^{-1/9}}{0.169\ Re_H^{-0.1}\ [13.2\ Pr - 10.16] + 0.9} \qquad (3.6.7)$$

Because the trip is at a distance of 11 trip-heights upstream of the step, it is necessary to enhance the result of Eqn. (3.6.7) by a factor of about 1.4 [8]. The reason, as will be shown graphically in a later chapter, is that the heat transfer coefficient beyond a step (in this case the trip is the step) never approaches the exact flat plate value.

For the back-step experiments of Moss and Baker [9] and Eaton and Johnston [20] all approach profiles are reported, except for the turbulence dissipation, which is obtained from the relationship below.

$$\varepsilon = \frac{k^{3/2}}{\ell_o} \quad , \quad \ell_o = 0.005\ d/2 \tag{3.6.8}$$

Results are not very sensitive to the choice of ℓ_o.

For the pipe expansions of Zemanick and Dougall [39] and Sparrow and O'Brien [41], fully developed turbulent inlet profiles are specified for the velocity and temperature. These are,

$$\frac{u}{U_o} = (1 - 2y/d)^{1/7} \tag{3.6.9}$$

and

$$\frac{T_w - T}{T_w - T_\infty} = (1 - 2y/d)^{1/7} \tag{3.6.10}$$

The profiles for k and ε are obtained by a piecewise linear fit of the data of Laufer [113]. Corresponding to Eqn. (3.6.6) for the flat plate, the friction velocity for fully developed turbulent pipe flow is,

$$u_\tau = 0.04\ U_o^2\ Re_D^{-1/4} \tag{3.6.11}$$

The heat transfer coefficients for the Zemanick and Dougall experiment [39] require calculations of the bulk temperature. It can be easily verified that the inlet bulk temperature is,

$$T_{b_o} = \frac{\int uTdA}{\int udA} = T_w - 0.833\ (T_w - T_\infty) \tag{3.6.12}$$

Presented in this study are correlations of back-step heat transfer coefficients for various Reynolds number. To rule out the effect of approach boundary layer thicknesses on heat transfer, constant momentum boundary layer thickness is assumed for all Reynolds numbers. (In the present study the effect of approach boundary layer thickness on reattachment length is shown to be negligible.) Also, the thermal and momentum boundary layers are assumed to have the same starting length. The momentum boundary layer thickness at the step is assumed to be,

$\delta_u = C\ H$, where C is a constant chosen as described below

(3.6.13)

From turbulent flat plate theory [103], the corresponding starting length is,

$$x_1 = \left[2.6219\ \delta_u \left(\rho U_o/\mu\right)^{0.2}\right]^{1.25} \qquad (3.6.14)$$

Using Eqn. (3.6.2), with $\xi = 0$, $\delta_T(x_1)$ at the step can be obtained. In Eqn. (3.6.13) the values of C examined are $0.4 \leq C \leq 2.0$. For the correlations C is taken to be 1.5. Discussion on the effects of the range of C on heat transfer coefficients is presented in a later chapter.

3.7 Final Remarks

In this chapter closure schemes for the turbulent viscosity and thermal diffusivity terms in Eqns. (3.3.2) - (3.3.4) have been presented together with some theoretical items relevant to the computational process. In the present study of turbulent recirculating heat transfer, approximations of the viscosity by a single mixing length scale proved to be inadequate. Variations and improvements of the k-ε model were then tested. The final calculations, the results of which are to be presented in a later chapter, employ the two-pass procedure with the improved version of the standard k-ε model discussed and the low-Reynolds number form of the model.

Direct application of the relatively complicated "second-order", Reynolds stresses and scalar fluxes closure schemes have not been attempted in this study. It was not necessary because the two-pass method, as seen in a later chapter, adequately predicts heat transfer coefficients for engineering purposes. Also, using the Reynolds stresses and scalar fluxes procedure would require initial conditions for each of the stresses and scalar fluxes. There is a lack of measurements of these correlations for approach boundary layers. Thus, the accuracy of the model cannot be thoroughly tested in the absence of well defined initial conditions. Moreover, engineering applications favor simple

modeling procedures and the present two-pass k-ε calculation is a simpler approach than complete Reynolds stress closure modeling.

In the next chapter the numerical procedures used to solve the set of differential equations, Eqns. (3.3.1) - (3.3.4) and Eqns. (3.4.7) -- (3.4.8), are presented.

CHAPTER IV

COMPUTATIONAL PROCEDURES

4.1 General Remarks

The computational procedure outlined herein is an outgrowth of the TEACH-T program described by Gosman [101]. The program in its original form features a variable, staggered grid arrangement and solves the hydrodynamic equations described in Chapter III by finite differencing procedures based on flux balances. In the present study, a temperature-field solution routine together with improvements upon differencing of the convective terms were incorporated into the code. The flow considered is two-dimensional and the equations are written in generalized cylindrical co-ordinates (x,r) and can be readily converted into Cartesian co-ordinates (x,y) by changing an index in the program.

4.2 Numerical Method

In this present work, attention is focused on solving the full Navier-Stokes and energy equations for steady two-dimensional flows. The numerical procedure used was developed by Gosman and coworkers [10] and is an outgrowth of the SIMPLE procedure of Patankar [95] developed for boundary layer flows. Details of the finite differencing procedures are discussed very thoroughly by Patankar [95,96]; therefore, only a brief overview of the solution procedure is presented herein.

4.2.1 TEACH-T Solution Algorithm with Heat Transfer

The equations in Chapter III, Eqns. (3.3.2) - (3.3.4) and Eqns. (3.4.7) - (3.4.8), can be written generally as,

$$\frac{1}{r}\left[\frac{\partial}{\partial x}(\rho r u\phi) + \frac{\partial}{\partial r}(\rho r v\phi) - \frac{\partial}{\partial x}\left(r\Gamma\frac{\partial\phi}{\partial x}\right) - \frac{\partial}{\partial r}\left(r\Gamma\frac{\partial\phi}{\partial r}\right)\right] - S_\phi = 0 \qquad (4.2.1)$$

where

$$\phi \equiv u,\ v,\ T,\ k \text{ or } \varepsilon$$

and $$\Gamma \equiv \mu_{eff} \text{ or } \Gamma_{eff}$$

In Cartesian coordinates, $r = 1$ and $\partial/\partial r = \partial/\partial y$. S_ϕ is the source term and represents the mechanism for the generation or destruction of ϕ. However, S_ϕ also represents all other terms that cannot be

conveniently expressed by the convection and diffusion terms of Eqn. (4.2.1), for example, the pressure gradient term ($\partial p/\partial x_i$) in the momentum equations. The mass flow rate in Eqn. (4.2.1) must satisfy the continuity equation. This condition is satisfied by updating the pressure solution so that the resulting velocity field satisfies the continuity equation. The solution for the pressure field is discussed later.

The discretized equations are obtained by integrating Eqn. (4.2.1) over a control volume. Figure (6) illustrates the control volumes and grid points used in the TEACH-T program. The control volumes are indicated by the broken lines, and the shaded area represents one such control volume. The grid points are placed at the geometric centers of the control volumes, the solid lines represent the grid lines. This procedure, often referred to as the staggered grid arrangement, aids in numerical stability [101]. Figure (6), for simplicity, shows grid lines of constant spacing; however, in this study non-uniform grid distributions are used. One such distribution is shown in Figure (7). (It should be pointed out that in Figure (7) the magnifications of the vertical and horizontal scales are not of the same order.) This grid distribution is devised to concentrate grid lines near the planes of the walls. As will be discussed later various near-wall grid densities were tested to obtain grid-independent heat transfer

results. Figure (6) also indicates the treatment of the near-wall control volumes; for instance, at a wall grid points are placed at the centers of the control volume faces. The advantage of this procedure is that it allows the treatment of different boundary conditions. For instance, the value of ϕ at the boundary or the flux across the control surface can be conveniently specified.

With the control volumes defined, Eqn. (4.2.2) can be integrated for each control surface. This procedure is exemplified by considering an isolated node point, P, as shown in Figure (8). Eqn. (4.2.1) then becomes,

$$\int_s^n \left[\left(\rho ru\phi - r\Gamma \frac{\partial \phi}{\partial x} \right)_e - \left(\rho ru\phi - r\Gamma \frac{\partial \phi}{\partial x} \right)_w \right] dr$$

$$+ \int_w^e \left[\left(\rho rv\phi - r\Gamma \frac{\partial \phi}{\partial r} \right)_n - \left(\rho rv\phi - r\Gamma \frac{\partial \phi}{\partial r} \right)_s \right] dx$$

$$- \int_V S_\phi \, r \, dr \, dx = 0 \qquad (4.2.2)$$

By having 'J' represent the total convection and diffusion flux in a given direction, and evaluating the integrals by the mean value theorem, Eqn. (4.2.2) reduces to,

$$J_w A_w - J_e A_e + J_s A_s - J_n A_n + \bar{S}_\phi \Delta V = 0 \qquad (4.2.3)$$

Approximation of the fluxes, J_i, in the original TEACH-T code is accomplished by the hybrid differencing schem [95]. In this study, the hybrid differencing scheme is replaced by the quadratic differencing scheme [98]. Both of these differencing schemes, together with the justification for the change, will be discussed in the next two sections. Often the source term contains the variable ϕ, and can be linearized,

$$\bar{S}_\phi = S_C + S_P \phi_P \qquad (4.2.4)$$

where, S_C is the part of $\bar{S}_\phi$ that has no ϕ dependency and S_P is the coefficient of ϕ_P. With these approximations Eqn. (4.2.3) can be discretized [95].

The final discretized equations are only quasi-linear; for instance, the coefficients may depend on values of ϕ and also on other dependent variables. As a result, the final solution is obtained iteratively. Convergence can be attained by a series of iterations. However, in most cases, convergence is not simply obtained as a result of successive iterations; for instance, the values of ϕ may oscillate or diverge. Controlling the changes in ϕ is accomplished by the under-relaxation technique [95]. For example,

$$\phi_P = \phi_P^* + \alpha \text{ [changes in } \phi_P \text{ in the current iteration]}$$

where ϕ_P^* is the value of ϕ_P from the previous iteration. To reduce the change in ϕ_P, α ranges from 0 to 1. Convergence is achieved

when $\phi p = \phi^{*} p$.

What finally remains, is a solution procedure for the resulting set of quasi-linear algebraic equations. A one-dimensional linear discretized set of equations can be solved efficiently by the tridiagonal matrix algorithm [95]. For two-dimensional problems, a line-by-line solution technique [95] incorporating the tridiagonal algorithm is utilized in the TEACH-T code. In this procedure, the equations for all the ϕ values along one grid line are considered, and the neighboring line values of ϕ are subsituted from the best known estimate. One iteration of the line-by-line technique is completed when all the lines in a chosen direction are swept.

The pressure is updated by using the equation of continuity in conjunction with a 'Poisson-like' equation [95]. For instance, the velocity is expressed in terms of pressure (for simplicity looking at only the w-direction of Figure (8)),

$$u_w = u_w^{*} + \frac{\partial u_w}{\partial (p_w - p_p)} (\tilde{p}_w - \tilde{p}_p) \qquad (4.2.5)$$

in which $\tilde{p}$ is pressure correction and the term $\partial u_w / \partial (p_w - p_p)$ is obtained from the solution of the u-momentum equation. The integrated form of the continuity equation is,

$$(\rho u A)_e - (\rho u A)_w + (\rho v A)_n - (\rho v A)_s = 0 \qquad (4.2.6)$$

Substituting for the velocities in Eqn. (4.2.6) by using relationships like that of Eqn. (4.2.5) for u_e, u_w, u_n and u_s result in a discretized equation for the pressure correction. The pressure obtained from solution of this equation is then used to correct the velocities to obtain velocity corrections, $\tilde{u}$ and $\tilde{v}$.

The numerical solution procedure for the TEACH-T code is as follows:

1. Initialize fields for all variables.
2. Assemble coefficients of momentum and energy equations and solve for new variables (u^*,v^*, etc.) by using previous pressure.
3. Solve for p in pressure correction equation.
4. Update all fluid flow variables, i.e., $p = p^* + \tilde{p}$, $u = u^* + \tilde{u}$, etc.
5. Assemble coefficients and solve for all other values, i.e., k, and ε.
6. Test for convergence.
7. If convergence not attained, continue solution procedure from step (2) until convergence is achieved.

In this study convergence of the solution is considered satisfactory when the normalized residuals, R, of each ϕ equation, summed over the entire calculation domain, are smaller than 0.005.

For example, for ϕ=u,

$$R = \frac{\int u \text{ - momentum equation}}{\int \rho\, u_{inlet}\, d\, A} \qquad (4.2.7)$$

In other words, convergence is achieved if Eqn. (4.2.2) is satisfied. In the TEACH-T code there are three basic termination procedures; first, if after 20 iterations and the maximum residual source is excessively large, then it will be impossible to have converged solutions, second, if convergence is obtained and third, if the number of iterations has reached the maximum value specified. In this study, the maximum number of iterations has been set at 400.

As mentioned previously, the TEACH-T computer code in its original form did not include temperature calculations. However, solution of the energy equation, Eqn. (3.3.4) is easily incorporated in the code by mimicking the numerical procedures of say the u - momentum equation. To validate the code initial calculations were performed for laminar heat transfer over a flat plate and more recently, in as yet unreported work by the Department of Mechanical Engineering, Howard University, for laminar heat transfer flows over a cavity.

4.2.2 TEACH-T Hybrid Differencing Scheme

The hybrid differencing procedure used in the solution algorithm is discussed in detail by Patankar [95]. This procedure uses both the central and upwind differencing schemes. Approximations for the convective terms in the transport equations are as follows: for face-Peclet number, Pe, ($\rho u_i \delta x_i / \Gamma$, convective to diffusive transport) less than 2, central differencing approximations are used and for face-Peclet number greater than 2, upwind differencing approximations are used. The diffusion terms are calculated by central differencing approximations.

From Figure (8), central differencing of ϕ_e is the average of ϕ_E and ϕ_P, and upwind differencing uses,

$$\phi_e = \phi_P \quad , \text{ for } u > 0$$

$$\phi_e = \phi_E \quad , \text{ for } u < 0$$

By using the above approximations differenced equations can be obtained, as presented below. Central differencing of the diffusion term is,

$$\left.\frac{\partial^2 \phi}{\partial x^2}\right|_i = \frac{\phi_{i+1} - 2\,\phi_i + \phi_{i-1}}{(\Delta x)^2} \qquad (4.2.8)$$

And the convection term is,

$$u \left.\frac{\partial \phi}{\partial x}\right|_i = u \left[\frac{\phi_{i+1} - \phi_{i-1}}{2\Delta x}\right] ; \quad Pe < 2 \qquad (4.2.9)$$

$$u \left.\frac{\partial \phi}{\partial x}\right|_i = u \left[\frac{\phi_i - \phi_{i-1}}{\Delta x}\right] ; \quad u > 0, \; Pe > 2 \qquad (4.2.10)$$

$$u \left.\frac{\partial \phi}{\partial x}\right|_i = u \left[\frac{\phi_{i+1} - \phi_i}{\Delta x}\right] ; \quad u < 0, \; Pe > 2 \qquad (4.2.11)$$

Leonard [98] showed that for convection dominated flows the hybrid procedure is only marginally superior to pure upwind differencing. He further demonstrated that the hybrid procedure severly restricts the grid densities (spacings), consequently, limiting the numerical accuracy, and also that the upwind differencing scheme is a main source of numerical diffusion. To eliminate some of these discrepancies Leonard [98] proposed the quadratic differencing scheme.

4.2.3 New Quadratic Differencing Scheme

The quadratic scheme of Leonard [98] seeks to combine the accuracy of the central difference scheme with the stability property of the upwind scheme. Rather than using the linear interpolation scheme of the central difference procedure, a

parabolic polynomial interpolation scheme is employed. The control volume surface values are obtained by fitting a parabola to the values of ϕ at three consecutive nodal positions. two located on either side of the face considered and the third located at the next node in the upstream direction. As such, consideration of all the faces for a point P, as in Figure (8), would require a 9-point star scheme in which the sign of all the face velocities must be taken into consideration. The quadratic approximations for say face 'e' (Figure (8)) are as follows [98]:

$$\phi_e = \frac{1}{2}(\phi_i + \phi_{i+1}) - \frac{1}{8}(\phi_{i-1} + \phi_{i+1} - 2\phi_i), \; u_e > 0 \qquad (4.2.12)$$

$$\phi_e = \frac{1}{2}(\phi_i + \phi_{i+1}) - \frac{1}{8}(\phi_i + \phi_{i+2} - 2\phi_{i+1}), \; u_e < 0 \qquad (4.2.13)$$

Similar expressions can be written for the other three faces. In Eqns. (4.2.12) and (4.2.13), the first bracketed terms represent the linear central differencing approximations, and the second bracketed terms represent the correction of ϕ by upstream weighted curvatures. Direct application of Eqns. (4.2.12) and (4.2.13) into the TEACH-T code (described previously) led to an increase in the number of iterations needed for convergence by as much as 100 percent. This is probably due to the loss of diagonal dominance as a result of the extra terms in the quadratic differencing

procedure. Increasing the rate of convergence is accomplished by grouping the quadratic (curvature) terms like those in Eqns. (4.2.12) and (4.2.13) with the source term S_ϕ of Eqn. (4.2.1) and then splitting up the source term and grouping a part of it with the coefficient of ϕ_p. This procedure is outlined for $\phi = \varepsilon$, Eqn. (3.4.8) for the standard k-ε model, in which S_ε is,

$$S_\varepsilon = -C_{\varepsilon 1} \frac{\varepsilon}{k} u_t G + C_{\varepsilon 2} \rho \frac{\varepsilon}{k}^2 + \text{Quadratic corrections}$$

Splitting S_ε,

$$S_\varepsilon = S_\varepsilon' + S_\varepsilon''$$

in which,

$$S_\varepsilon' = C_{\varepsilon 2} \rho \frac{\varepsilon^2}{k} + \text{Quadratic corrections}$$

and

$$S_\varepsilon'' = -C_{\varepsilon 1} \frac{\varepsilon}{k} \mu_t G$$

The final discretized equation for the n^{th} iteration for point P (Figure (8)), from Eqn. (4.2.3) is,

$$\left(C_p + S_\varepsilon' \right)^{(n-1)} \varepsilon_p = C_E \varepsilon_E^{(n-1)} + C_W \varepsilon_W^{(n)}$$

$$+ C_N \varepsilon_N^{(n)} + C_S \varepsilon_S^{(n-1)} + S_\varepsilon''^{(n-1)}$$

Similar expressions are obtained for the other ϕ - values.

In the present study, initially quadratic differencing

was only applied to the momentum and energy transport equations. This was because the recent study of Leschziner and Rodi [63] has shown that solutions of k and ε are insensitive to the discretization scheme, particularly in the high shear regions bordering recirculating zones. However, in order to obtain grid independent solutions, grid refinements were necessary in the near-wall region; for instance, about a 10 percent increase over what was needed when all the transport equations incorporate the hybrid difference scheme. Recently, by extensive numerical experimentations, Han, Humphrey and Launder [100] showed that for grid distributions less than (22 x 22) in cavity driven flows, quadratic differencing approximations, for the convective terms should be used for all variables. As a result, subsequent calculations in this study did incorporate quadratic differencing in all of the transport equations. With this procedure grid independent solutions were very easily obtained with about a (25 x 28) grid distribution.

As a final remark, some of the advantages gained by using the quadratic differencing procedure have been demonstrated by Leonard [98]. The list below represents a brief summary of Leonard's [98] study, where quadratic differencing of the convective terms results in:

(i) Reduction of the presence of false diffusion.

(ii) More stability at high Peclet numbers.

(iii) Less grid-dependent solutions than the upwind scheme.

As a result of the above conclusions this improved scheme is much more realiable in testing the validity of turbulent models.

4.3 Treatment of Boundary Conditions

In order to avoid an excessively fine grid at a wall, functional relationships are specified to describe the rapidly varying quantities in the wall region. The procedure of obtaining these functions are two fold: the values for some variables (e.g., u,v,T) at the nodes adjacent to the wall (near-wall nodes) are directly obtained from 'wall-function' relations, and where 'wall-function' approximations are not strictly valid, approximate solutions of the transport equations for the other variables (e.g., k and ε) are solved in the near-wall region. In this study, as mentioned previously, two forms of the k-ε model are employed in a two-pass procedure. The standard model is applied to the entire flow field in a first pass procedure to establish the recirculating zone, and in a second pass the standard model is maintained up to reattachment and the low-Reynolds number version is applied downstream of reattachment. The boundary conditions for each model require slightly different treatments, consequently in the following sub-sections each procedure is analyzed separately.

4.3.1 Single Pass Procedure

The standard k-ε model, is discussed in Chapter III, is valid for regions outside the buffer zone (Figure (C2)) where the flow is fully turbulent. Beyond this region, $13 < y^+(u_\tau y/\nu) < 250$, is the 'log-law region' (Figure (C2)), and in this region

functional relations are assigned to the velocities and temperature [58]. These relationships, often referred to as 'wall-functions', are approximate solutions of the transport equations. The functional relationships for the entire near-wall region (Figure (C2)) for momentum and energy transfer are obtained by integrating the governing boundary layer transport equations in each region with the appropriate assumptions applied. The procedure is briefly described below and in Appendix (C) the mathematical procedure is carried out for the u-momentum equation. In the linear sublayer, $y^+ < 5$, the flow is assumed laminar and the solution of the Navier-Stokes and energy equation is obtained by assuming the shear-stress (and heat flux) is constant throughout this region. This results in,

$$u_i^+ = x_i^+ \tag{4.3.1}$$

$$T^+ = x_i^+ \tag{4.3.2}$$

in which $u^+ \equiv u_i/u_\tau$

$$x^+ \equiv x_i u_\tau / \nu$$

and

$$T^+ \equiv (T_w - T)/T_\tau$$

where

$$T_\tau \equiv \dot{q}_w''/\rho c_p u_\tau$$

In the buffer region, $5 < y^+ < 13$, both laminar and turbulent shear stresses (and scalar fluxes) are important, so approximate solution

of the wall layer transport equations results in an integral equation. In the log-wall region, $13 < y^+ < 250$, the flow is assumed fully turbulent, and the Boussinesq approximations of Chapter III are applied. Solution of the transport equations result in,

$$u_i^+ = \frac{1}{\kappa} \ln x_i^+ + C, \quad \kappa = 0.42 \tag{4.3.3}$$

$$T^+ = \frac{1}{\kappa} \ln x_i^+ + D \tag{4.3.4}$$

In the TEACH-T code the boundary conditions are expressed through wall shear stress and heat flux. For the standard k-ε model the 'wall-function' relations are summarized below, and they are those proposed by Launder and Spalding [58]. These relationships are modifications of the boundary layer results (presented above) so as to reflect the presence of recirculating flow.

(i) Mean velocity: the wall shear stress,

$$\tau_w = \rho_w u_p C_\mu^{\frac{1}{4}} k_p \frac{\kappa}{\ln (E y_p^+)}, \quad E = 9.8 \tag{4.3.5}$$

where subscripts 'w' and 'P' refer to values at the wall and a point P close to the wall. The point y_p^+ is established by the value of y_p,

$$y_p^+ = \frac{y_p}{\nu} \left(C_\mu^{\frac{1}{2}} k_p \right)^{\frac{1}{2}} \tag{4.3.6}$$

In this study $y_p^+ \simeq 15$ for most cases.

(ii) Mean Temperature: the heat flux,

$$\dot{q}_w'' = \frac{(T_w - T_p)\ \rho\ c_p\ C_\mu^{\frac{1}{4}}\ k_p^{\frac{1}{2}}}{Pr_t\left[u^+ + P(Pr)/Pr_t\right]} \qquad (4.3.7)$$

The function P(Pr) has been modeled by Jayatilleke [114],

$$\frac{P(Pr)}{Pr_t} = 9.24\left[\left(\frac{Pr}{Pr_t}\right)^{\frac{3}{4}} - 1\right]\left[1 + 0.28\ \exp\ (-0.007\ \frac{Pr}{Pr_t})\right]$$

Specification of Pr_t, in the near-wall region, has been presented in Section (3.4.1).

(iii) Turbulent kinetic energy,

kp is calculated from the differential equation (Eqn. (3.4.7)) with the assumption that the diffusion of energy to the wall is zero. With this assumption Eqn. (3.4.7) reduces to,

$$\frac{d}{dy}\left(\frac{\mu_t}{\rho\sigma_k}\frac{dk}{dy}\right) + \mu_t\ G - \rho\varepsilon = 0 \qquad (4.3.8)$$

The dissipation rate of turbulent energy in Eqn. (4.3.8) is approximated as,

$$\int_0^{y_p} \varepsilon\ dy = C_\mu\ \frac{k_p^{\frac{3}{2}}}{\kappa}\ \ell n\left[\frac{E\ y_p\ C_\mu^{\frac{1}{4}}\ k_p^{\frac{1}{2}}}{\nu}\right]$$

(iv) Dissipation rate of Turbulent energy,

$$\varepsilon_p = C_\mu^{\frac{3}{4}} k_p^{\frac{3}{2}} / (\kappa y_p) \qquad (4.3.9)$$

The above relations describe wall functions for the horizontal wall, the obvious modifications are made for the vertical walls.

4.3.2 Two-Pass Procedure

Figure (5) illustrates the solution domains for each model during the second calculation. In implementing the low-Reynold number procedure from the reattachment point, the calculation proceeds to the wall with grid lines placed inside the linear sublayer. This creates an upstream boundary for the low-Reynolds number solution in the sublayer at the vertical plane through the reattachment point. Boundary conditions along this plane for momentum and energy in this region are $u^+=y^+$ and $T^+=y^+$ (as discussed in the previous section). The boundary condition for the turbulent variable k is obtained by integrating its near-wall transport equation and ε is obtained by empirical formula directly from k, as outlined in the previous section.

The boundary conditions for the entire flow field during the second pass are summarized in Table (4.1).

TABLE 4.1

SUMMARY OF INLET AND BOUNDARY CONDITIONS

Variable	Inlet Plane	Exit Plane	At Walls	Free Stream (Symmetry) Plane	Upstream vertical plane through reattachment point for Low-Reynolds number model
u	Prescribed from Experiment or Simulated	Satisfies Continuity Equation, $\frac{\partial u}{\partial x} = 0$	τ_w specified (base wall)	Flux Condition, $\frac{\partial u}{\partial y} = 0$	Linear Sublayer approximation $u^+ = y^+$
v	0	Satisfied Continuity Equation, $\frac{\partial v}{\partial x} = 0$	τ_w specified (side wall)	Flux Condition, $\frac{\partial v}{\partial y} = 0$	$v^+ = 0$
T	Simulated	Flux Condition, $\frac{\partial T}{\partial x} = 0$	$\dot{q}''$ specified (both walls)	Flux Condition, $\frac{\partial T}{\partial y} = 0$	Linear Sublayer approximation $T^+ = y^+$
k	Prescribed by Experiment or Curve fitted	$\frac{\partial k}{\partial x} = 0$	Prescribed from k transport Equation or $k = 0$	Flux Condition, $\frac{\partial k}{\partial y} = 0$	Prescribed from k transport equation
ϵ	Obtained from k profile or Curve fitted	$\frac{\partial \epsilon}{\partial x} = 0$	Prescribed from ϵ transport Equation or $\epsilon = 0$	Flux Condition, $\frac{\partial \epsilon}{\partial y} = 0$	Obtained empirically from k transport Equation

CHAPTER V

PREDICTIONS OF TURBULENT RECIRCULATING HEAT TRANSFER

5.1 General Remarks

The turbulent models described in Chapter III, together with the computational procedures of Chapter IV, are examined by application to the two-dimensional back-step and the pipe expansion geometries where experimental data exist. In addition to the heat transfer experiments of Aung and Goldstein [8], Zemanick and Dougall and Sparrow and O'Brien [41] (which did not include detailed hydrodynamic measurements), flow field comparisons are made with the pure hydrodynamic measurements of other investigators [9,20].

All calculations are performed with air as the working fluid. The values of the fluid properties of air, such as density (ρ), dynamic viscosity (μ), specific heat at constant property (C_p) and molecular Prandtl number (Pr) are taken from Eckert and Drake [115]. In the back-step experiments of Aung and Goldstein [8], the walls are heated to uniform temperatures. The difference between free stream and wall temperature is 18°C. For the pipe expansion of Zemanick and Dougall [39], the wall temperature distribution is given in Zemanick [116]. For the pipe expansion results of Sparrow and O'Brien [41] obtained from napthalene sublimation measurements, the wall temperature is taken as the sublimation temperature of napthalene. For the back step calculation the Reynolds number is

based on the mean inlet velocity and step height and for the pipe expansion it is based on mean inlet velocity and downstream pipe diameter.

Figure (4) shows the schematics of the two-dimensional back-step and sudden pipe expansion geometries considered in this study. The point y = 0, for the back-step is at a location well outside the approach boundary layer, and for the pipe expansion it is located at the symmetry axis. Table (5.1) lists the actual dimensions used in the various numerical and physical experiments. In this table all distances are in centimeters, the distance X/H (in terms of step or expansion height) represents the final station at which measurements were taken and the expansion ratio d/D, for the back-step, represent the actual dimensions of the upper grid boundary used in the present numerical study.

The results presented in this chapter are obtained by solving the system of equations of Chapter III by the numerical procedures of Chapter IV. For a better appreciation of the tasks involved in the present study, initial calculations are presented (mainly for the back-step geometry) justifying the need for the various improvements and modifications implemented during the development of this research. Following this overview, detailed flow, temperature and turbulence intensity fields and heat transfer calculations obtained with the two-pass procedure incorporating

TABLE 5.1

PHYSICAL DIMENSIONS CONSIDERED IN TEST CASES

Geometry	Experimenters	H	d/2	d/D	x/H	Re
Back Step	Aung and Goldstein [8]	0.04	2.5H	0.71	11	6.3×10^{2} -1.7×10^{3}
Back Step	Moss and Baker [9]	7.6	2.0H	0.67	9	5×10^{4}
Back Step	Eaton and Johnston [20]	5.08	2.2H	0.688	12	3.4×10^{4}
Pipe Expansion	Zemanick and Dougall [39]	0.673	0.508	0.43	18	4×10^{3} -5×10^{4}
		0.5428	0.8372	0.54	18	4×10^{3} -7×10^{4}
Pipe Expansion	Sparrow and O'Brien [41]	2.54	2.54	0.5	Not Applicable	5×10^{3} -4.5×10^{3}

improvements to the model and code (as discussed earlier) are presented. Table (5.1) lists the geometries considered for which comparisons between the present numerical calculations and experimental measurements are made.

Before proceeding directly to the presentation of the numerical results, a few general comments regarding the calculation procedures are presented. For most of the calculations in the standard k-ε model $y_p^* \simeq 15$. For a single (first) pass with quadratic differencing, a typical non-uniform grid distribution used is (25 x 28), convergence is obtained after about 250 iterations with central processor times on an IBM 3033 Processor Complex averaging about 4 minutes. In the second pass, in the redeveloping region the number of horizontal grids are increased to about 32. In early calculations, using hybrid differencing with the standard k-ε model, a typical non-uniform grid used was (28 x 32), and convergence was obtained after about 190 iterations. Grid independence of results, in the present study was verified for all test cases. Figure (9) illustrates the verification procedure for the back-step experiments of Aung and Goldstein [8]. Nusselt number at one location is plotted as a function of y-grid densities. The x/H location chosen is purely arbitrary, for most cases a value just downstream of the reattachment point is chosen. The first point on Figure (9) corresponds to 15 y-grids uniformly

spaced across the channel. All the other points correspond to non-uniform grid densities, with a higher concentration of grids in the near-wall region. As the number of horizontal grid densities are increased from 20 y-grids to about 35 y-grids, but keeping the near-wall grid location the same so as to maintain the y_p^+ condition, the Nusselt number increases slightly. Beyond 30 y-grids the changes is less than about 2 percent. In most of the present calculations the number of y-grids used is about 30. A similar verification procedure was also adopted for the x-grid densities.

Typical grid distributions used in the present study for both the back-step and pipe expansion geometries are shown in Figures (7) and (10), for a single and double pass, respectively. The grid distribution shown in Figure (7) is arranged such that for the entire calculation domain the near-wall nodes are outside the viscous sublayer. Typical near-wall distances are shown in the figure. This procedure is necessary (as discussed previously) when using the standard k-ε model in a single pass. Upon establishing the reattachment length by the previous single-pass procedure, a typical grid distribution, as that shown in Figure (10), is then employed for the second pass. The figure also shows near-wall nodes outside the viscous sublayer for the side wall and up to the reattachment point, x_R, for the bottom wall, again consistent with

the computational domain for the standard k-ε model. Beyond reattachment, at the very next downstream node, grid points are placed close to the wall, inside the viscous sublayer, and the solution procedure utilizes the Low-Reynolds number version of the k-ε model. The initial and boundary conditions described in Table (4.1) are applied at the following locations: initial conditions at the plane x = 0, boundary conditions at the near wall nodes, free stream (or symmetry) conditions at the plane y = 0, exit conditions along the plane x = NI and upstream condition for the Low-Reynolds number model along the plane $x = x_R$.

A brief discussion concerning the dependency of reattachment length with Reynolds number and step height is now presented for the back-step geometry. For turbulent flows reattachment length is independent of Reynolds number. However, for laminar and transitional flows there is a significant Reynolds number dependency. Initially (laminar regime), reattachment length increases sharply with an increase in Reynolds number, and reaching a maximum (in the transitional regime) then gradually decreasing to a fairly constant value. Figure (11) illustrates the effects of Reynolds number (based on momentum thickness at the step), on reattachment length for laminar, transitional and turbulent regimes. The experimental data points are that of Eaton and Johnston [20] and the solid line joins the experimental points.

Initial calculations were performed using three different step heights to examine the effects of step heights on reattachment lengths. Figure (12) illustrates that x_R/H remains constant with H. These results were obtained by using the original standard k-ε model (i.e. no modifications to C_μ). However, the same constant behavior is expected when using the improved model, the only difference lies in the magnitude of the reattachment length.

5.2 Initial Results (Single Pass)

Initial calculations were performed for the two-dimensional back-step and pipe expansions by incorporating both the mixing length and standard k-ε models. For the k-ε model C_μ was assumed a constant value of 0.09 and Pr_t approximated by Eqn. (3.4.2). Approach and boundary conditions used have been discussed previously. Presented here is a summary of typical initial heat transfer results for the back-step in which Nusselt number (normalized by its value just upstream of the step) is plotted at various downstream distance (normalized by step height) for a Reynolds number (based on step height) of 1728.4. More extensive standard k-ε results obtained in the present research including hydrodynamic and turbulence flow field predictions are presented in Ref. [106]. In results to be presented here for the initial calculations comparison is made between numerical prediction and experimental data of Aung and Goldstein [8] for their highest Reynolds number case. Figure (13) shows results obtained from the initial calculations in which the mixing length model was employed. It is apparent from the figure that this simple model consisting of a single turbulence scale does not account for the complex turbulence phenomena, particularly in the recirculating region. This is evident by the comparitively small values of heat transfer obtained when using the mixing length model. Figure (14) shows

heat transfer results obtained for the same case by the standard k-ε model. With this model, the predictions consistently overestimate the experimental data particularly in the redeveloping region. However, the overall agreement is fairly satisfactory considering the inherent 'simplicity' of the k-ε model. The constraints on the choice of the near wall grid line in these calculations, as discussed previously, are that it must lie outside the linear sublayer and yet, be close enough to the wall, particularly for heat transfer calculations, to provide accurate resolution of the flow in the near-wall region. For most of the present calculations y_p^+ averages about 15, which is the approximate average value in the recirculation zone.

Since the Reynolds numbers of the present flow calculations for the step are comparatively low, the physical distance of y_p^+ from the wall is large and therefore resolution of the details of the near-wall flow is not possible. In an attempt to improve the results by increasing resolution near the walls the low-Reynolds number form of the model was employed for the entire region downstream of the step. A typical result obtained by utilizing this model is shown in Figure (15). The heat transfer results underestimate the data for the recirculating region, but fairly good agreement is obtained for the redeveloping region. This behavior is understandable since the justifications of the

low-Reynolds number terms in this model was based on studies with accelerated boundary layer type flows [60]. Such a model was needed for it yielded an additional improvement by permitting resolution of the near-wall region downstream of reattachment. This is extremely important when a local extremum in the velocity profile occurs near the wall as is the tendency in the present cases. The results obtained by the standard k-ε model and the low-Reynolds number model indicate that the standard model gives better overall prediction in the recirculation zone and that the low-Reynolds number model is better for the redeveloping region. The two-pass procedure exploits this phenomena. However, the feasibility of such a procedure would depend on the reliability of predicting reattachment lengths. This is accomplished by incorporating various improvements in the standard k-ε model especially. Results utilizing these improved models are discussed in the next section.

To yield overall better predictions of heat transfer results another variation of the model was tested. This is discussed in Section (3.4.3) with the additional term to the ε-equation given by Eqn. (3.4.9). This procedure is often referred to as the 'sensitivity' correction of Hanjalic and Launder [62]. Results obtained by this procedure are shown in Figure (16). Again, no substantial improvement in heat transfer results are obtained.

Predictions of flow field variables by the two-pass procedure will be presented in a later section. All of the above calculations (except for the mixing length model) yield reattachment lengths of about 4.5 step-heights downstream of the step, with the maximum (peak) value of Nusselt number occuring about one step-height upstream of reattachment. (Reattachment lengths obtained by the various procedures are summarized in the next section). The value of 4.5 is consistent within the range of values obtained experimentally by Aung and Goldstein [8] for a tripped approach boundary layer. However, the models in their present form underestimate the reattachment length for all the other test cases considered. This phenomenon is also discussed in detail in the next section.

5.3 Improved Results (Single Pass)

As discussed in Chapter III the standard k-ε model and the low-Reynolds number form of the model were improved in the present work by functionalizing C_μ and Pr_t through Eqns. (3.4.36) and (3.4.37), respectively. These (and all subsequent) calculations incorporated quadratic approximations for the convective terms, as discussed previously. Figure (17) compares the heat transfer coefficients obtained by the quadratic and by hybrid differencing schemes. The quadratic procedure yields slightly improved predictions of heat transfer for the recirculating region. However, improvements in predictions of reattachment lengths are more significant and further the scheme requires lower near-wall grid densities for grid independent solutions, as indicated on the figure.

Figure (18) compares heat transfer obtained by both the present improved standard k-ε and low-Reynolds number models. The trend is the same as discussed previously. For instance, the standard model and low-Reynolds number form of the model better represent the flow in the recirculating and redeveloping regions, respectively, thus, re-emphasising the need for the two-pass procedure. Figure (19) shows similar heat transfer results, but for a different value of Reynolds number.

In an attempt to yield better overall heat transfer

predictions for the entire region by the improved standard k-ε model, without resorting to the two-pass procedure for which results are described later, the 'sensitivity' correction of Leschziner and Rodi [64] were tested. In this procedure to the ε-equation an additional term is introduced, as given by Eqn. (3.4.10). Results obtained by this procedure are shown in Figure (20). Again, no substantial improvement in heat transfer results for the redeveloping region are obtained.

Heat transfer results for the pipe expansion case (for a Reynolds number of 66,260) by the improved standard k-ε model is presented in Figure (21). Also indicated on the figure are the experimental data of Zemanick and Dougall [39]. Again predicted results are larger than experimental ones.

The two-pass procedure described in Chapter III requires partitioning of the flow field into two regions: recirculating and redeveloping regions. Consequently, the applicability of the procedure relies on the accuracy and consistency to which the reattachment length can be predicted. It is for this reason that various numerical experiments were undertaken with emphasis on reliable predictions of reattachment lengths. Table (5.2) summarized reattachment lengths obtained by the various turbulent approximation procedures discussed previously. In the table, the expression "partially improved C_μ" refers to exclusion of

TABLE 5.2

SUMMARY OF REATTACHMENT LENGTHS OBTAINED BY THE VARIOUS MODELING PROCEDURES

Geometry	Experimental Values of x_R/H	Mixing length Model	Present Predictions of x_R/H				
			Standard k-ε Model				
			$C_\mu = 0.09$	Partially Improved C_μ	Fully Improved C_μ	'Sensitized' ε- Eqn. (Eqn. 3.4.10)	Simulation of Trip Conditions at Step With Fully Improved C_μ
Back Step	4.5 - 5.0 [8]	9.1	4.5	5.2	5.8	6.0	5.3
Back Step	5.7 - 6.0 [9]	—	4.9	5.3	6.0	—	—
Back Step	7.97 [20]	—	5.1	5.9	7.5	—	—
Pipe Expansion	6 - 9 [39]	—	6.4	7.1	8.4	—	—

wall-damping corrections and imposing the equilibrum of turbulence energy assumption in the derivation of the function for C_μ, i.e., $\Lambda'' = 0$ and $P/\varepsilon = 1$ in Eqn. (3.4.36). Fully improved C_μ refers to Eqn. (3.4.36). The results indicate that by employing the fully improved expression for C_μ in the standard k-ε model (together with quadratic differencing for the convective terms) yields reattachment lengths that are consistent with experiments, except for the Aung and Goldstein [8] case. However, the reason for the over-prediction is explainable. In their experiments the boundary layer trip was located at eleven trip-heights upstream of the step, which results in a higher level of turbulence intensity at the step. In order to gain some appreciation for the magnitude of this effect, a numerical experiment was conducted by using the improved k-ε model to perform a turbulent back-step flow field calculation with the step height taken as the height of the trip. The results then were examined to obtain quantitative estimates of the level of k and ε at 11 trip heights downstream. These values were then used as upstream condition input for the regular back-step calculation in lieu of the method described earlier.

Although the effect on heat transfer of the higher level of turbulence is slight, as shown in Figure (22), the reattachment length is reduced, and essentially comparable with the experiment. The reattachment length obtained is indicated in the last column of

Table (5.2). Since there remains some questions of whether or not the physics are really improved by this method of obtaining upstream conditions and also as to whether or not heat transfer results using it are actually in closer agreement with experiment, it was not adopted for the final calculations.

5.4 Improved Results (Two-Pass)

The two-pass method was the procedure which as previously indicated gave the best overall prediction of heat transfer. In applying it during the first pass, calculations are performed according to the previous section to obtain the reattachment length. Specifically, for the best results, the first pass employed the improved standard k-ε model, with C_μ and Pr_t given by Eqns. (3.4.36) and (3.4.37), respectively. For the second pass, the above procedure is maintained up to reattachment, and beyond reattachment the improved low-Reynolds number form of the model is used with C_μ and Pr_t given by Eqns. (3.4.38) and (3.4.39), respectively.

5.4.1 Results for Back-Step

Before presenting the heat transfer predictions from the two pass method, the hydrodynamic and turbulence flow field predictions are discussed. The purpose is to illustrate that although the emphasis of the present study is on heat transfer, the present procedure reliably predicts the other turbulent flow field variables as well. Typical computed velocity profiles for two different experimental cases are shown in Figure (23) and (24). As can be seen, the agreement between the experimental data and present predictions is good. Figures (25) and (26) represent cross-stream pressure variation and surface pressure coefficient

downstream of the step, respectively. In the recirculating region, the pressure is not uniform, as is expected, but approaches a uniform value in the redeveloping boundary layer. Figure (27) is a comparison of computed temperature profiles for one Reynolds number with the corresponding data of Aung and Goldstein [8] and is typical of the agreement of results at the other two Reynolds number as well. Figure (28) and (29) compare mean velocity and temperature profiles in the reattached boundary layer with their universal 'log-wall' functions. The computed slopes deviate slightly from that of the universal slopes. This is typical of a reattached boundary layer [8,25]. Figures (30) and (31) depict the computed behavior of turbulent kinetic energy. Figure (30) shows the profiles at selected streamwise locations; the experimental data points represent $\overline{u'^2}$ only. The same qualitative trend is observed in the figure between the prediction's and the experiment, and further in the recirculating region k is about 40 percent higher than $\overline{u'^2}$ [25], since in this region all three components of the Reynolds stresses are important. Figure (31) is a plot of the streamwise variation of the maximum (peak) value of k and the experimental data points are the total k values. As can be seen that the agreement between predictions and experimental data is again very good.

A comparison of the streamwise variation of the computed

heat transfer coefficients with the experimental data of Aung and Goldstein [8] is given in Figures (32) through (34). The overall agreement is acceptable. Figure (32) summarizes the results obtained by the improved procedure with a single pass only and the two-pass procedure.

5.4.2 Results for Pipe Expansion

Heat transfer results for three pipe expansion cases are plotted in Figures (35) through (37). The results of previous k-ε calculations by Chieng and Launder [59] together with the experimental data of Zemanick and Dougall [39] are also shown for comparison. In the recirculating region the Nusselt number obtained by the present improved standard k-ε model differs significantly from that obtained by Chieng and Launder [59]. The reasons for this difference are that Chieng and Launder [59] in their calculations assumed constants for both C_μ and Pr_t and more importantly, their calculations proceeded from the buffer zone. Starting the solution inside the buffer zone is only possible by specifying k and ε for this region. Early attempts were made in the present study to incorporate the Chieng and Launder [59] functions valid for the buffer zone [106]. However, for some unresolved reason the predictions obtained did not correspond with the results of Chieng and Launder [59]. It is obvious that the results from the present two-pass procedure are a marked

improvement over the Chieng and Launder [59] calculations and also are in reasonably good agreement with experimental results in the entire flow field.

Figure (38) shows the maximum (peak) Nusselt number dependence on Reynolds number. The predictions exhibit a slightly greater sensitivity to Reynolds number than do the measurements. This slight difference is insignificant when considering the range of Reynolds number studied. The predicted maximum Nusselt number is represented by the following expression.

$$(Nu)_{max} = cRe_H^{0.75}, \quad c = 0.145$$

5.5 Downstream Face Heat Transfer

Figure (39) shows the side-wall heat transfer coefficient for the back-step for two Reynolds numbers. The Nusselt number is normalized by its average value and the horizontal axis is normalized to vary from 0 to 1, the former corresponding to a point adjacent to the opening and the latter to a point where the side-wall meets the horizontal wall. The results obtained (though not possibly evident from the figure) indicate that the Nusselt numbers are very small compared to say the base wall (about 10 percent of base-wall value). The highest heat transfer occurs on the portion of the side-wall adjacent to the main flow and the lowest occurs in the corner region. No experimental data are available for comparison.

Figure (40) through (42) show similar predicted results of heat transfer coefficients for three Reynolds number for the downstream face of a pipe expansion. Comparison is made with the experimental data of Sparrow and O'Brien [41]. Agreement with the experiment is better for the larger Reynolds numbers. This observed phenomena can be explained by the fact that in the region adjacent to the downstream facing wall the improved standard k-ε model is used; and, as mentioned previously, the near-wall resolution of this model, particularly for low-Reynolds numbers, is severly restricted. Figure (43) shows the dependence of the

a verage Nusselt number on Reynolds number, the growth law is essentially the same as that of the experimental data. The predicted growth law is represented by the following expression.

$$(Nu)_{side} = cRe_H^{0.69}, \quad c = 0.057$$

5.6 Correlations of Back-Step Heat Transfer

Results related to correlations of heat transfer coefficients are presented in Figures (44) through (48) for the back step geometry. All calculations were performed by assuming, at the step, an untripped turbulent boundary layer having a heated starting length. Also, the same momentum thickness for the incident boundary layer is assigned to all Reynolds numbers. This is not too damaging an assumption because the heat transfer coefficients beyond the step are fairly independent of approach boundary layer thicknesses. This is demonstrated in Figure (44) for three different approach boundary layer thicknesses. The region that shows the greatest sensitivity of heat transfer coefficients to different approach boundary layer thicknesses is the region bordering the reattachment point.

Figure (45) is a logarithmic plot of Nusselt number, $Nu_{\bar{x}}$, based on distance $\bar{x}$, downstream of reattachment versus Reynolds number, $Re_{\bar{x}}$, for five Reynolds number cases. The flat plate turbulent boundary layer theory for heat transfer is also shown for comparison. The computed results all tend to the 0.8 power growth law of the flat plate relation sufficiently far downstream of the step. Here this occurs between 10 to 13 step heights downstream of the step. These results demonstrate the fact that the flat plate boundary layer theory based on distance downstream of reattachment

cannot be used to predict the heat transfer in the redeveloping boundary layer region. Even at significant distances downstream where the same power law behavior is followed, it will always tend to underestimate the heat transfer rate. In the present predictions, the computed results exceed the flat plate theory by factors ranging from 1.3 to 1.8.

Figures (46) and (47) show the dependence of the maximum (peak) and side-wall Nusselt numbers with Reynolds numbers, respectively. This power law dependence, for convenient reference purposes, is summarized in Table (5.3) and should be of use to the designer. The power law behavior for the maximum Nusselt number is used in an attempt to correlate the distribution of heat transfer coefficients for design purposes. This result is presented in Figure (48). Figure (48) presents results for $Nu\ Re^{0.68}$ versus x/H, where the exponent 0.68 represents the power law dependence of the maximum Reynolds number. Also plotted on the figure are the experimental data of Aung and Goldstein [8]. The data points fall within the expected range, except for the peak values. This is probably due to the slight influence of the difference in approach boundary layer thicknesses on heat transfer coefficients. The graphs of Figures (46) through (48) can be used with some confidence to predict back-step heat transfer coefficients with accuracy sufficient for most design purposes, within the range of

TABLE 5.3

CORRELATION OF MAXIMUM (PEAK) AND AVERAGED (FOR DOWNSTREAM FACE) NUSSELT NUMBER WITH REYNOLDS NUMBER FOR BACK STEP

$Nu = c\,Re_H^m$		
Quantity	m	c
$(Nu)_{max}$	0.68	0.1066
$(Nu)_{side}$	0.55	0.0839

Reynolds number considered. As a final comment, the results shown in Figures (46) through (48) are very restrictive in the sense that they represent heat transfer coefficients for a constant step-height (H) of 0.64 cm. and a constant approach boundary layer thickness of 1.5H. Future studies to be undertaken will examine the effects of step-height on heat transfer coefficient beyond the step.

5.7 Discussion of Results

The present results indicate that using the usual two-equation models of turbulence (standard and low-Reynolds number form with C_μ a constant) yields unacceptable predictions of reattachment lengths and heat transfer coefficients for the entire flow field downstream of a sudden change in geometry. A great improvement in results are obtained by using the improved versions of the two-equation models in the two-pass procedure. Comparison of computed results with experimental results, and with calculations of previous investigators indicate that at moderate Reynolds number the two-pass method with the improved two equation models allows accurate calculation of heat transfer over the entire flow field.

CHAPTER VI

CONCLUDING REMARKS

6.1 Achievements of Present Analysis

The results presented in Chapter V demonstrate that by employing modified versions of the k-ε model applied in a sequence of two passes, predictions of heat transfer coefficients can be obtained fairly accurately for recirculating and subsequent redeveloping flows beyond abrupt expansions where the Reynolds numbers range from low to moderate values. The procedures developed herein impose minim al restrictions on near-wall grid densities, are numerically efficient and employ fairly simple turbulence modeling. They are therefore, particularly appropriate for engineering applications.

Important turbulence phenomena, such as streamline curvature effects, and pressure-strain (scalar) interactions including 'wall-damping' effects have been incorporated in the k-ε model through functionalizing two parameters (C_μ and Pr_t) that were heretofore assumed as constants. Thus, some of the most important turbulence interactions are included in this improved k-ε model and at the same time, side-stepping the cumbersome numerical calculations necessary for the more complex higher order schemes. This functionalization is accomplished by employing the basic ideas of the 'second-order' algebraic stress level of closure without actually employing the full method in the calculation.

The eventual modeling and numerical procedures adopted for the present study yield consistently acceptable predictions of reattachment lengths, correlations of heat transfer coefficients and flow and turbulence intensity fields of the entire flow field. Throughout the course of this study, emphasis has focused on evaluating the capabilities and feasibilities of both the numerical and turbulent closure procedures. Consequently, the numerical code used is structured in such a way that it can be readily used to evaluate various modifications of turbulent viscosity models.

6.2 Limitations of Present Analysis

The major shortcoming of the present analysis lies in the inherent assumption that underlies all turbulent viscosity models, i.e. use of the Boussinesq assumption. By this assumption the shear stress is forced to instantaneously respond to changes in the mean strain field. This concept is not strictly valid in non-equilibruim flows, of which recirculating flow unfortunately is an example. A shortcoming of the two-pass procedure used is that it requires, a priori, fairly accurate prediction of reattachment lengths. For abrupt expansion geometries, as those examined in this study, fairly accurate reattachment lengths were obtained. However, for other engineering heat exchanger geometries it is not certain if the same level of success can be achieved. There are other minor limitations of the present research which become even less significant when viewed in the context of applications of heat exchange equipment; for example, neglection of the intermittent and fine scales structure of turbulence. As a final remark, Chandrsuda and Bradshaw [25] presented detailed measurements of Reynolds shear stress and triple products for the entire flow field beyond the back-step. Their results indicate that the triple products play an important role in the 'spreading' of the shear-layer, particularly around reattachment. However, the $k-\varepsilon$ viscosity model in its present form is not 'sensitized' to reflect triple products.

6.3 Suggestions for Future Studies

(a) Direct application of the procedures developed in this study can be applied to study turbulent heat transfer flows over a cavity, for which experimental measurements are reported [46]. For such a geometry the flow recirculates inside the cavity and the original shear layer is only slightly disturbed, consequently, the single pass procedure might suffice.

(b) By making the appropriate changes in the transport equations, buoyancy driven flows (such as that in a vertical sudden expansion) can be studied. It is expected that the present improvements to the code and to the basic model are adequate for analyzing such flow fields.

(c) Further improvements on modeling the dissipation equation is necessary. The improved model should more precisely account for near-wall effects and probably triple products. If such a model is devised, then it is possible to predict results for the entire flow field by a single pass.

(d) In present studies the length scales ($k^{3/2}/\varepsilon$) for both the velocity and temperature are assumed proportional. As discussed previously this will only be true if $P/\varepsilon \approx$

$P_\theta/\varepsilon_\theta$, which is rarely approached in a recirculating region. The way forward would be to replace the temperature length scale by $\overline{\theta'^2})^{3/2}/\varepsilon_\theta$, and then obtain differential equations of transport for both $\overline{\theta'^2}$ and ε_θ.

APPENDIX A

CLOSURE LEVELS OF TURBULENCE

The mathematics of some of the most common closure techniques for the stresses $\overline{u_i' u_j'}$ and $\overline{u_j' \theta'}$ are presented in this appendix.

(1) Turbulent Viscosity Models

According to the Boussinesq [54] idea, the tensorial representation of the Reynolds stresses and scalar fluxes, respectively, are,

$$-\rho \overline{u_i' u_j'} = \mu_t \left(\frac{\partial u_i}{\partial x_j} + \frac{\partial u_j}{\partial x_i} \right) + \frac{1}{3} \delta_{ij} \overline{u_m' u_m'} \qquad \text{(A1)}$$

$$-\rho \overline{u_j' \theta'} = \Gamma_t \frac{\partial T}{\partial x_j} \qquad \text{(A2)}$$

where μ_t and Γ_t are the turbulent viscosity and diffusivity of temperature respectively. The term $1/3\, \delta_{ij} \overline{u_m' u_m'}$ in Eqn. (A1) simply ensures that the normal stresses do not vanish in the absence of mean strain, and they are equal in magnitude. The approximations for the turbulent viscosity, μ_t, will now be discussed.

(a) Algebraic Expressions

By Prandtl's mixing length hypothesis [53],

$$\mu_t = \rho \ell_o^2 \left| \frac{\partial u_i}{\partial x_j} \right| \qquad \text{(A3)}$$

where ℓ_o is the mixing (characteristic) length, and is approximated as,

$$\ell_o = \kappa y \tag{A4}$$

where κ is Von Karman constant (=0.4). Such an approximation for ℓ_o is clearly only valid for regions remote from the wall, excluding the sublayer and buffer layer close to the wall. An improvement of this length scale was suggested by Van Driest [56] for the near-wall region. The expression is

$$\ell_o = \kappa y \left[1 - \exp\left(-y^+ \tau_w / A^+\right)\right] \tag{A5}$$

In the fully turbulent region Eqn. (A5) reduces to Eqn. (A4), as is expected.

(d) Differential Expressions

In this procedure the viscosity is again approximated by scales (length or velocity) which are in turn approximated by transport differential equations.

(i) One Equation Model

This modeling procedure has been developed and tested by Bradshaw et al [57]. The viscosity is approximated by

$$\mu_t = C \rho k^{\frac{1}{2}} \ell_o , \quad k = \frac{1}{2} \overline{(u_i' u_i')} \tag{A6}$$

where C is a constant, $k^{\frac{1}{2}}$ is the velocity scale and ℓ_o (as described above) is the length scale. The turbulent kinetic energy, k, is expressed by a transport differential equation. The differential equation is obtained by a tensorial contraction of the

the Reynolds stress equation. The Reynolds stress equation is developed in the next section, thus, development of the differential equation for k is deferred to the next section.

(ii) Two Equation Model

This modeling procedure is based on approximating the turbulent viscosity by two scales, length and velocity [60].

$$\mu_t = C_\mu \rho v_o \ell_o \tag{A7}$$

where $v_o = k^{\frac{1}{2}}$

$\ell_o = k^{\frac{3}{2}} / \varepsilon$

and C_μ normally assumed a constant value of 0.09. The dissipation of turbulent energy, ε, is expressed by a transport differential equation. For the same reason as mentioned for k, the ε equation is deferred to the next section.

(2) Stress and Flux Transport Models

Transport equations for the Reynolds stress and scalar flux is derived and a brief discussion of the closure techniques is discussed. (The unsteady form of the governing equations are maintained, although in the present study, the steady form of the equations are considered). The instantaneous values of the Navier-Stokes equation, Eqn. (1.2.1) are replaced by the sum of the

mean and fluctuating quantities, as described in Section (1.2), and applying the time-averaged continuity equation to further simplify, results in a differential equation for the fluctuating velocity, u_i',

$$\frac{\partial u_i'}{\partial t} + u_k' \frac{\partial \bar{u}_i}{\partial x_k} + \bar{u}_k \frac{\partial u_i'}{\partial x_k} + \frac{\partial}{\partial x_k}(u_i'u_k' - \overline{u_i'u_k'}) = -\frac{1}{\rho}\frac{\partial p'}{\partial x_i} + \nu \frac{\partial^2 u_i'}{\partial x_\ell \partial x_\ell} \qquad (A8)$$

Writing a similar equation for the u_j' fluctuation, and multiplying the u_i' equation by u_j', and the u_j' equation by u_i', and adding the two resulting equations, yields,

$$\begin{aligned} &u_j'\frac{\partial u_i'}{\partial t} + u_i'\frac{\partial u_j'}{\partial t} + u_j'u_k'\frac{\partial \bar{u}_i}{\partial x_k} + u_i'u_k'\frac{\partial \bar{u}_j}{\partial x_k} + u_j'\bar{u}_k\frac{\partial u_i'}{\partial x_k} \\ &+ u_i'\bar{u}_k\frac{\partial u_j'}{\partial x_k} + u_j'\frac{\partial}{\partial x_k}(u_i'u_k' - \overline{u_i'u_k'}) + u_i'\frac{\partial}{\partial x_k}(u_j'u_k' - \overline{u_j'u_k'}) \\ &= -\frac{1}{\rho}u_j'\frac{\partial p'}{\partial x_i} - \frac{1}{\rho}u_i'\frac{\partial p'}{\partial x_i} + \nu u_j'\frac{\partial^2 u_i'}{\partial x_\ell \partial x_\ell} + \nu u_i'\frac{\partial^2 u_j'}{\partial x_\ell \partial x_\ell} \end{aligned} \qquad (A9)$$

Time-averaging Eqn. (A9) and grouping some of the expressions results in the Reynolds stress transport equation for the correlation $\overline{u_i'u_j'}$. Omitting the usual overbars for the mean fluid

dynamic variables results in Eqn. (3.4.13).

A similar analysis is performed for the scalar (energy) equation. The procedure is as follows: substitute the Reynolds procedure of Section (1.2) into the instantaneous energy equation, Eqn. (1.2.4), and multiply the new equation by u_i', the result is then added to the product of Eqn. (A8) and θ'. Time-averaging the resulting equation yields the transport equation for the scalar flux, $\overline{u_j' \theta'}$. Again by omitting the usual overbars for the mean quantities, Eqn. (3.4.14) is obtained.

The transport differential equations for k and ε, as used in the two-equation model, are now developed. Performing a contraction on the Reynolds stress equation, Eqn. (3.4.13), i.e., setting i=j, and replacing $\overline{u_i'u_j'}/2$ by k results in the transport equation for k,

$$\frac{Dk}{Dt} = \underbrace{-\overline{u_i'u_j'}\frac{\partial u_j}{\partial x_i}}_{I} \underbrace{- \nu \overline{\frac{\partial u_j'}{\partial x_i}\frac{\partial u_j'}{\partial x_i}}}_{II} \qquad \text{(A10)}$$

$$\underbrace{- \frac{\partial}{\partial x_i}\overline{u_i'\left(\frac{p'}{\rho} + k\right)}}_{IV} + \nu \frac{\partial^2 k}{\partial x_i \partial x_i}$$

Eqn. (A10) is the differential equation that governs the transport of turbulent kinetic energy, k, and Terms I,II, and IV have the

same physical interpretations as those of Eqn. (3.4.13).

The derivation of the transport equation for ε, the dissipation rate of turbulent energy, is slightly more algebraically involved. The mathematical procedure is briefly outlined below. By definition, from Eqn. (3.4.13) the dissipation (Term II), ε, is,

$$\varepsilon = \nu \overline{\frac{\partial u_i'}{\partial x_j} \frac{\partial u_i'}{\partial x_j}} \tag{A11}$$

Differentiate Eqn. (A8) with respect to $\partial/\partial x_\ell$ and multiply throughout by $2\nu \partial u_i/\partial x$, time-average the results and use the definition of ε, Eqn (A11). By grouping various terms, the result is the transport equation for ε,

$$\frac{D\varepsilon}{Dt} = \underbrace{-2\nu \overline{\frac{\partial u_i'}{\partial x_k} \frac{\partial u_i'}{\partial x_\ell} \frac{\partial u_k'}{\partial x_\ell}}}_{\text{I}} \underbrace{-2\nu \overline{\left(\frac{\partial^2 u_i'}{\partial x_k \partial x_\ell}\right)^2}}$$

$$\underbrace{-2\nu \left\{ \overline{\frac{\partial u_i'}{\partial x_\ell} \frac{\partial u_k'}{\partial x_\ell}} + \overline{\frac{\partial u_\ell'}{\partial x_i} \frac{\partial u_\ell'}{\partial x_k}} \right\} \frac{\partial u_i}{\partial x_k} - 2\nu \overline{u_k' \frac{\partial u_i}{\partial x_\ell}} \frac{\partial^2 u_i}{\partial x_k \partial x_\ell}}_{\text{II}}$$

$$\underbrace{-\frac{\partial}{\partial x_k} \left\{ \overline{u_k' \varepsilon} + \frac{2\nu}{\rho} \overline{\frac{\partial u_k}{\partial x_\ell} \frac{\partial p'}{\partial x}} - \nu \frac{\partial \varepsilon}{\partial x_k} \right\}}_{\text{III}} \tag{A12}$$

Terms I,II, and III retain their respective physical meanings as given in Eqn. (3.4.13). These differential equations for the transport of k and ε must be closed so as to be applicable. The

closure of Eqn. (A10) for the turbulent kinetic energy is accomplished by comparing each of the terms with experimental measurements, and deriving empirical relationships. For the ε equation, Eqn (A12), this is not possible for none of the terms are accessible to measurements; however, closure is accomplished by gross simplifications. Launder [69] presented the closure details for both equations.

Within the framework of the turbulent viscosity model, Eqns. (A11) and (A12) reduces to [69],

$$\rho \frac{Dk}{Dt} = \frac{\partial}{\partial x_j}\left(\frac{\mu_t}{\sigma_k} \frac{\partial k}{\partial x_j}\right) + \mu_t\left(\frac{\partial u_i}{\partial x_j}\right)^2 - \rho\varepsilon \qquad \text{(A13)}$$

$$\rho \frac{D\varepsilon}{Dt} = \frac{\partial}{\partial x_j}\left(\frac{\mu_t}{\sigma_\varepsilon} \frac{\partial \varepsilon}{\partial x_j}\right) + C_{\varepsilon 1} \frac{\varepsilon}{k} \mu_t\left(\frac{\partial u_i}{\partial x_j}\right)^2 - C_{\varepsilon 2} \frac{\rho\varepsilon^2}{k} \qquad \text{(A14)}$$

where σ_k, σ_ε, $C_{\varepsilon 1}$ and $C_{\varepsilon 2}$ are empirical constants, their values are listed in Table (3.1).

Often analogous transport equations are needed for $\overline{\theta'^2}$ and $\varepsilon_\theta (= 2\Gamma \overline{(\partial\theta'/\partial x_k)^2})$. However, in this study, as will be shown in Appendix B, these terms are omitted.

APPENDIX B

DERIVATION OF C_μ AND Pr_t FUNCTIONS FOR ENTIRE FLOW FIELD

Relationships for C_μ and Pr_t are first developed in streamline co-ordinates for the recirculating region. Figure (B1) shows a schematic of the streamline co-ordinate system. In the present formulation the following assumptions of Leschziner and Rodi [64] are used.

$$v/r = \partial u_s/\partial s = 0 \tag{B1}$$

Re-writing Eqn. (3.4.27) for each component in (s,n) co-ordinate system,

$$\overline{u_s' u_n'} = P_{ns} \frac{k}{\varepsilon} (\Lambda' + \Lambda'') - \frac{k}{\varepsilon} \Lambda'' D_{ns} \tag{B2}$$

$$\overline{u_n'^2} = P_{nn} \frac{k}{\varepsilon} (\Lambda' + \Lambda'') - \frac{2}{3} k (\Lambda' \frac{P}{\varepsilon} - 1)$$

$$- \frac{k}{\varepsilon} \Lambda'' D_{nn} \tag{B3}$$

$$\overline{u_s'^2} = P_{ss} \frac{k}{\varepsilon} (\Lambda' + \Lambda'') - \frac{2}{3} k (\Lambda' \frac{P}{\varepsilon} - 1)$$

$$- \frac{k}{\varepsilon} \Lambda'' D_{ss} \tag{B4}$$

in which, $P = \frac{\mu_t}{\rho} \left(\frac{\partial u_s}{\partial n} - \frac{u_s}{R_c} \right)^2$

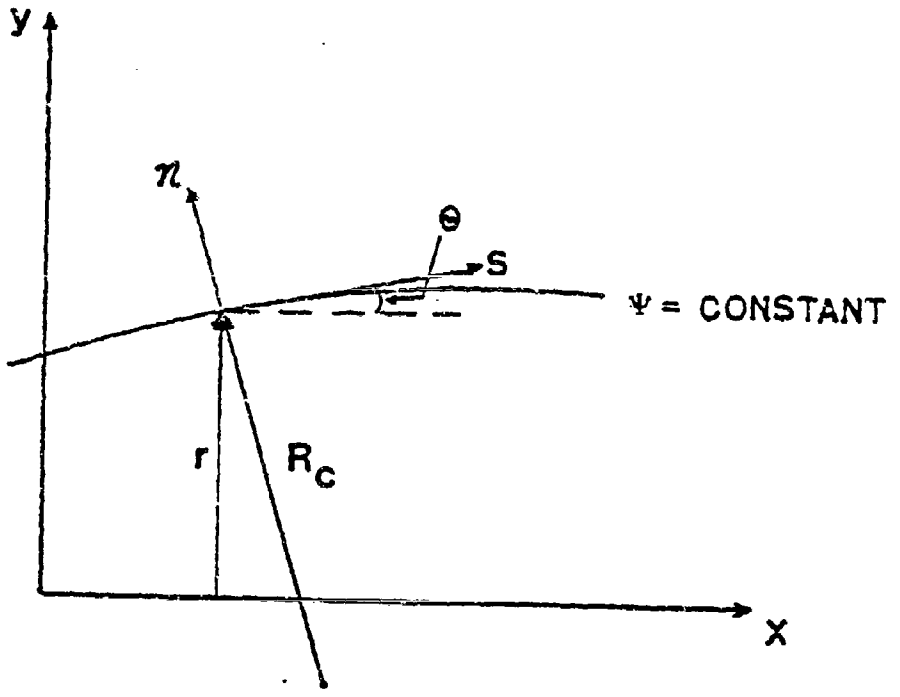

Figure B1. Sketch of Streamline Co-ordinate System

In the framework of the Boussinesq approximation, the k-ε model is,

$$-\overline{u_s' u_n'} = C_\mu \frac{k^2}{\varepsilon}\left(\frac{\partial u_s}{\partial n} - \frac{u_s}{R_c}\right) \tag{B5}$$

Similarly, writing P_{ij} and D_{ij}, Eqns. (3.4.15) and (3.4.16) in streamline co-ordinates and using the assumptions given in Eqn. (B1),

$$P_{ns} = -\overline{u_n'^2}\frac{\partial u_s}{\partial n} + \left(2\overline{u_s'^2} - \overline{u_n'^2}\right)\frac{u_s}{R_c} \tag{B6}$$

$$P_{nn} = 4\,\overline{u_n' u_s'}\,\frac{u_s}{R_c} \tag{B7}$$

$$P_{ss} = -2\,\overline{u_s' u_n'}\left(\frac{\partial u_s}{\partial n} + \frac{u_s}{R_c}\right) \tag{B8}$$

$$D_{ns} = -\overline{u_s'^2}\frac{\partial u_s}{\partial n} + \left(2\overline{u_n'^2} - \overline{u_s'^2}\right)\frac{u_s}{R_c} \tag{B9}$$

$$D_{nn} = -2\,\overline{u_s' u_n'}\left(\frac{\partial u_s}{\partial n} + \frac{u_s}{R_c}\right) \tag{B10}$$

$$D_{ss} = 4\,\overline{u_s' u_n'}\,\frac{u_s}{R_c} \tag{B11}$$

Substitution of Eqns. (B6)-(B11) into Eqns. (B2)-(B4) results in the following,

$$-\overline{u_s' u_n'} = \overline{u_n'^2}\left[\frac{k}{\varepsilon}\Lambda'\left(\frac{\partial u_s}{\partial n} + \frac{u_s}{R_c}\right) + \frac{k}{\varepsilon}\Lambda''\left(\frac{\partial u_s}{\partial n} + 3\frac{u_s}{R_c}\right)\right]$$

$$+ \overline{u_s'^2}\left[-\frac{k}{\varepsilon}\Lambda'\left(2\frac{u_s}{R_c}\right) - \frac{k}{\varepsilon}\Lambda''\left(\frac{3u_s}{R_c} + \frac{\partial u_s}{\partial n}\right)\right] \qquad (B12)$$

$$\overline{u_n'^2} = \overline{u_s' u_n'}\left[4\frac{k}{\varepsilon}\Lambda'\frac{u_s}{R_c} + \frac{k}{\varepsilon}\Lambda''\left(6\frac{u_s}{R_c} + 2\frac{\partial u_s}{\partial n}\right)\right]$$

$$-\frac{2}{3}k\left(\Lambda'\frac{P}{\varepsilon} - 1\right) \qquad (B13)$$

$$\overline{u_s'^2} = \overline{u_s' u_n'}\left[-\frac{2k}{\varepsilon}\Lambda'\left(\frac{\partial u_s}{\partial n} + \frac{u_s}{R_c}\right)\right]$$

$$-\frac{2k}{\varepsilon}\Lambda''\left(\frac{\partial u_s}{\partial n} + 3\frac{u_s}{R_c}\right) - \frac{2}{3}k\left(\Lambda'\frac{P}{\varepsilon} - 1\right) \qquad (B14)$$

Eqns. (B12)-(B14) represent three algebraic equations with three unknown stresses, $\overline{u_s' u_n'}$, $\overline{u_n'^2}$ and $\overline{u_s'^2}$. Elimination of $\overline{u_n'^2}$ and $\overline{u_s'^2}$ in Eqn. (B12) results in the expression for $\overline{u_s' u_n'}$ as given by Eqn. (3.4.32). Comparing Eqn. (3.4.32) with the Boussinesq approximation, Eqn. (B5), results in the functional form for C_μ, as given by Eqn. (3.4.36).

Following a similar procedure as outlined above, the

functional representation for Pr_t is obtained. Writing Eqn. (3.4.31) in (s,n) co-ordinates, for both fluxes,

$$-\overline{u_s'\theta'} = \phi_T \frac{k}{\varepsilon}\left(\overline{u_s'^2}\frac{\partial T}{\partial s} + \overline{u_s'u_n'}\frac{\partial T}{\partial n}\right) + \phi_T' \frac{k}{\varepsilon}\left[\overline{u_n'\theta'}\left(\frac{\partial u_s}{\partial n} + \frac{u_s}{R_c}\right)\right] \quad \text{(B15)}$$

$$-\overline{u_n'\theta'} = \phi_T \frac{k}{\varepsilon}\left(\overline{u_s'u_n'}\frac{\partial T}{\partial s} + \overline{u_n'^2}\frac{\partial T}{\partial n}\right) + \phi_T' \frac{k}{\varepsilon}\left[\overline{u_s'\theta'}\left(-2\frac{u_s}{R_c}\right)\right] \quad \text{(B16)}$$

The Boussinesq approximation is,

$$-\rho\,\overline{u_n'\theta'} = \frac{\mu_t}{Pr_t}\frac{\partial T}{\partial n} \quad \text{(B17)}$$

Elimination of $\overline{u_s'\theta'}$ in Eqn. (B16) by Eqn. (B15) and comparing the result with Eqn. (B17) give the functional form of Pr_t. To isolate the main contributions of curvature effects on Pr_t, the following assumption is made,

$$\frac{\partial T}{\partial s} \Big/ \frac{\partial T}{\partial n} = 0$$

With this assumption the expression for Pr_t is obtained as given by Eqn. (3.4.37). Expressions are now developed for R_c and $\partial u_s/\partial n$. Using the definition of the radius of curvature,

$$\frac{1}{R_c} = \left. \frac{d^2y/dx^2}{\left[1 + (dy/dx)^2\right]^{3/2}} \right|_{\psi = c} \qquad (B18)$$

Using the functional relationship for ψ,

$$\left. \frac{dy}{dx} \right|_{\psi = c} = \frac{v}{u}$$

and

$$\left. \frac{d^2y}{dx^2} \right|_{\psi = c} = \frac{v}{u^2}\left[\frac{\partial v}{\partial y} - \frac{\partial u}{\partial x}\right] + \frac{1}{u}\frac{\partial v}{\partial x} - \frac{v^2}{u^3}\frac{\partial u}{\partial y}$$

Substituting these expressions into Eqn. (B18) result, in the expressions for R_c as given by Eqn. (3.4.12).

$\partial u_s/\partial n$ is determined in the following manner. Transforming from (x,y) to (s,n) co-ordinates,

$$S_{k\ell}^{(2)} = S_{ij}^{(1)} C_{ik} C_{j\ell} \qquad (B19)$$

where the C's are the direction cosines. Rewriting equation (B19) in (n,s) system,

$$S_{ns} = \frac{1}{2}\sin(2\theta)\left[S_{yy} - S_{xx}\right] + S_{xy}\cos(2\theta) \qquad (B20)$$

Taking S to be the shear stresses,

$$S_{xx} = 2\frac{\partial u}{\partial x} \; ; \; S_{yy} = 2\frac{\partial v}{\partial y}$$

$$S_{xy} = \frac{\partial u}{\partial y} + \frac{\partial v}{\partial x}$$

$$S_{ns} = \frac{\partial u_s}{\partial n} - \frac{u_s}{R_c}$$

Substituting these relationships into Eqn. (B20) and solving for $\partial u_s/\partial n$, results in the expression as given by Eqn. (3.4.11).

Expressions for C_μ and Pr_t are now obtained in (x,y) co-ordinates valid for the redeveloping region. The procedure is analagous to that as outlined above, and therefore discussion will be very brief. Rewriting Eqn. (3.4.27) for each of the stress, substituting for P_{ij} and D_{ij} and eliminating $\overline{u'^2}$ and $\overline{v'^2}$ results in a unique expression for $\overline{u'v'}$. Comparing with the Boussinesq approximation for $\overline{u'v'}$ results in the expression for C_μ as given in Eqn. (3.4.38). In this region, P, P_{ij} and D_{ij} take on the relationships as given below.

$$P = \mu_t G,$$

in which G is defined by Eqn. (3.4.8).

$$P_{xy} = -2\overline{v'^2}\frac{\partial u}{\partial y} - \overline{u'^2}\frac{\partial v}{\partial x} + j\,\overline{u'v'}\frac{v}{y}$$

$$P_{xy} = -2\overline{u'^2}\frac{\partial u}{\partial x} - 2\overline{u'v'}\frac{\partial u}{\partial y}$$

$$P_{yy} = -2\overline{u'^2}\frac{\partial u}{\partial y} - 2\overline{u'v'}\frac{\partial v}{\partial x}$$

$$D_{xy} = -\overline{u'^2}\frac{\partial u}{\partial y} - \overline{v'^2}\frac{\partial v}{\partial x}$$

$$D_{xx} = -2\overline{u'^2}\frac{\partial u}{\partial x} - 2\overline{u'v'}\frac{\partial v}{\partial x}$$

$$D_{yy} = -2\overline{v'^2}\frac{\partial v}{\partial y} - 2\overline{u'v'}\frac{\partial u}{\partial y}$$

In the above expression j=0,1 correspond to the rearward facing step and pipe expansion geometries, respectively. In the expression for C_μ , Eqn. (3.4.38), the coefficients are defined as,

$$C_\ell = \left\{ \frac{k}{\epsilon}\frac{v}{y}\left[\frac{1 - C_{s2} + C_{s2w}f}{\frac{P}{\epsilon} + C_{s1} - C_{s1w}f}\right]\right\}^j$$

$$A = -\frac{\Lambda''}{\Lambda' + \Lambda''} \quad ; \quad B = \left(\frac{\Lambda' P}{\epsilon} - 1\right); \quad C = \frac{1-\beta}{A\alpha\beta}$$

$$E = C_\ell^j - \frac{1}{2}\frac{2k\Lambda''}{\epsilon A}\frac{\partial u}{\partial y}\left[\frac{A(\alpha+\beta)}{\alpha\beta} + \frac{1-\beta}{A\alpha\beta}\right]$$

$$F = \frac{1}{3}\, k\, \frac{B}{E}\left(\frac{\partial u}{\partial y}\right)^2\left(\frac{2k\Lambda''}{\epsilon A}\right)^2\left[\frac{1+A}{\alpha\beta} + \left(\frac{1-\beta}{A\alpha\beta}\right)\right]$$

$$\alpha = 1 + 2\frac{\Lambda' k}{\epsilon}\frac{\partial u}{\partial x}$$

$$\beta = 1 - \frac{2k}{\epsilon}\Lambda''\frac{\partial u}{\partial y}$$

A similar analysis for Pr_t is performed, the final result is given by Eqn. (3.4.39).

APPENDIX C

SIMULATION OF INITIAL CONDITIONS AND TREATMENT OF NEAR-WALL FLOWS

C.1 Simulation of Initial Conditions

Figure (C1) illustrates the schematic procedure for the simulation of approach boundary layer thicknesses for the Aung and Goldstein [8] experiment. The experiment was performed with an unheated starting length, ξ_1. The actual dimensions are,

ξ_1 = 15 cm. $\xi_1 = x'' - x''$, $\xi = x_1 - x_2$

x_1 = 45.5 cm.

x_2 = 30.5 cm.

x_S = 10 cm.

From laminar flat plate boundary layer theory [103]

$$\delta_u' = 4.64\left(\frac{ux_1'}{\rho U_o}\right)^{1/2} \qquad (C1)$$

$$\delta_T' = \frac{\delta_u'}{1.026\ (Pr)^{1/3}}\left[1 - \left(\frac{\xi_1}{x_1'}\right)^{3/4}\right]^{1/3} \qquad (C2)$$

Equating the turbulent boundary layer thicknesses, Eqns. (3.6.1) and (3.6.2) with Eqns (C1) and (C2) results in expressions for the respective starting lengths. The effective starting lengths are,

$x_1 = x_S + x_1''$

$x_2 = x_S + x_2''$

Inserting these lengths into Eqns. (3.6.1) and (3.6.2) results in

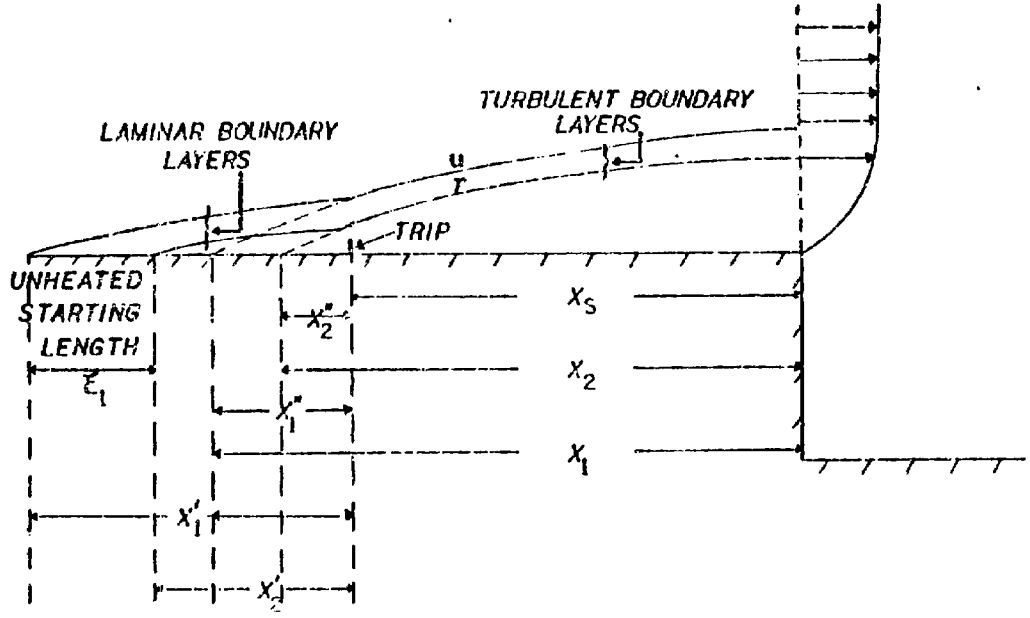

Figure C1. Simulation of Approach Momentum and Thermal Thicknesses for the Back-Step Experiment of Aung and Goldstein 8

the momentum and thermal boundary layer thicknesses at the step.

D.2 Wall Boundary Condition

Figure (C2) illustrates the mean velocity distribution in a boundary layer [12], also indicated are the names associated with each region. A brief mathematical description is presented for the functional behavior of the mean velocity in each of the regions. The analysis is formulated for the u-velocity; however, similar procedures can be carried out for the v-velocity and temperature.

1. Linear Sublayer

The viscous sublayer is approximately equal to 0.1 percent of the total boundary layer thickness, this corresponds to $y^+ < 5$. The total shear stress is,

$$\tau = \tau_\ell + \tau_t \qquad (C3)$$

where,

τ_ℓ (laminar) $= \mu \frac{\partial u}{\partial y}$

τ_t (turbulent) $= -\rho \overline{u'v'}$ (Boussinesq Approximation)

The momentum equation for a two-dimensional, incompressible, turbulent boundary layer with zero pressure gradient is,

I LINEAR SUBLAYER
II BUFFER ZONE
III LOG-LAW REGION

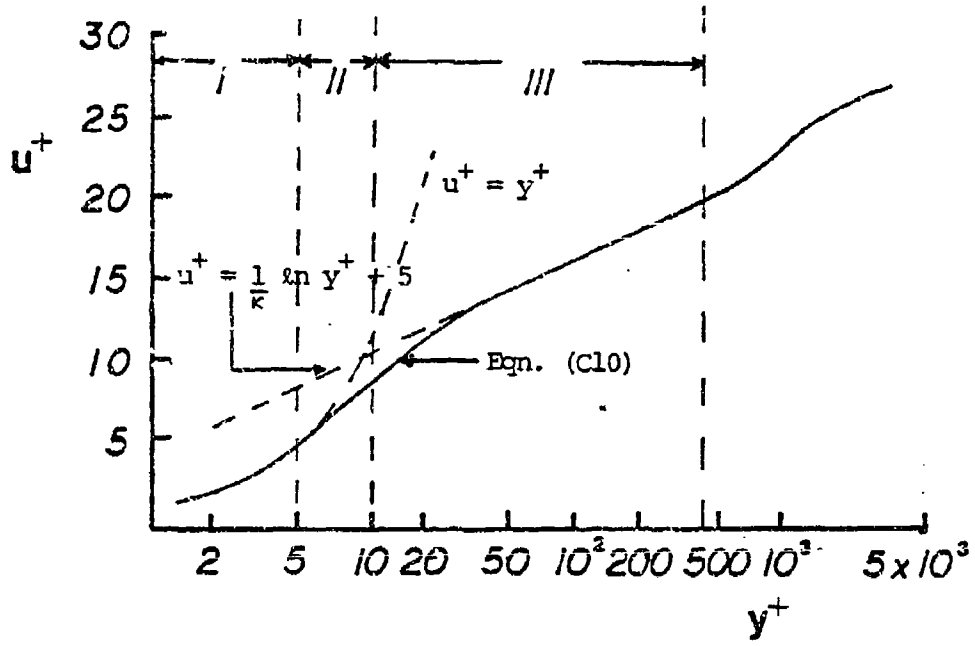

Figure C2. Mean Velocity Distribution in Turbulent Boundary Layer

$$u \frac{\partial u}{\partial x} + v \frac{\partial u}{\partial y} = \frac{1}{\rho} \frac{\partial \tau}{\partial y} \qquad (C4)$$

where,

$$u = v = 0, \quad \text{at} \quad y = 0$$

It can be shown that,

$$\left(\frac{\partial^2 \tau}{\partial y^2} \right)_{y=0} = 0$$

Thus, for a small distance away from the wall,

$$\frac{\partial \tau}{\partial y} = 0$$

This implies that the region close to the wall is a constant shear stress region. Re-writing Eqn. (C3),

$$\frac{\tau}{\rho} = \nu \frac{du}{dy} - \overline{u'v'} = \frac{\tau_w}{\rho} \equiv u_\tau^2 \qquad (C5)$$

In the viscous sublayer region, Eqn. (C5) reduces to (since $\overline{u'v'}$ =

0 at y = 0),

$$\nu\left(\frac{du}{dy}\right) = u_\tau^2 \tag{C6}$$

Integrating Eqn. (C6), and using the definition of,

$y^+ = \frac{yu_\tau}{\nu}$ and $u^+ = \frac{u}{u_\tau}$, result in,

$$u^+ = y^+ \tag{C7}$$

2. Buffler Layer

For this region, often referred to as the transition or inner region, y^+ ranges from about 5 to 13. In this range both τ_ℓ and τ_t are important. From the mixing length hypothesis,

$$-\rho\overline{u'v'} = \rho\,\ell_o^2\left|\frac{\partial u}{\partial y}\right|\frac{\partial u}{\partial y} \tag{C8}$$

Using the Van Driest [56] length scale (Eqn. (3.4.4)) and subsituting into Eqn. (C8), yields,

$$\nu\frac{du}{dy} + (\kappa y)^2\left[1 - \exp\left(-y/A^+\right)\right]^2\left(\frac{du}{dy}\right)^2 = u_\tau^2 \tag{C9}$$

For $a\,(y^+) = (\kappa y^+)^2\left[1 - \exp\left(-y/A^+\right)\right]^2$

and, $b = 1$

Eqn. (C9) reduces to,

$$a\,(y^+)\left(\frac{du^+}{dy^+}\right)^2 + b\left(\frac{du^+}{dy^+}\right) - 1 = 0$$

or,

$$\frac{du^+}{dy^+} = \frac{-b + (b^2 + 4a)^{1/2}}{2a}$$

or,

$$u^+ = \int_0^{y^+} \frac{2}{b + \left[b^2 + 4a(y^+)\right]^{1/2}}\, dy^+ \qquad (C10)$$

Eqn. (C10) agrees very well with the experimental data of Klebanoff [112] and Laufer [113] in the buffer zone [12].

3. Log-wall Region

For this region, sometimes referred to as the fully turbulent part of the inner region, $y^+ > 13$. Eqn. (C3), reduces to,

$$\frac{\tau_t}{\rho} = -\overline{u'v'} = u_\tau^2 \qquad (C11)$$

By substituting the Boussinesq approximation, Eqn. (3.2.1) and the expression for the turbulent viscosity, μ_t, Eqn. (3.4.22), into Eqn. (C 11), result in

$$\kappa\, u_\tau\, y \frac{du}{dy} = u_\tau^2 \qquad (C12)$$

Integrating Eqn. (C 12) results in,

$$u^+ = \frac{1}{\kappa} \ln y^+ + c \qquad (C13)$$

REFERENCES

1. Bergles, A.E., "Survey and Evaluation of Techniques to Augment Convective Heat and Mass Transfer, "Progress in Heat and Mass Transfer, Vol. 1, 1969, pp. 331-424.
2. Lancet, R.T., "The Effect of Surface Roughness on the Convection Heat-Transfer Coefficient for Fully Developed Turbulent Flow in Ducts with Uniform Heat Flux," J. Heat Transfer Trans. ASME, Vol. 81, 1959, pp. 168-174.
3. Dipprey, D.F. and Sabersky, R.M., "Heat and Momentum Transfer in Smooth and Rough Tubes at Various Prandtl Numbers," Int. J. of Heat and Mass Transfer, Vol. 6, 1963, pp. 329-363.
4. Zaherdadeh, N.H. and Jagdish, B.S., "Heat Transfer in Decaying Swirl Flow," Int. J. Heat Mass Transfer, Vol. 18, 1975, p. 941.
5. Huang, F.C., "Numerical Computations of Friction and Heat Transfer in Free Swirling Pipe Flow," Ph.D. Thesis, Drexel University, 1980.
6. Seban, R.A., Emery, A. and Levy, A., "Heat Transfer to Separated and Reattached Subsonic Turbulent Flows Obtained Downstream of a Surface Step," J. Aerospace Sci., Vol. 26, No. 12, 1959, pp. 809-814.
7. Prandtl, L. and Tietjens, O., Fundamentals of Hydro and Aero Mechanics, McGraw Hill, N.Y., 1934.

8. Aung, W. and Goldstein, R.J., "Heat Transfer in Turbulent Separated Flow Downstream of a Rearward-Facing Step," Israel J. of Tech., Vol. 10., 1972, pp. 35-41.

9. Moss, W.D. and Baker, S. "Re-circulating Flows Associated with Two-Dimensional Steps," The Aeronautical Quarterly, Vol. 31, Part 3, 1980.

10. Abbott, D.E., and Kline, S.J., "Experimental Investigation of Subsonic Turbulent Flow over Single and Double Backward Facing Steps," J. Basic Engng. Trans. ASME, Vol. D84, 1962, pp. 317-325.

11. Fraser, S.M. and Sidding, M.H., "Turbulent Flow Over a Normal Wall," J. of Mech. Engrg. Sc., Vol. 22, No. 4, 1980.

12. Cebecci, T. and Smith, A.M.O., Analysis of Turbulent Boundary Layers, Academic Press, New York, 1974.

13. Orszag, S.A., The Statistical Theory of Turbulence, Gordon and Beach Co., 1974.

14. Deardorff, J.W., "A Numerical Study of Three-Dimensional Turbulent Channel Flow at Large Reynolds Numbers, J. Fluid Mech., Vol. 41, 1970, p. 453.

15. Deardorff, J.W., "Three-Dimensional Numerical Study of Height and Mean Structure of a Heated Planetary Boundary Layer," Boundary-Layer Metero., Vol. 7, 1974, pp. 81-106.

16. Hinze, J.O., Turbulence, McGraw Hill, New York, 1975.

17. Launder, B.E., Reece, G.J., and Rodi, W., "Progress in the Development of a Reynolds Stress Turbulence Closure," J. Fluid Mech., 68, part 3, 1975, pp. 537-566.

18. Launder, B.E., "Heat and Mass Transport," Turbulence-Topics in Applied Physics, Vol. 12, Springer-Verlag, New York, 1976,

19. Launder, B.E., and Spalding, D.B., Mathematical Models of Turbulence, Academic Press, London, 1972.

20. Eaton, J.K. and Johnston, J.P., "Turbulent Flow Reattachment: An Experimental Study of the Flow and Structure Behind a Backward-Facing Step," Report MD-39, Thermo. Div., Dept. of M.E., Stanford Univ., 1980.

21. Hsu, H.C., "Characteristics of Mean Flow and Turbulence at an Abrupt Two-Dimensional Expansion," Ph.D. Thesis, State Univ. of Iowa, 1950.

22. Tani, I., Iuchi, M. and Komoda, H., "Experimental Investigation of Flow Separation Associated with at Step or Groove," Report No. 364, Aero. Res. Inst., Univ. of Tokyo, 1961.

23. Bradshaw, P., and Wong, F.Y.F., "The Reattachment and Relaxation of a Turbulent Shear Layer," J. Fluid Mech., Vol. 52, part 1, 1972, pp. 113-135.

24. Bradshaw, P., "Review - Complex Turbulent Flows," J. of Fluids Engrg. Trans, ASME, Vol. 97, 1975, pp. 146-154.

25. Chandrsuda, C. and Bradshaw, P., "Turbulence Structure of a Reattaching Mixing Layer," J. of Fluid Mech., Vol. 110, 1981, pp. 171-194.

26. Hussain, A.K.M.F. and Zedan, M.F., "Effects of the Initial Condition on the Axisymmetric Free Shear Layer: Effects of the Initial Momentum Thickness," Phys. Fluids, Vol. 21, No. 7, 1978, pp. 1100-1112.

27. Narayanan, B., et al., "Similarities in Pressure Distribution in Separated Flow Behind Backward-Facing Steps," Aeronautical Quarterly, 23, part 4, 1974, pp. 305-312.

28. Kim, J., et al., "Investigation of a Reattaching Turbulent Shear Layer: Flow over a Backward-Facing Step," J. Fluids Engrg. Trans. ASME, Vol 102, 1980, pp. 302-308.

29. Mehta, P.R., "Separated Flow Through Large Sudden Expansions," J. Hyd. Div. ASCE, Vol. 107, No. Hy4, 1981, pp. 451-460.

30. Denham, M.K., and Patrick, M.A., "Laminar Flow Over a Downstream-Facing Step in a Two-Dimensional Flow Channel," Trans. Instn. Chem. Engrs., 52, 1974, pp. 361-364.

31. Etheridge, D.W., and Kemp, P.H., "Measurements of Turbulent Flow Downstream of a Rearward-Facing Step," J. Fluid Mech., 86, part 3, 1978, pp. 545-566.

32. Smyth, R., "Turbulent Flow Over a Plane Symmetric Sudden Expansion," J. of Fluids Eng Trans, ASME, Vol 100, 1979, pp. 348-353.

33. Armaly, B.F. et al., "Measurements and Predictions of Flow Downstream of a Two-Dimensional Single Backward Facing Step," Sonderforschungsbereich 80-172, Universitat Karlsruhe, July 1980.

34. Back, L.H. and Roschke, E.J., "Shear-Layer Flow Regimes and Wave Instablities and Reattachment Lengths Downstream of an Abrupt Circular Channel Expansion," J. of App. Mechs. Trans. ASME, Vol. 94, 1972, pp. 677.

35. Kuehn, D.M., "Effects of Adverse Pressure Gradient on the Incompressible Reattaching Flow over a Rearward-Facing Step," AIAA Journal, 18, No. 3, 1980, pp. 343-344.

36. Hanson, F.B. and Richardson, P.D., "Mechanisms of Turbulent Separated Flows as Indicated by Heat Transfer: A Review," ASME Symp. on Fully Turbulent Flows, New York, 1964.

37. Fletcher, L.S., Briggs, D.G. and Hage, R.E., "Heat Transfer in Separated and Reattaching Flows: An Annotated Review," Israel J. of Tech., Vol. 12, 1974, pp. 235-261.

38. Aung, W. and Watkins, C.B., "Heat Transfer Mechanisms in Separated Forced Convection," Proceedings of the NATO Institute on Turbulent Forced Convection in Channels and Rod

Bundles, Hemisphere Publications Inc., Washington, D.C., 1979.

39. Zemanick, P.P. and Dougall, R.S., "Local Heat Transfer Downstream of Abrupt Circular Channel Expansion," J. Heat Transfer Trans. ASME, Vol. 92, p. 53, 1970.

40. Ede et al., "Effect of an Abrupt Disturbance of the Flow on the Local Heat Transfer Coefficient in a Pipe," HEAT 164, NEL, Glasgow, Scotland, 1959.

41. Sparrow, E.M. and O'Brien, "Heat Transfer Coefficients on the Downstream Face of an Abrupt Enlargement or Inlet Constriction in a Pipe," J. Ht. Tr. Trans. ASME, Vol. 102, 1980, pp. 408-414.

42. Seki, N. et al., "Turbulent Fluctuations and Heat Transfer for Separated Flow Associated with a Double Step at Entrance to an Enlarged Flat Duct," J. Heat Transfer Trans. ASME, 98, 1976, pp. 588-593.

43. Seki, N. et al., "Effect of Stall Length on Heat Transfer in Reattached Region Behind a Double Step and Entrance to an Enlarged Flat Duct," Int. J. Heat and Mass Transfer, 19, 1976, pp. 700-702.

44. Koram, K.K. and Sparrow, E.M., "Turbulent Heat Transfer Downstream of an Unsymmetric Blockage in a Tube," J. Heat Transfer Trans. ASME, 100, 1978, pp. 588-594.

45. Symth, R., "Turbulent Heat Transfer Measurements in Axisymmetric External Separated and Reattached Flows," Letters in Heat and Mass Transfer, 6, 1979, pp. 405-412.

46. Haugen, R.L. and Dhanak, A.M., "Heat Transfer in Turbulent Boundary-Layer Separation Over a Surface Cavity," J. Ht. Transfer Trans. ASME, Vol. 89, 1967, pp. 335-340.

47. Ota, T. and Kon, N., "Heat Transfer in the Separated and Reattached Flow Over Blunt Flat Plates-Effects of Nose Shape," Int. J. Of Heat and Mass Transfer, Vol. 22, 1979, pp. 197-206.

48. Ota, T. and Kon, N., "Turbulent Transfer of Momentum and Heat in a Separated and Reattached Flow Over a Blund Flat Plate," J. Ht. Transfer Trans. ASME, Vol. 102, 1980, p. 749.

49. Lamb, J.P., "Convective Heat Transfer Correlations for Planar, Separated Flows," J. of Ht. Transfer Trans. ASME, Vol. 102, 1980, p. 351.

50. Bradshaw, P., "The Understanding and Prediction of Turbulence," Aero. Journal, 1972, pp. 403-418.

51. Rodi, W., "Turbulence Models and Their Application to Hydraulics - A State of the Art Review," Report SFB 80/T/127, University of Karlsruhe, Germany.

52. Reynolds, W.C., "Computation of Turbulent Flows," Ann. Rev. Fluid Mech., Vol. 8, 1976, pp. 183-209.

53. Mellor, G.L. and Herring, H.J., "A Survey of the Mean Turbulent Field Closure Models," AIAA Journal, 11, No. 5, 1973, pp. 509-599.

54. Boussinesq, J., "Theorie de L'ecoulement Tourbillant," Mem. Pre. par. div., Sav. 23, Paris.

55. Prandtl, L., "Bericht uber Untersuchungen Zur Ausgebildeten Turbulenz," ZAMM, 5, 1925, p. 136.

56. Van Driest, E.R., "On Turbulent Flow Near a Wall," J. Aero. Sci., Vol. 23, 1956, p. 1007.

57. Bradshaw, P., Ferriss, D.H. and Atwell, N.P., "Calculation of Boundary Layer Development Using the Turbulent Energy Equation," J. Fluid Mech., Vol. 28, 1976, p. 593.

58. Launder, B.E. and Spalding, D.B., "The Numerical Computation of Turbulent Flows," Comput. Methods Appl. Mech. Eng., Vol. 3, 1974, pp. 269-289.

59. Chieng, C.C. and Launder, B.E., "On the Calculation of Turbulent Heat Transport Downstream from an Abrupt Pipe Expansion," Numerical Heat Transfer, Vol. 3, 1980, pp. 189-207.

60. Jones, W.P. and Launder, B.E., "The Prediction of Laminarization with a 2 - Equation Model of Turbulence," Int. J. Heat Mass Transfer, Vol. 15, 1972, pp. 301-313.

61. Hanjalic, K. and Launder, B.E., "Sensitizing the Dissipation Equation to Irrotational Strains," J. Fluids Engrg. Trans. ASME, Vol. 102, 1980, p. 34.

62. Hanjalic, K. and Launder, B.E., "Preferential Spectral Transport by Irrotational Straining," Proceedings to the ASME Symposium on Turbulent Boundary Layers, Niagara Falls, New York, June 1979, pp. 101-110.

63. Ljuboja, M. and Rodi, W., "Calculation of Turbulent Wall Jets with an Algebraic Reynolds Stress Model," Proceedings of the ASME Symposium on Turbulent Boundary Layers, Niagara Falls, New York, June 1979, pp. 131-138.

64. Leschziner, M.A. and Rodi, W., "Calculation of Annular and Twin Parallel Jets Using Various Discretization Scheme and Turbulence-Model Variations," J. Fluids Eng. Trans. ASME, Vol. 103, 1981, pp. 352-360.

65. Humphrey, J.A.C. and Pourahmadi, F., "A Generalized Algebraic Relation for Predicting Developing Curved Channel Flow with a k-ε Model of Turbulence," Third Symposium on Turbulent Shear Flow, Univ. of California, Davis, Sept. 9-11, 1980.

66. Gooray, A., Watkins, C.B. and Aung, W.," k-ε Calculations of Heat Transfer in Redeveloping Turbulent Boundary Layers Downstream of Reattachment," To be Presented, AIAA/ASME Fluids, Plasma, Thermophysical and Heat Transfer Conference,

St. Louis, Missouri, June 7-11, 1982.

67. So, R.M.C., "Heat Transfer Modeling for Turbulent Shear Flows on Curbed Surfaces," ZAMP, Vol. 32, 1981, pp. 514-532.

68. Bradshaw, P., "Effect of Streamwise CUrvature on Turbulent Flows", AGARDDograph No. 169, 1973.

69. Launder, B.E., Progress in the Modeling of Turbulent Transport, Supplementary Notes, Dept. of Chem. Eng., McGill Univ., Canada, 1976.

70. Hanjalic, K., and Launder, B.E., "A Reynolds Stress Model of Turbulence and its Application to Thin Shear Flows," J. Fluid Mech. Vol. 52, 1972, pp. 609-638.

71. Hanjalic, K., and Launder, B.E., "Contribution Towards a Reynolds Stress Closure for Low-Reynolds Number Turbulence". J. Fluid Mech., Vol. 74, 1976, pp. 593-610.

72. Cormack, D.E., et al., "An Evaluation of Mean Reynolds Stress Turbulence Models: The Triple Velocity Correlation," J. Fluids Engrng. Trans. ASME, Vol. 100, 1979, pp. 47-54.

73. So, R.M.C., "Comments on Extended Pressure-Strain Correlation Models," J. of Applied Math. and Phys. (ZAMP), Vol. 31, 1980, pp. 56-65.

74. Speziale, C.G., "Closure Relations for the Pressure-Strain Correlation of Turbulence," Phys. Fluids, 23, No. 3, 1980, pp. 459-463.

75. Gessner, F.B., and Emery, A.F., "A Reynolds Stress Model for Turbulent Corner Flows-part 1 Development of the Model", J. of Fluids Engrng. Trans. ASME, Vol. 98, 1976, pp. 261-268,

76. Gessner, F.B., "Turbulence and Mean Flow Characteristics of Fully Developed Flow in Rectangular Channel," Ph.D. Thesis, Purdue Univ., 1974.

77. Gibson, M.M., and Launder, B.E., "On The Calculation of Horizontal Turbulent, Free Shear Flows Under Gravitational Influence," J. Heat Trans. ASME, 98C, 1976, pp. 81-87.

78. Samaraweera, D.S.A., "Turbulent Heat Transfer in Two - and Three-Dimensional Temperature Fields," Ph.D. Thesis, University of London, 1978.

79. Gibson, M.M., "An Algebraic Stress and Heat-Flux Model for Turbulent Shear Flow with Streamline Curvature," Int. J. Ht. and Mass Transfer, Vol. 21, 1978, pp. 1609-1617.

80. Antonia, R.A., and Danh, H.Q., "A Local Similarity Model for the Heat Flux Equation in a Turbulent Boundary Layer, Int. J. Heat Mass Transfer, 21, 1979, pp. 1002-1005.

81. Gessner, F.B., and Po, J.K., "A Reynolds Stress Model for Turbulent Corner Flows - Part II: Comparisons between Theory and Experiment," J. Fluids Engrng. Trans. ASME, 98, 1976, pp. 269-277.

82. So, R.M.C., "A Note in Comment on A Reynolds Stress Model for Turbulent Corner Flows", J. Fluids Eng. Trans. ASME, 99, 1977, pp. 593-598.

83. Irwin, H.P.A.H. and Smith, P.A., "Prediction of the Effect of Streamline Curvature on Turbulence," Physics of Fluids, Vol. 18, 1975, pp. 624-630.

84. Taylor, C., et al., "F.E.M. and the Two-Equation Model of Turbulence," Proc. 2nd Int. Conf. Num. Method in Laminar and Turbulent Flow, Venice, Italy, 1981, pp. 639-5=651.

85. Oliver, A.J., "The Prediction of Turbulent Flow and Heat Transfer Over Rearward Facing Steps," Computer Methods in Fluid, London, Pentech Press Ltd., 1980.

86. Spalding, D.B., "A Simple Formula for the "Law of the Wall", J. App. Mech. Trans. ASME, Vol. 28, 1961, pp. 455-457.

87. Durst, F. and Rastogi, A.K., "Turbulent Flow Over 2D-Fences," Turbulent Shear Flows, Vol. 2, Spinger-Verlag, 1980.

88. Roache, P.J. and Mueller, T.J., "Numerical Solutions of Laminar Separated Flows," AIAA Journal, Vol. 8 No. 3, 1970, p. 530.

89. Atkins, D.J., et al. (1980), "Numerical Prediction of Separated Flows". Int. J. Num. Meth. Engrg.," 15, 1980, pp. 129-144.

90. Minh, H.H., and Chassaing, P., "Some Numerical Predictions of Incompressible Turbulent Flows," Proc. 1st Int'l. Conf. on Numerical Methods in Laminar and Turbulent Flow, Swansea, Wales, 1978.

91. Castro, I.P., "The Numerical Prediction of Recirculating Flows," Proc. 1st. Int'l. Conf. on Numerical Methods in Laminar and Turbulent Flow, Swansea, Wales, 1978.

92. Richards, C.W., and Crane, C.M., "The Accuracy of Finite Difference Schemes for the Numerical Solution of the Navier-Stokes Equations" Appl. Math. Modeling, 13, 1979, pp. 205-211.

93. Biringen, S., "Calculation of Axisymmetric Jets and Wakes with a Three-Equation Model of Turbulence," J. Fluid Mech., 86, part 4, 1978, pp. 745-759.

94. Barrett, K.E. and Demunshi, G., "Numerical Methods For Recirculating Flow," Proc. 1st. Int'l. Conf. on Numerical Methods in Laminar and Turbulent Flow, Swansea, Wales, 1978.

95. Patankar, S.V., Numerical Heat Transfer and Fluid Flow, Hemisphere Publishing, 1980.

96. Patankar, S.V., "A Calculation Procedure for Two-Dimensional Elliptic Situations," Num. Heat Transfer, Vol. 4, 1981, pp. 409-425.

97. Raithby, G.D., "Skew Upstream Differencing Schemes for Problems Involving Fluid Flow," Computer Methods Appl. Mec. Eng., Vol. 9, 1976, pp. 153-164.

98. Leonard, B.P., "A Stable and Accurate Convective Modeling Procedure Based on Quadratic Upstream Interpolation," Computer Methods Appl. Mech. Eng., Vol. 19, 1979, pp. 59-98.

99. Leschziner, M.A., "Practical Evaluation of Three Finite Difference Schemes for the Computation of Steady-State Recirculating Flows," Computer Methods Appl. Mech. Eng., Vol. 23, 1980, pp. 293-312.

100. Han, T., Humphrey, J.A.C. and Launder, B.E., "A Comparison of Hybrid and Quadratic-Upstream Differencing in High Reynolds Number Elliptic Flows," Comp. Meth. App. Mech. Engrg., Vol. 28, 1981.

101. Gosman, A.D., "The TEACH-T Computer Program - Strucutre," Flow Heat and Mass Transfer in Turbulent Recirculating Flows - Prediction and Measurements, McGill University, Canada, 1976.

102. Blackwell, B.F., Ph.D. Thesis, Stanford University, 1972.

103. Kays, W.M., and Crawford, M.W., Convective Heat and Mass Transfer, McGraw Hill, New York, 1980.

104. Antonia, R.A., "Behavior of the Turbulent Prandtl Number Near the Wall," Int. J. Heat Transfer, Vol. 23, 1980, pp. 906-908.

105. El-Hawary, M.A. and Nicoll, W.B., "A Relation for the Length-Scale of Turbulence to Mean Flow Characteristics for Flows Close to the Wall," Letters in Heat and Mass Transfer, Vol. 7, 1980, pp. 401-411.

106. Gooray, A., Watkins, C.B. and Aung, W., "Numerical Calculations of Turbulent Heat Transfer Downstream of a Rearward-Facing Step," Proc. 2nd. Int. Cont. Num. Method in Laminar and Turbulent Flow, Venice, Italy, 1981, pp. 639-651.

107. Lam, C.K.G. and Bremhorst, K., "A Modified Form of the k-ε model for Predicting Wall Turbulence," J. Fluids Eng. Trans. ASME, Vol. 103, 1981, pp. 456-460.

108. Launder, B.E. and Ying, W.M., "Prediction of Flow and Heat Transfer in Ducts of Square-Cross-Section," Proc. Inst. Mech. Eng., Vol. 187, 1973, p. 455.

109. Gibson, M.M., Jones W.P. and Younis, B.A., "Calculation of Turbulent Boundary Layers on Curved Surfaces," Phys. Fluids, Vol. 24, No. 3, 1981, pp. 386-395.

110. Ellis, L.B. and Joubert, P.N., "Turbulent Shear Flow in a Curved Duct," J. Fluid Mech., Vol. 62, 1974, pp. 65-84.

111. So, R.M.C., and Mellor, G.L., "Experiment on Convex Curvature Effects in Turbulent Boundary Layers," J. Fluid Mech., Vol. 60, 1973, pp. 43-62.

112. Klebanoff, P.S., "Characteristics of Turbulence in a Boundary Layer with Zero Pressure Gradient," NACA TN, 3178, 1954.

113. Laufer, J. The Structure of Turbulence in Fully Developed Pipe Flow," NACA Rept. 1174, 1954, p. 18.

114. Jayatilleke, C.L.V., "The Influence of Prandtl number and Surface Roughness on the Resistance of the Laminar Sub-Layer to Momentum and Heat Transfer," Prog. Heat Mass Transf., Vol. 1, 1969, p. 193.

115. Eckert, E.R.G. and Drake, R.M., Analysis of Heat and Mass Transfer, McGraw Hill, New York, 1972.

116. Zemanick, P.A., "Local Heat Transfer Downstream of Abrupt Expansion in Circular Channel with Subsonic Turbulent Air Flow," Ph.D. Thesis, Univ. of Pittsburgh, 1968.

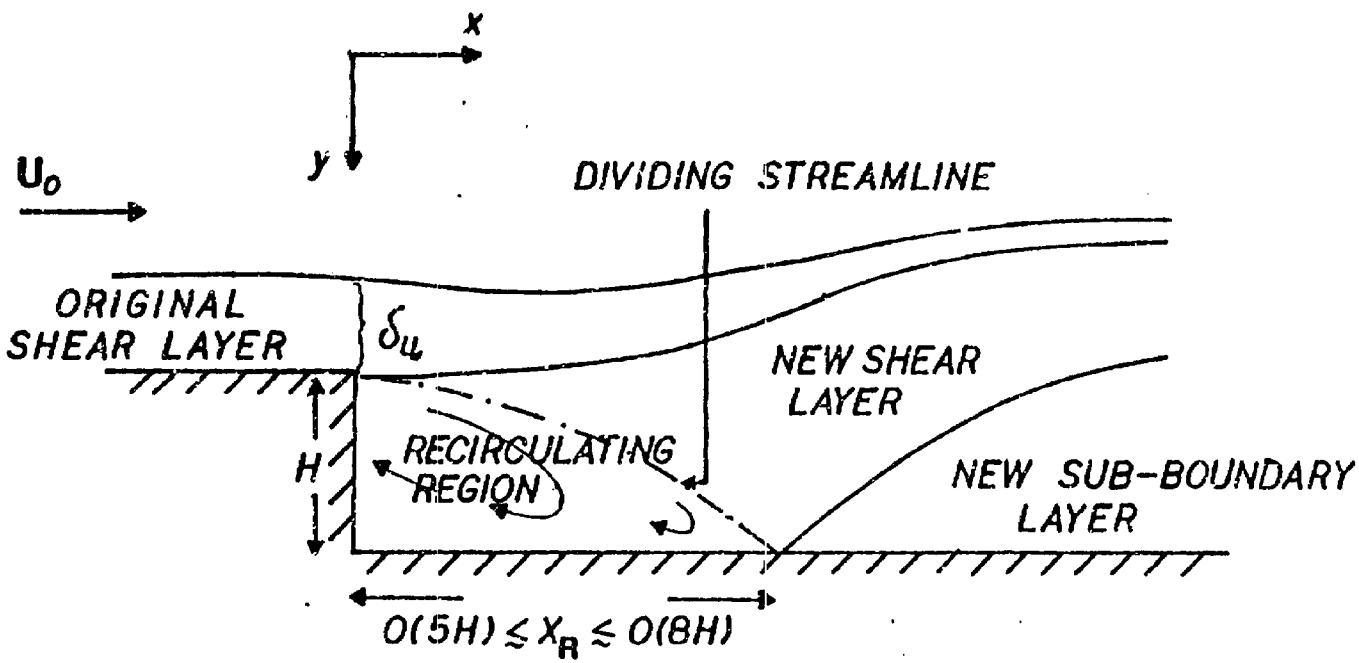

Figure 1. General Behavior of Reattaching Flow

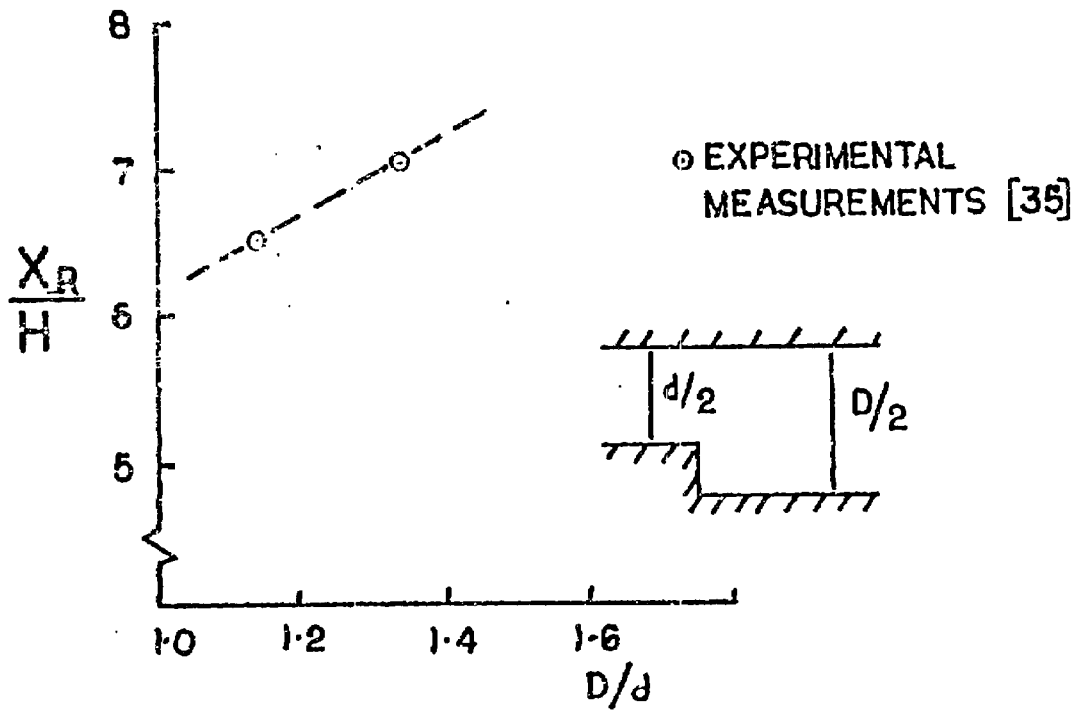

Figure 2. Effect of Pressure Gradient Due to Spacing Between Step and Wall on Reattachment Length

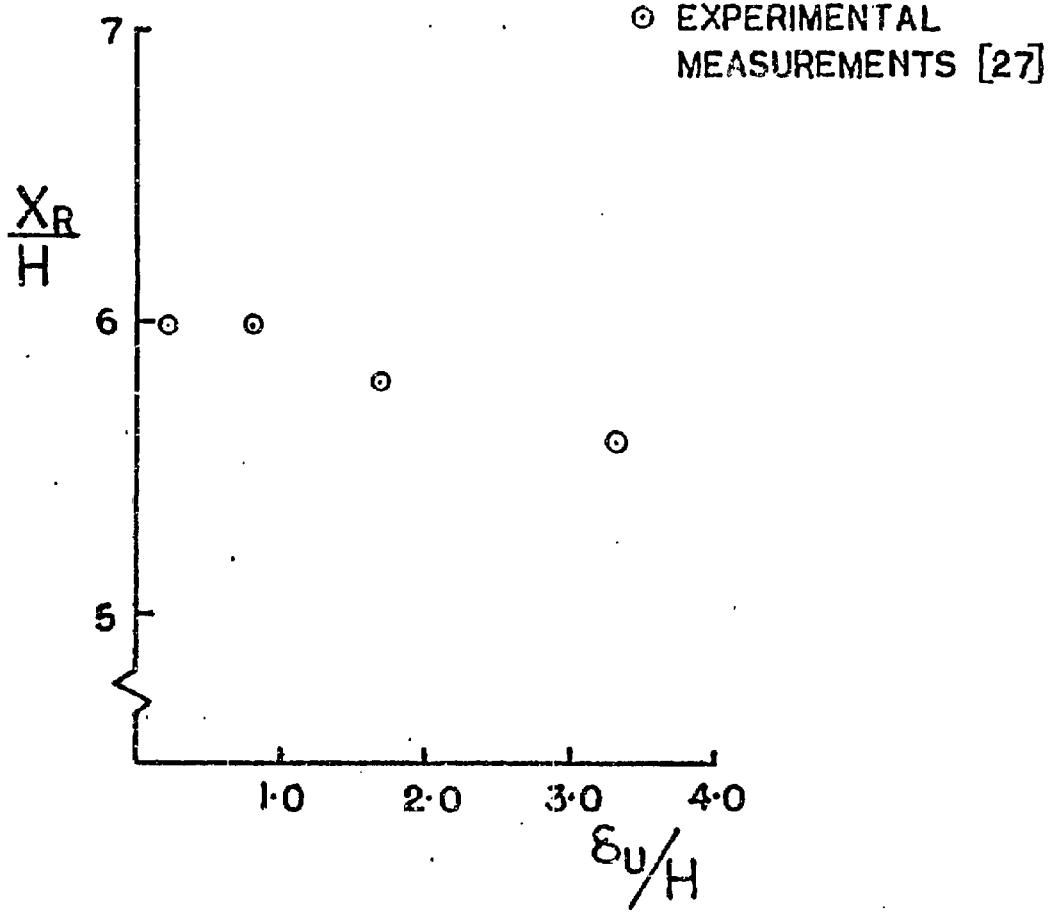

Figure 3. Effect of Approach Boundary Layer Thickness On Reattachment Length

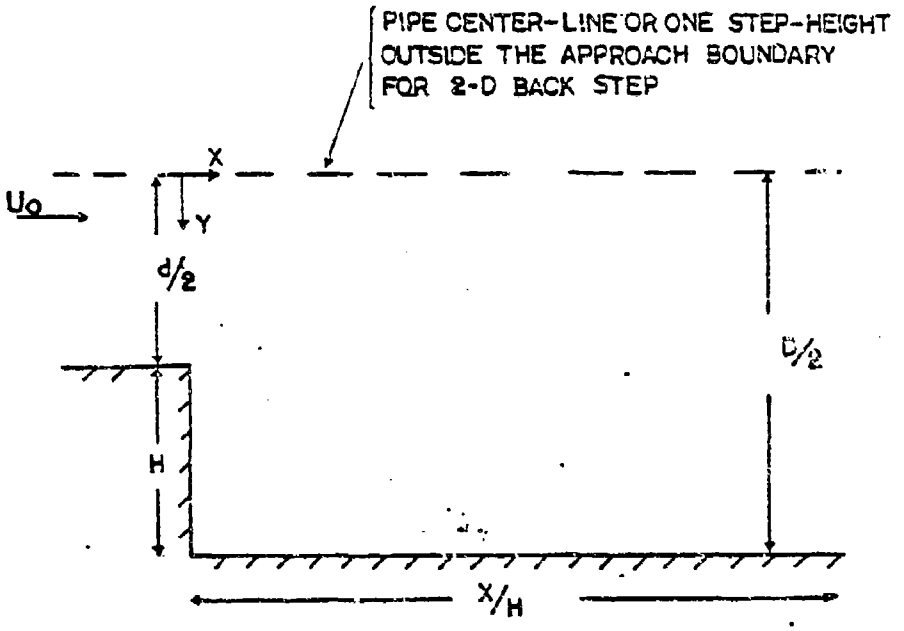

Figure 4. Geometrical Representation of Two-Dimensional Back-Step and Sudden Pipe Expansion

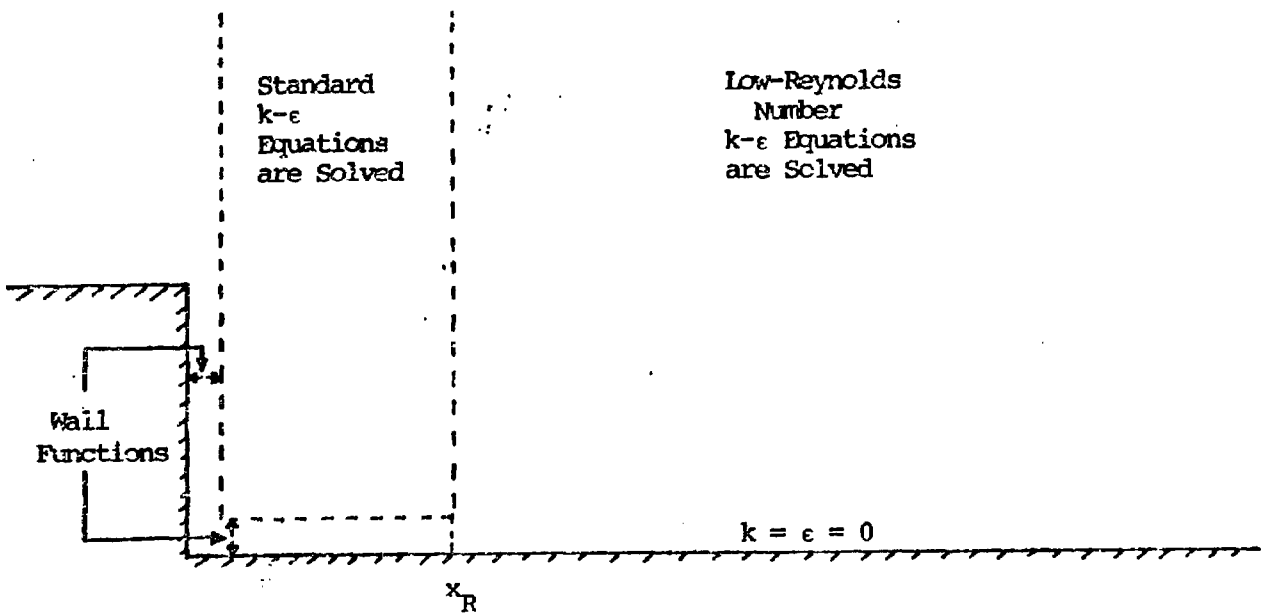

Figure 5. Solution Domain for Second-Pass Procedure

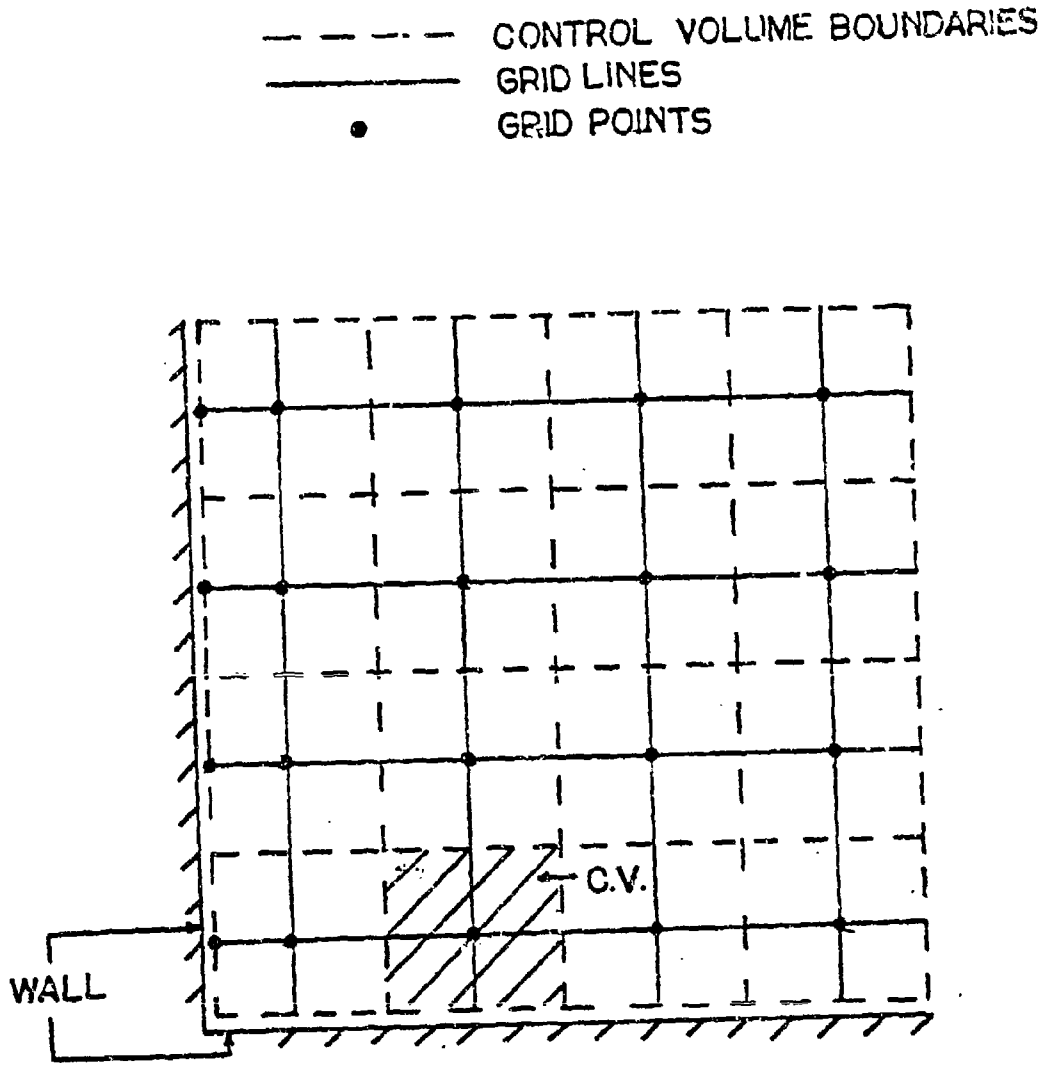

Figure 6. Control Volume and Grid Nodes Distribution

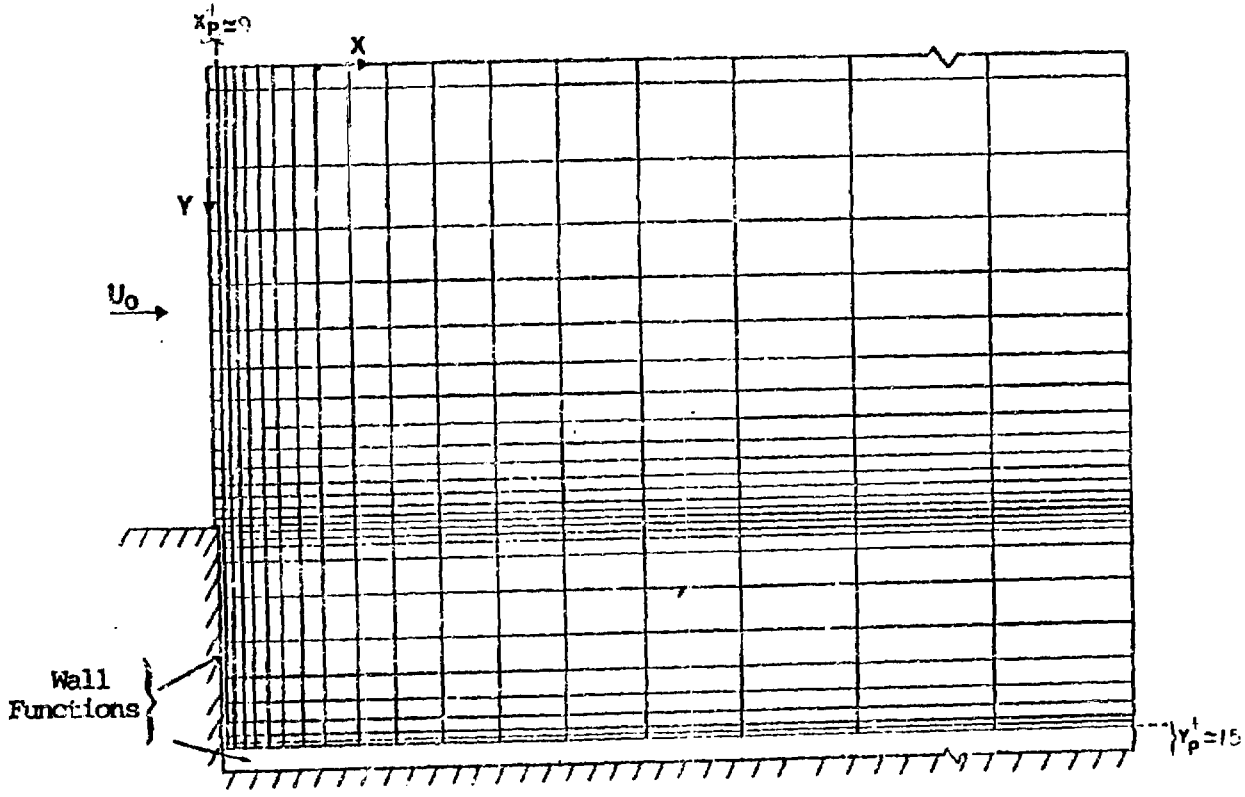

Figure 7. Typical Grid Distribution in Single-Pass Procedure

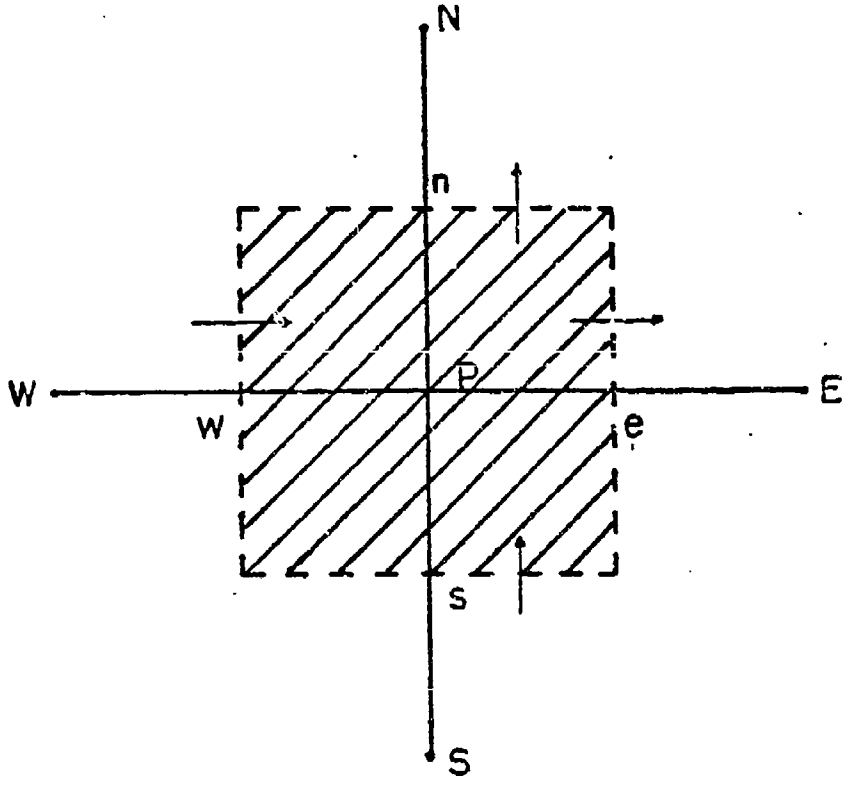

Figure 8. Control Volume for Node P

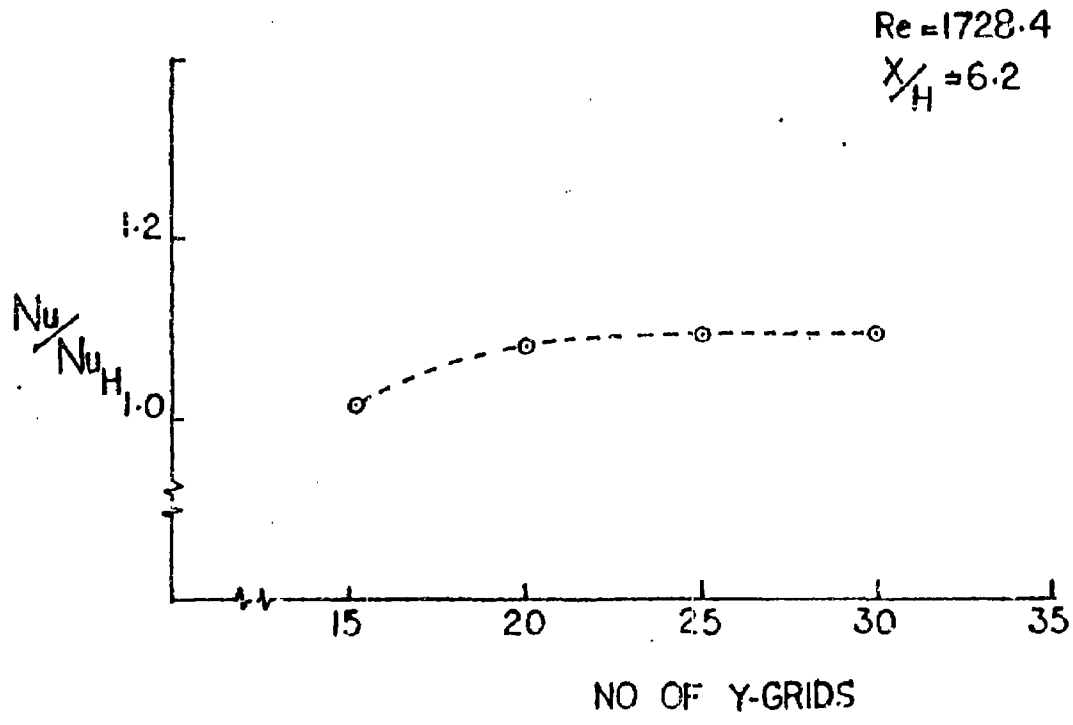

Figure 9. Procedure for Establishing Grid-Independent Solutions

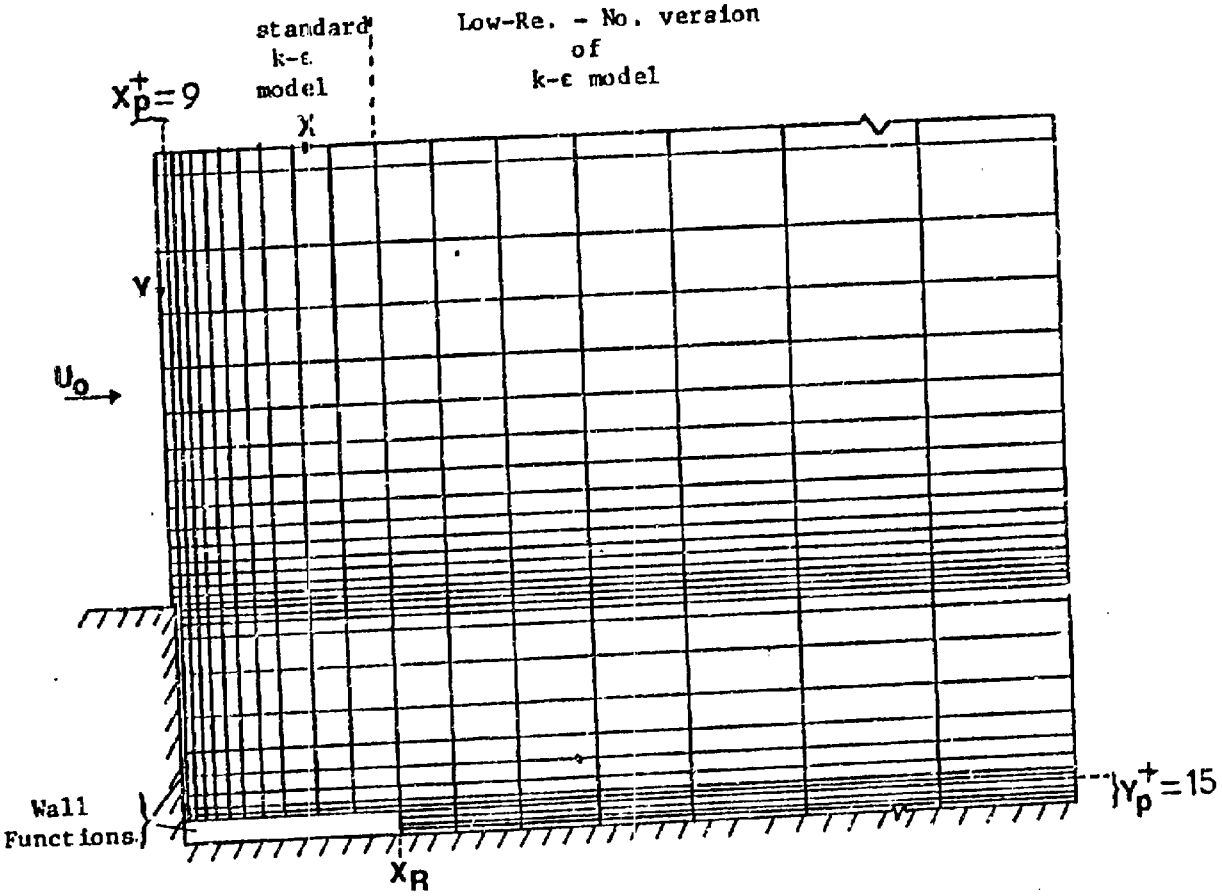

Figure 10. Typical Grid Distribution in Two-Pass Procedure

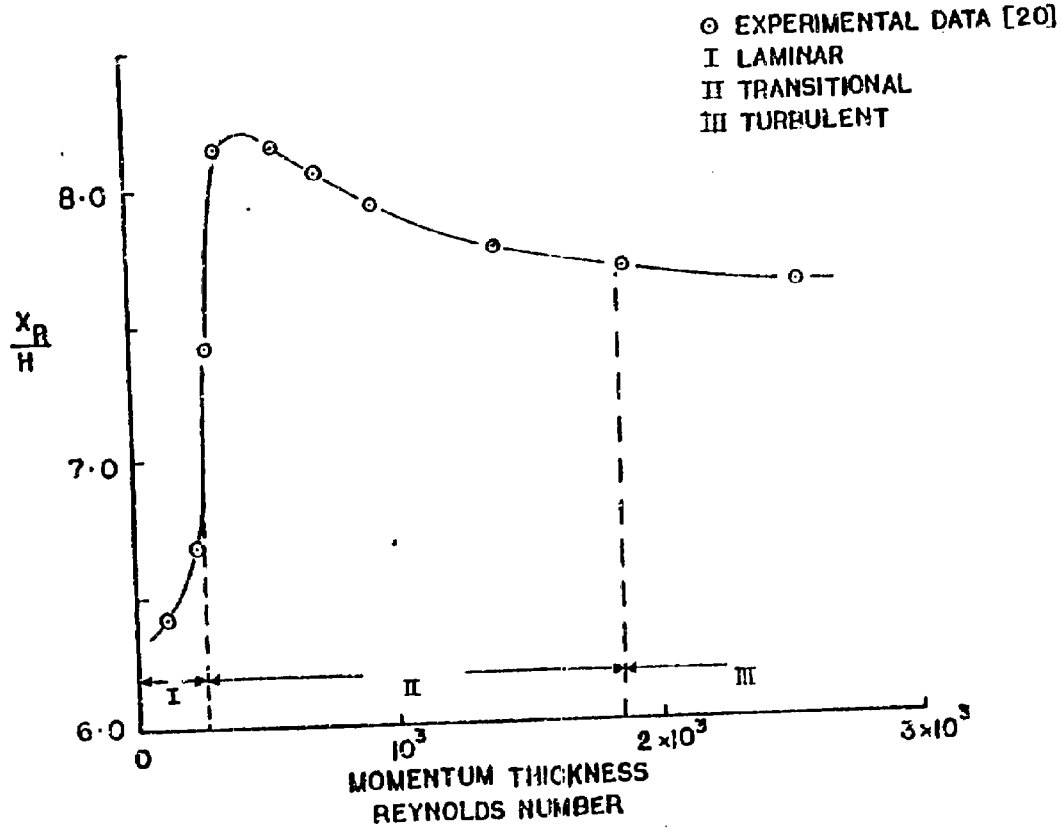

Figure 11. Effects of Reynolds Number on Reattachment Lengths

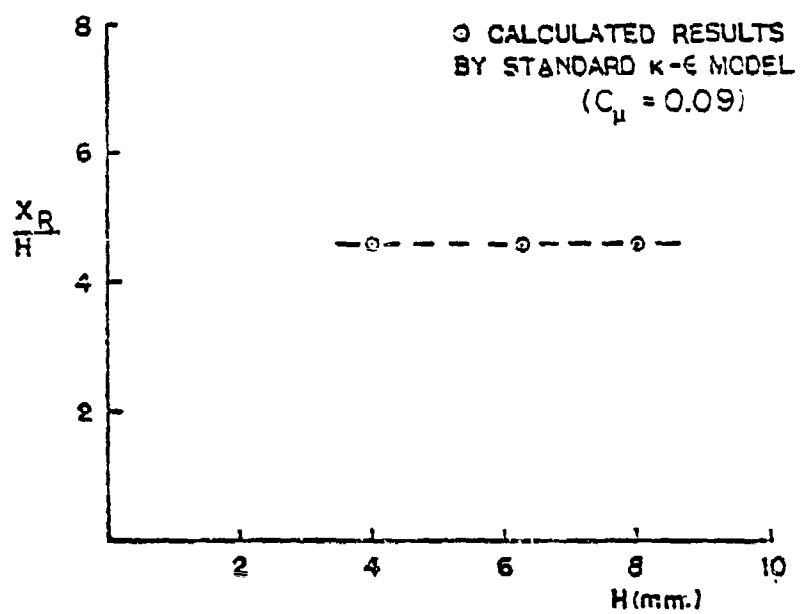

Figure 12. Effects of Step Height on Reattachment Length

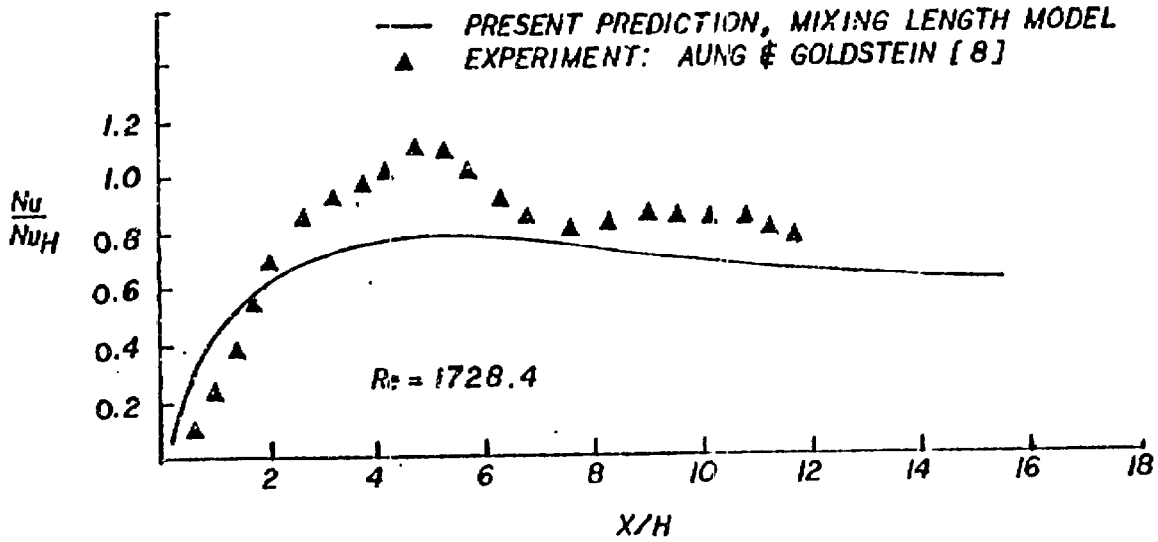

Figure 13. Streamwise Variation of Nusselt Number Downstream of Step for Mixing Length Model

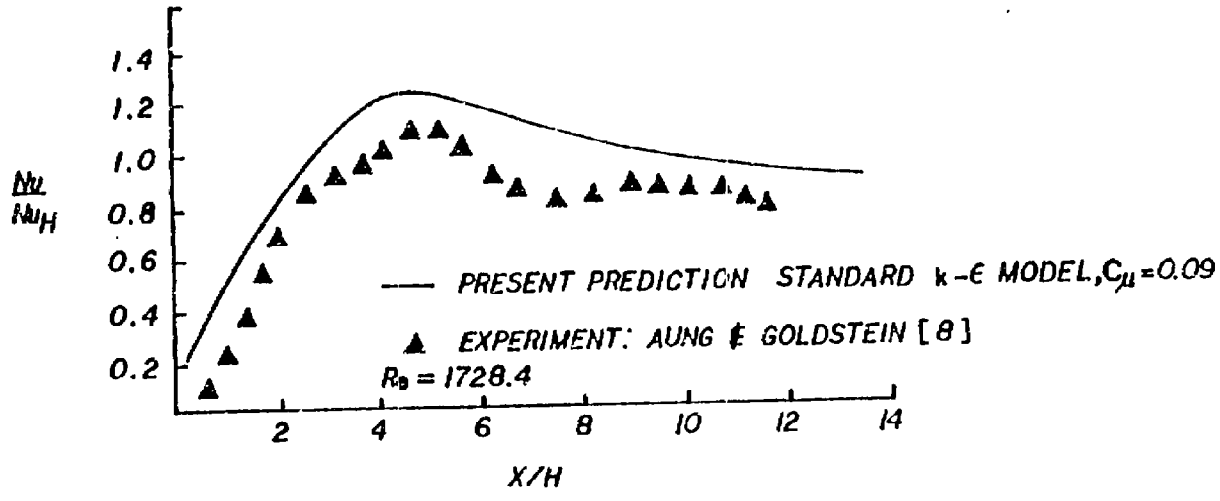

Figure 14. Streamwise Variation of Nusselt Number Downstream of Step for Standard k-ε Model

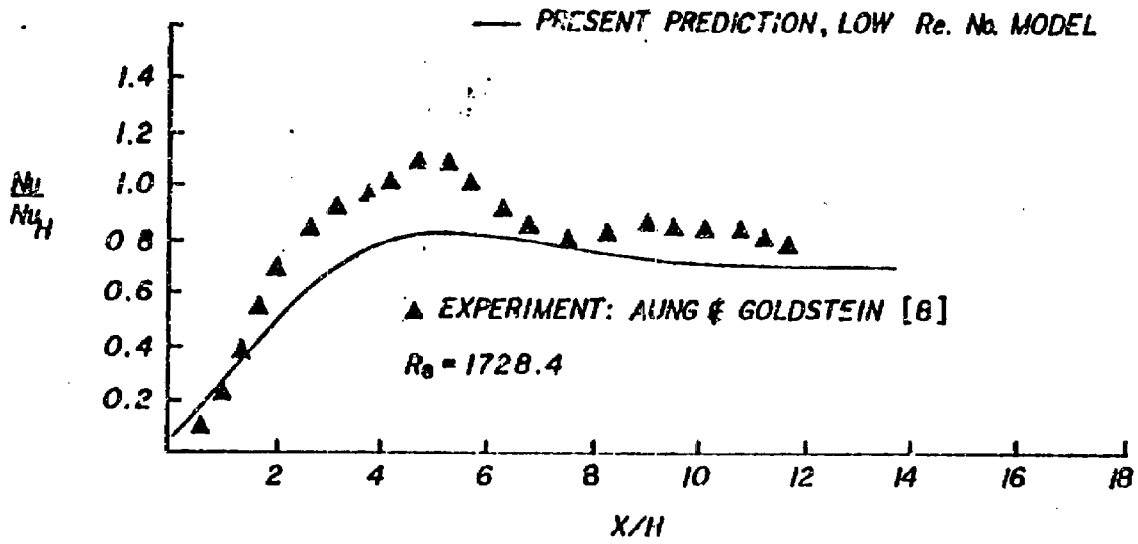

Figure 15. Streamwise Variation of Nusselt Number Downstream of Step for Low-Reynolds Number

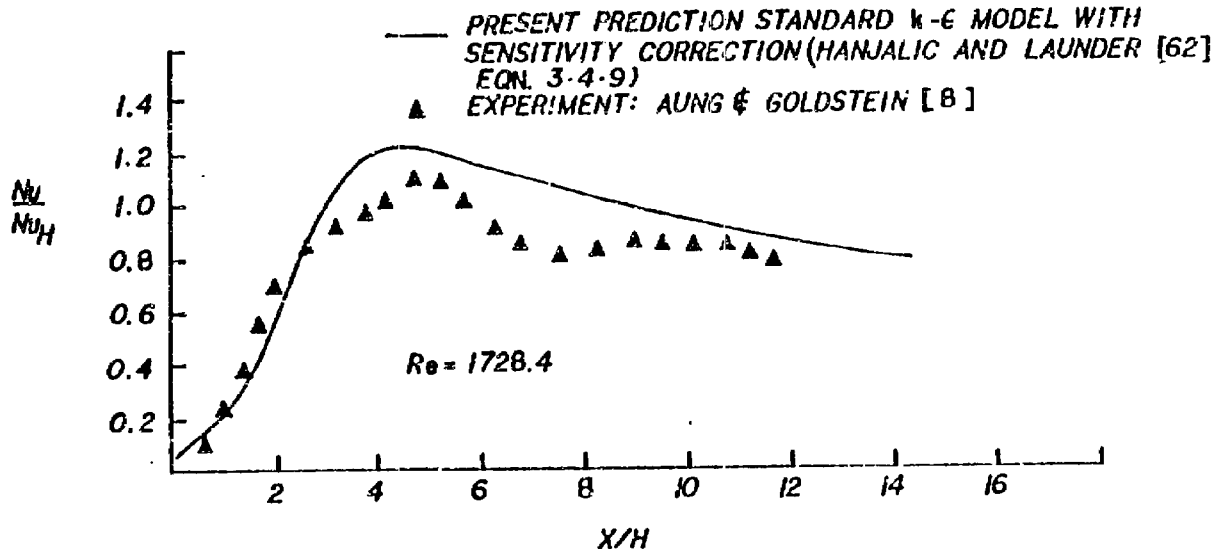

Figure 16. Streamwise Variation of Nusselt Number Downstream of Step for 'Sensitized' ε-Equation

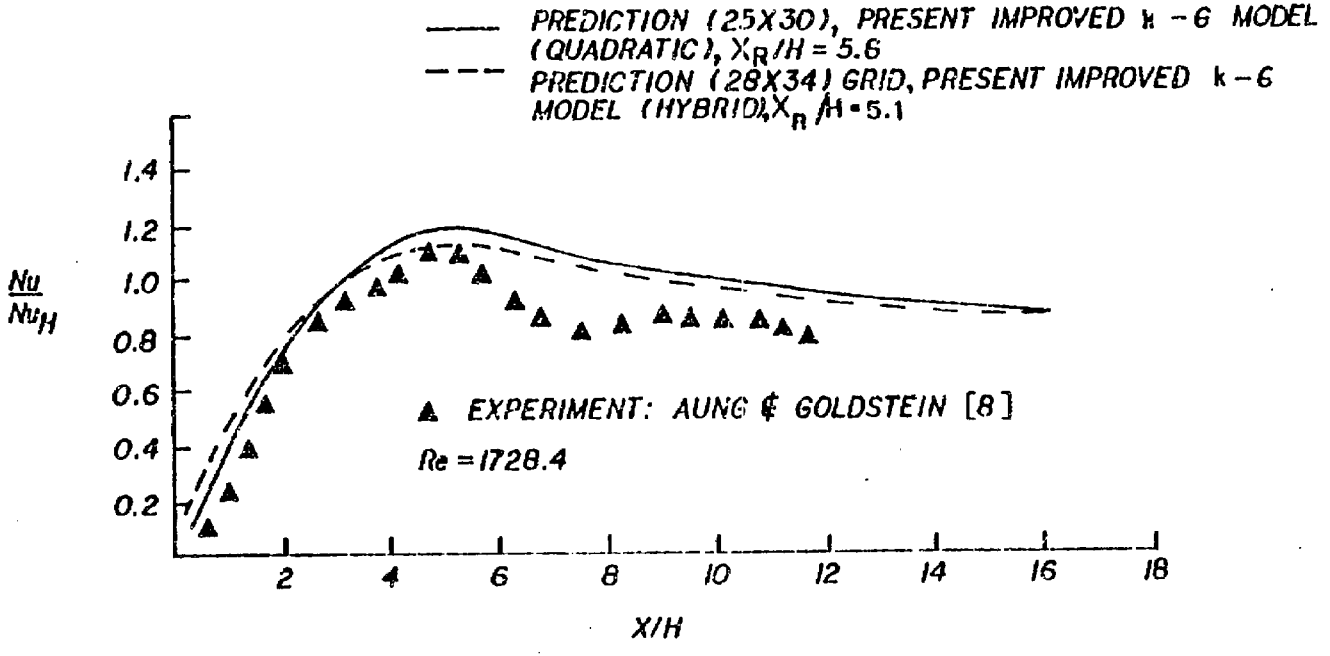

Figure 17. Comparison of Streamwise Nusselt Number Downstream of Step by Quadratic and Hybrid Differencing Schemes for Present Improved k-ε Model

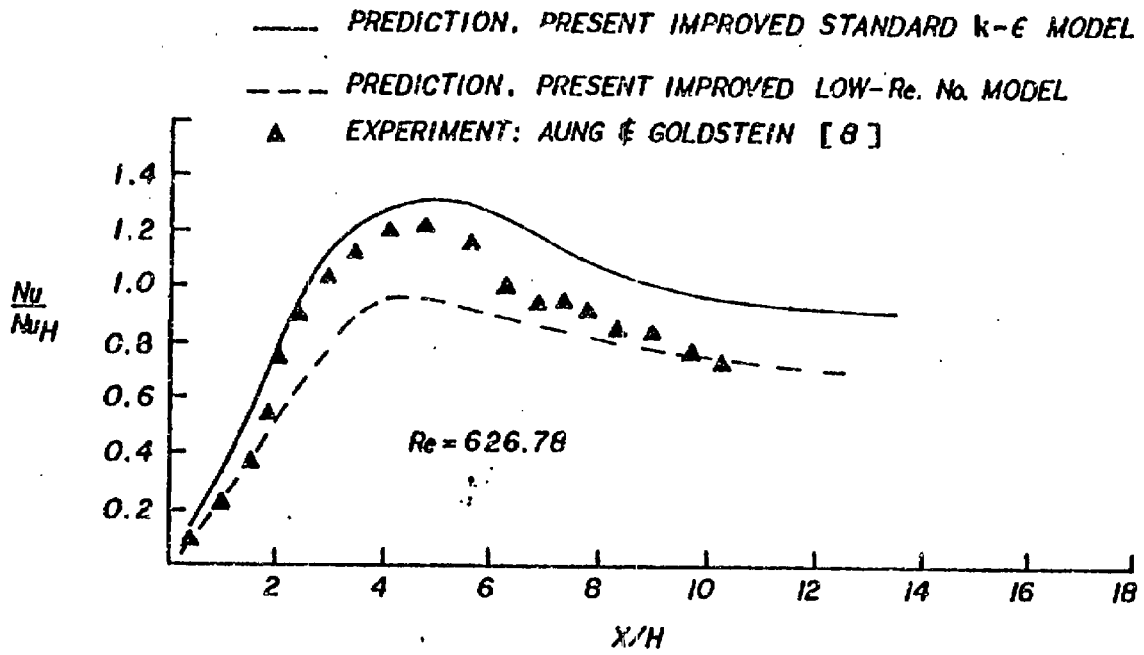

Figure 18. Streamwise Variation of Nusselt Number Downstream of Step for Present Improved Standard k-ε and Low-Reynolds Number Models

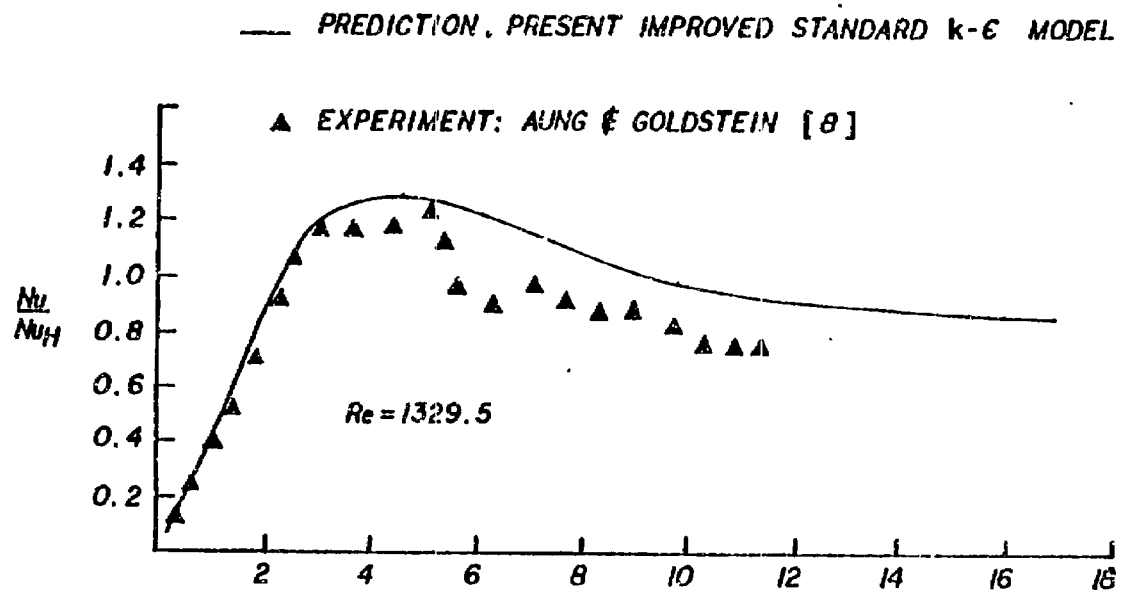

Figure 19. Streamwise Variation of Nusselt Number Downstream of Step for Improved Standard k-ε Model

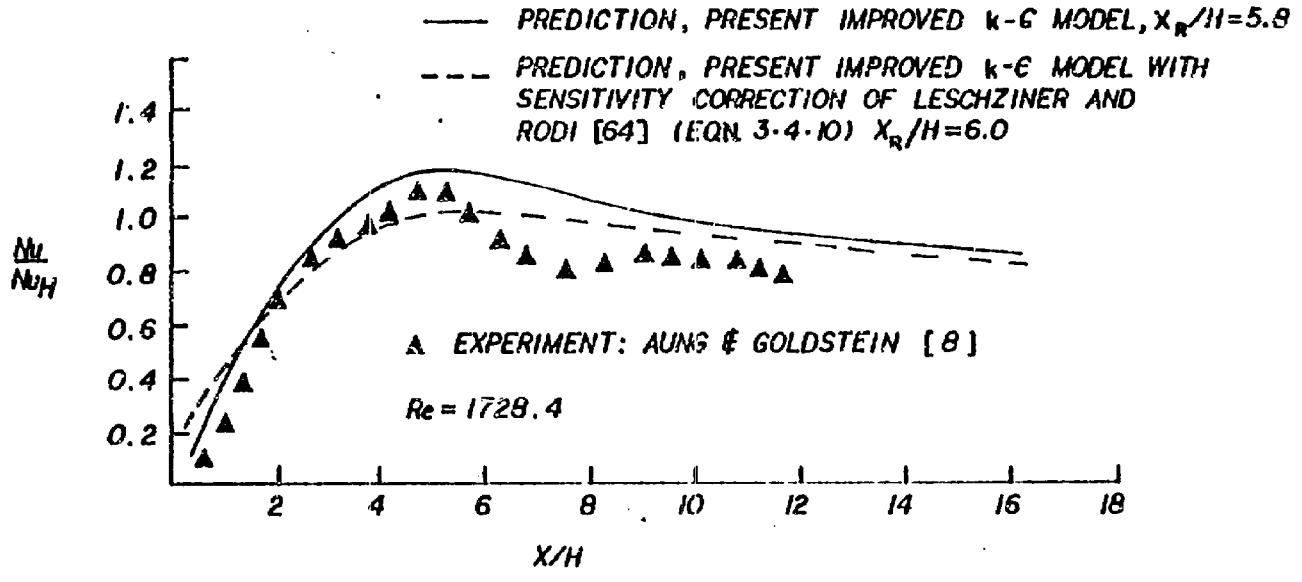

Figure 20. Streamwise Variation of Nusselt Number Downstream of Step for Improved Standard k-ε and 'Sensitized' ε- Equation Models

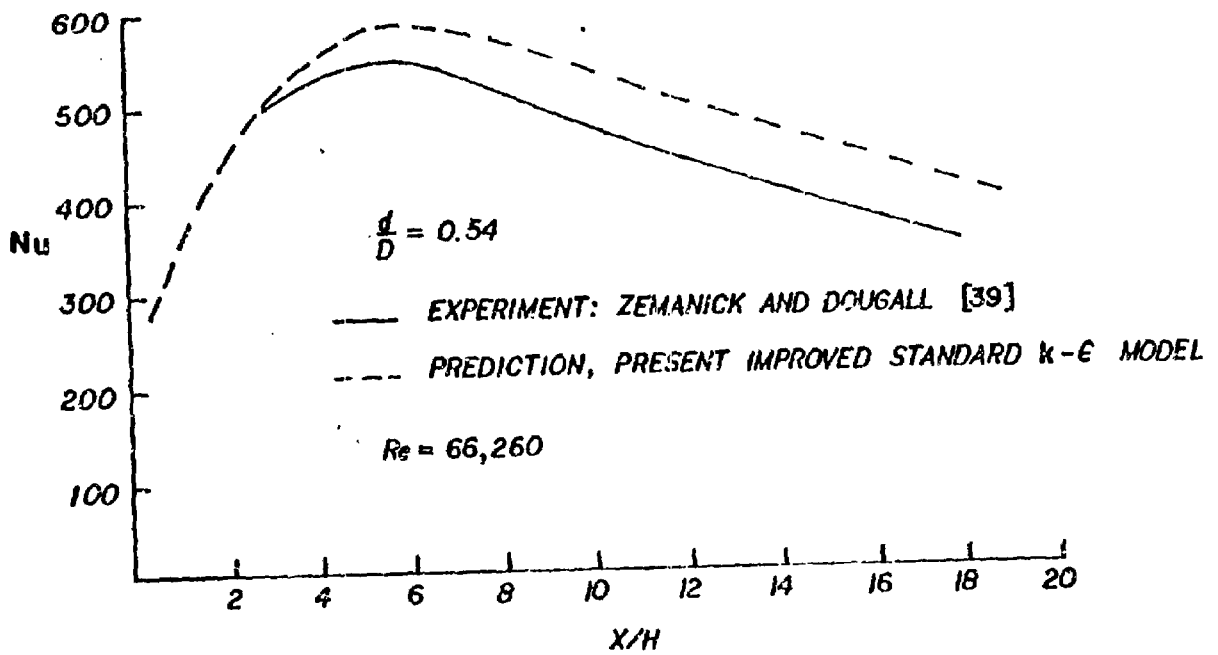

Figure 21. Streamwise Variation of Nusselt Number Downstream of Pipe Expansion for Present Improved Standard k-ε Model

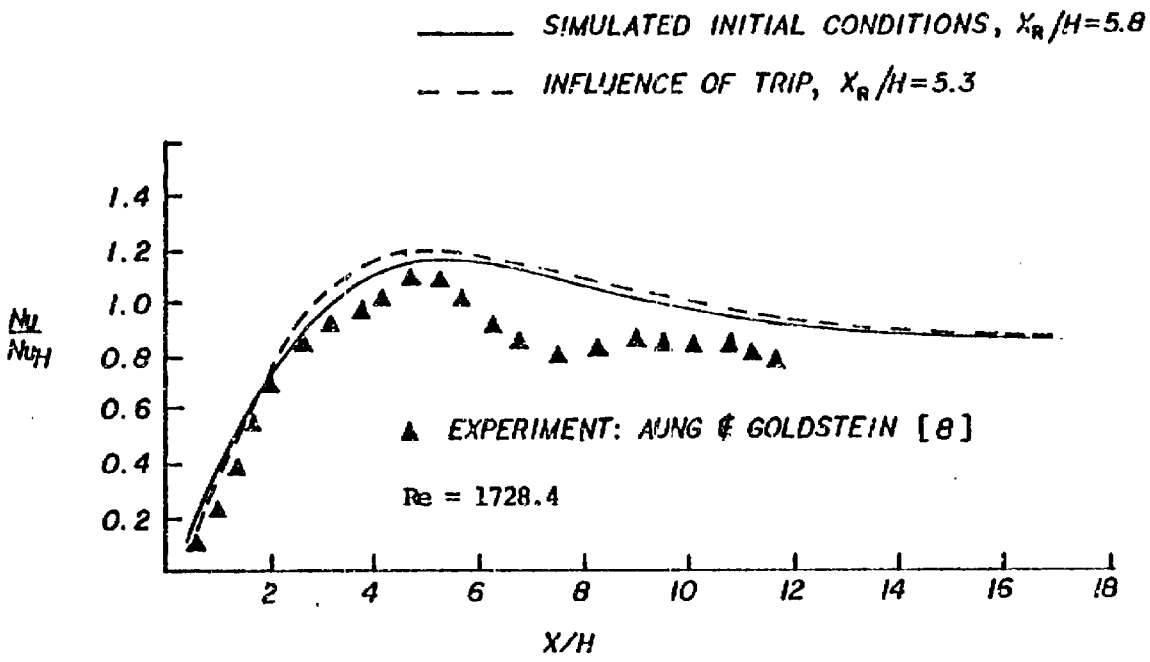

Figure 22. Effects of Initial Conditions on Streamwise Variation of Nusselt Number Downstream of Step for Present Improved Standard k-ε Model

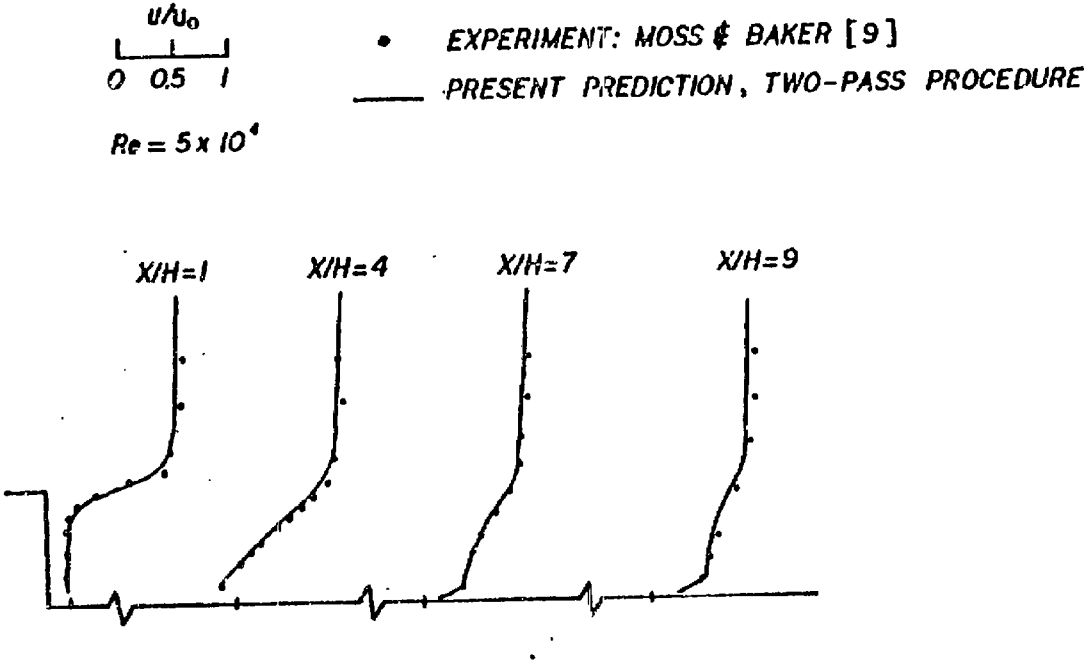

Figure 23. Streamwise Mean Velocity Downstream of Step

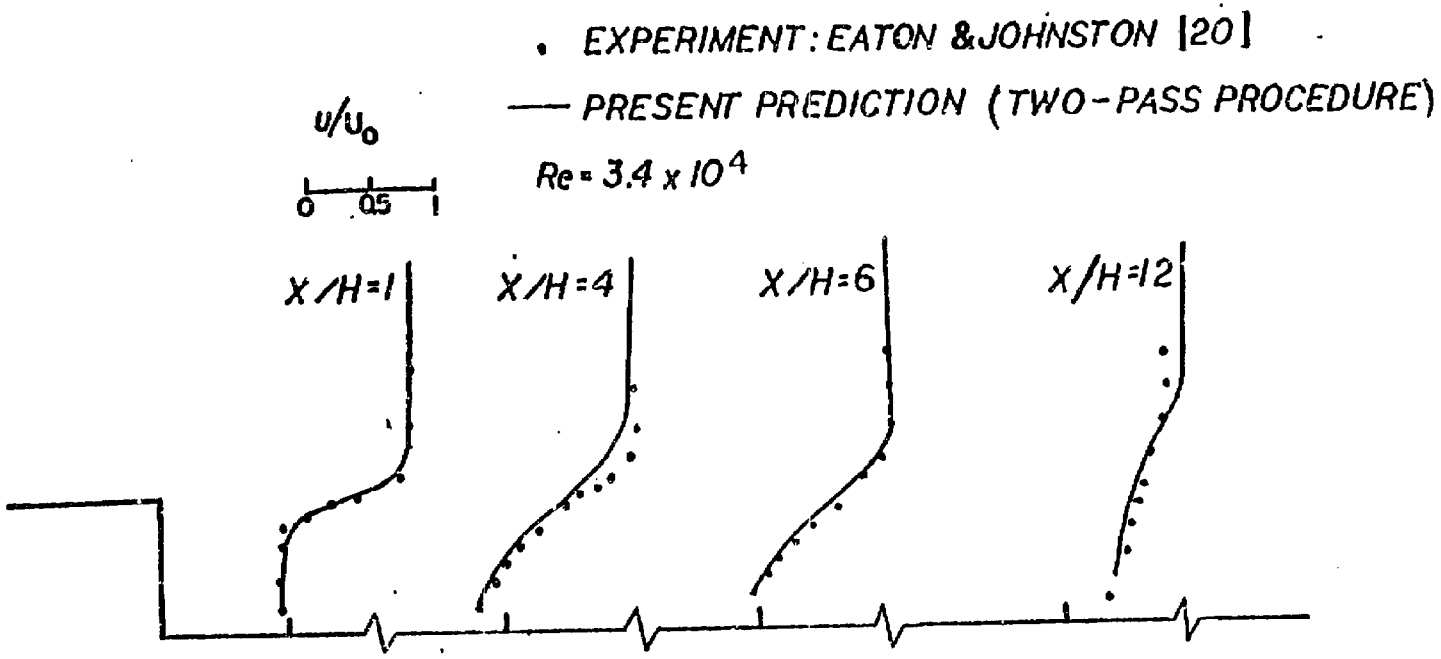

Figure 24. Streamwise Mean Velocity Downstream of Step

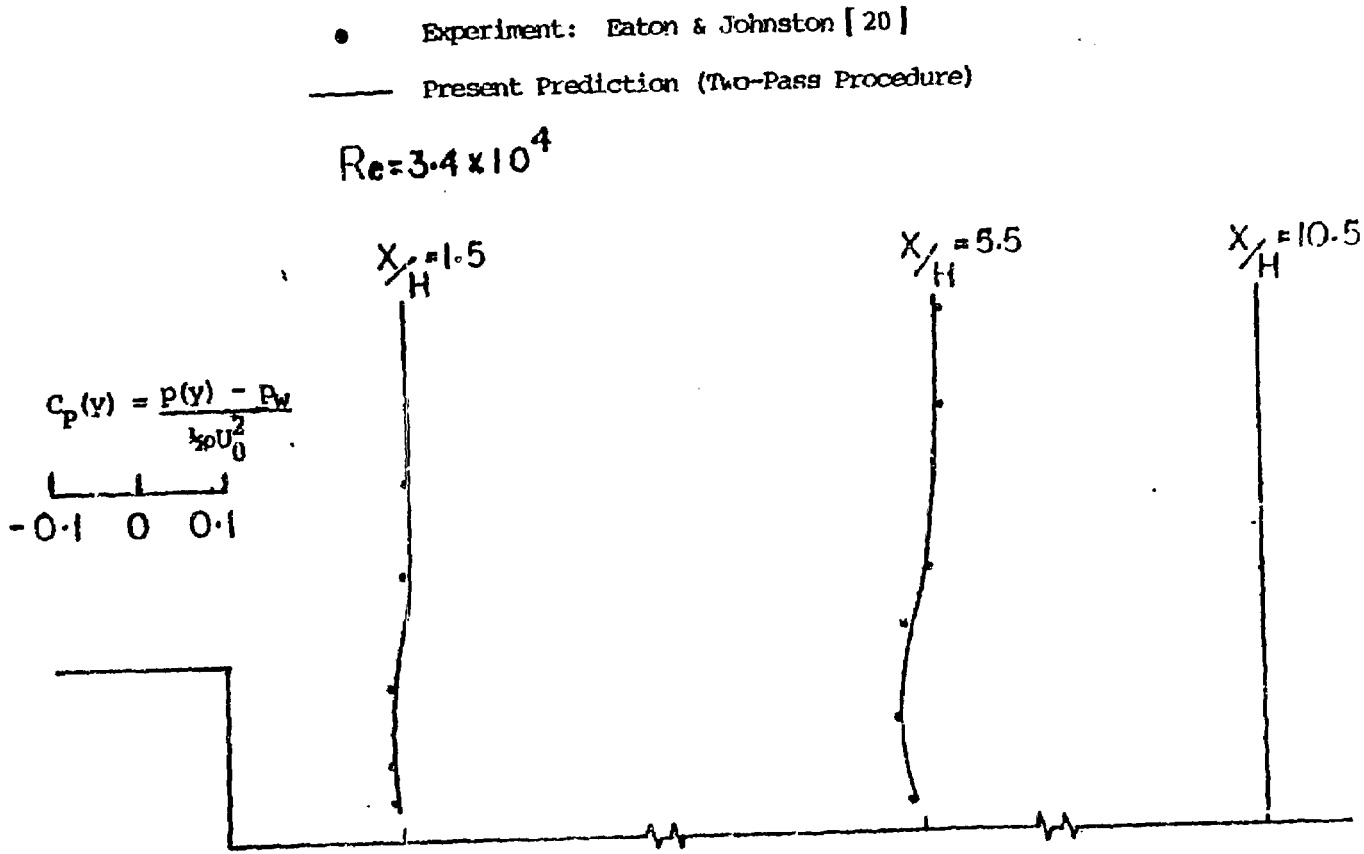

Figure 25. Cross Stream Pressure Variation for Back-Step

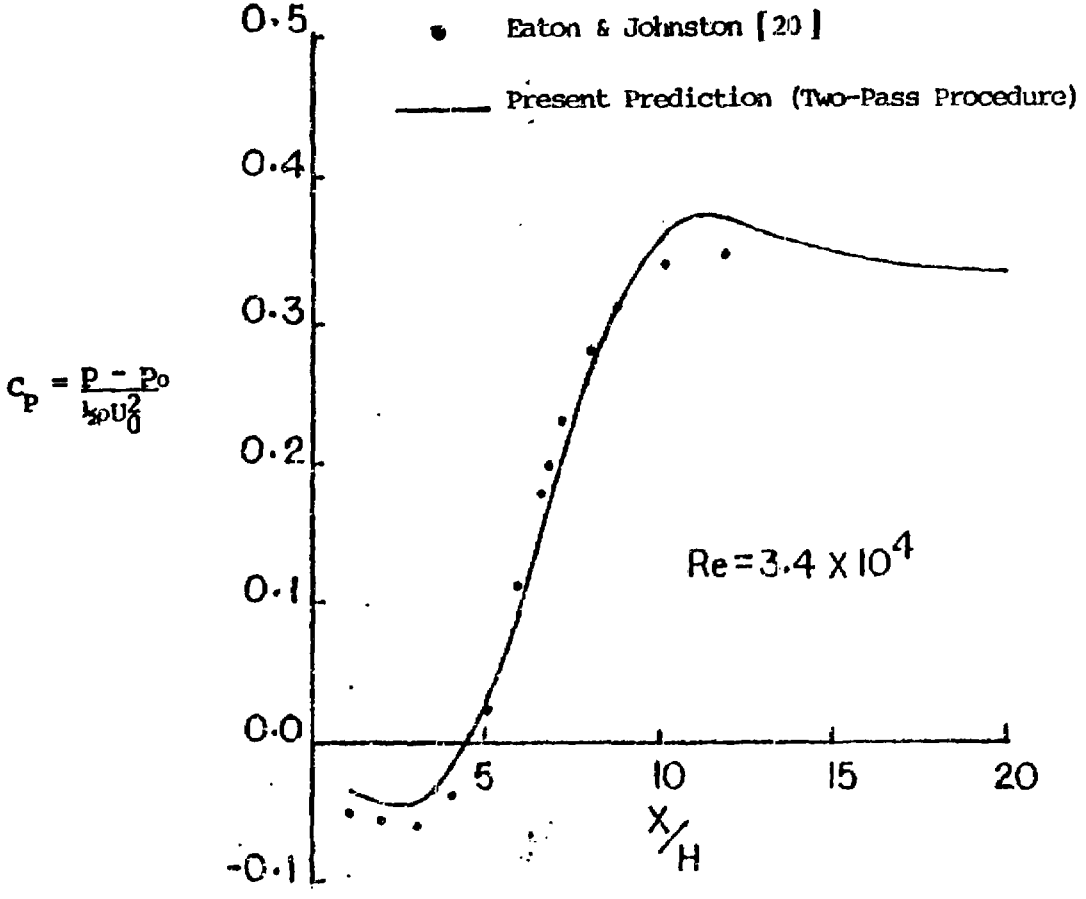

Figure 26. Streamwise Surface Pressure Coefficient Downstream of Step

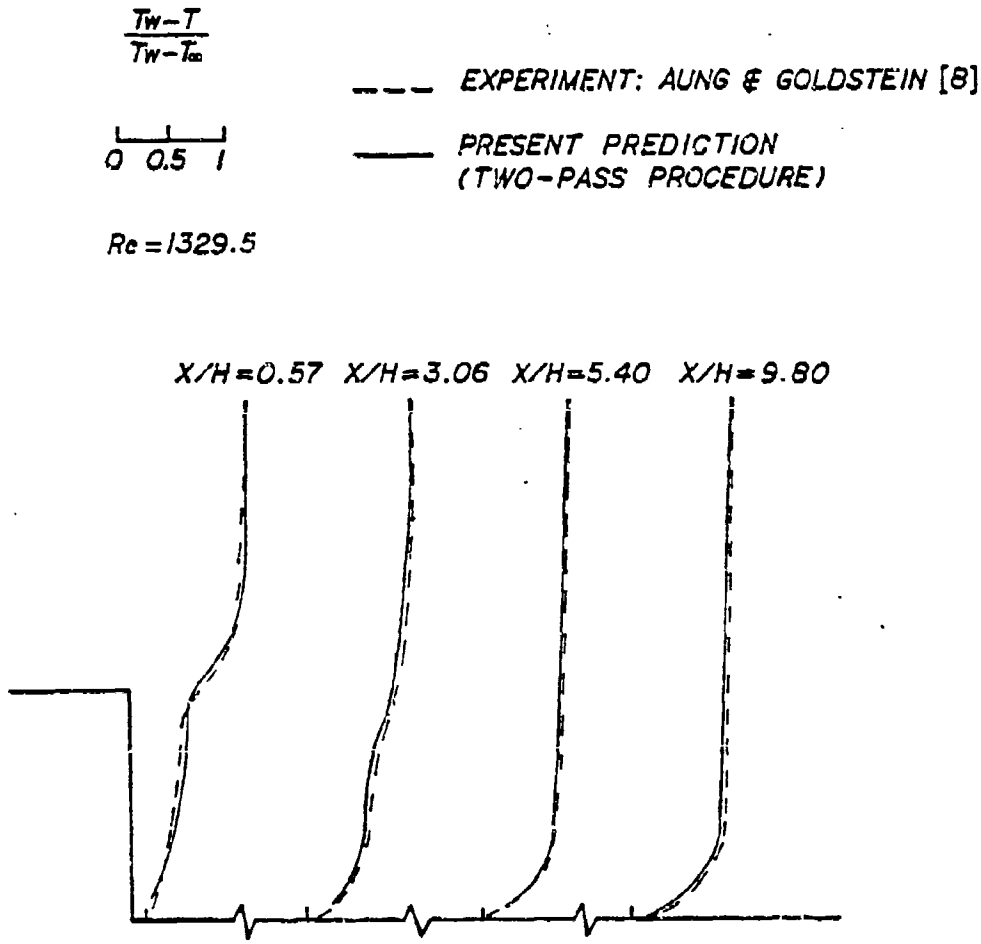

Figure 27. Temperature Distribution Downstream of Step

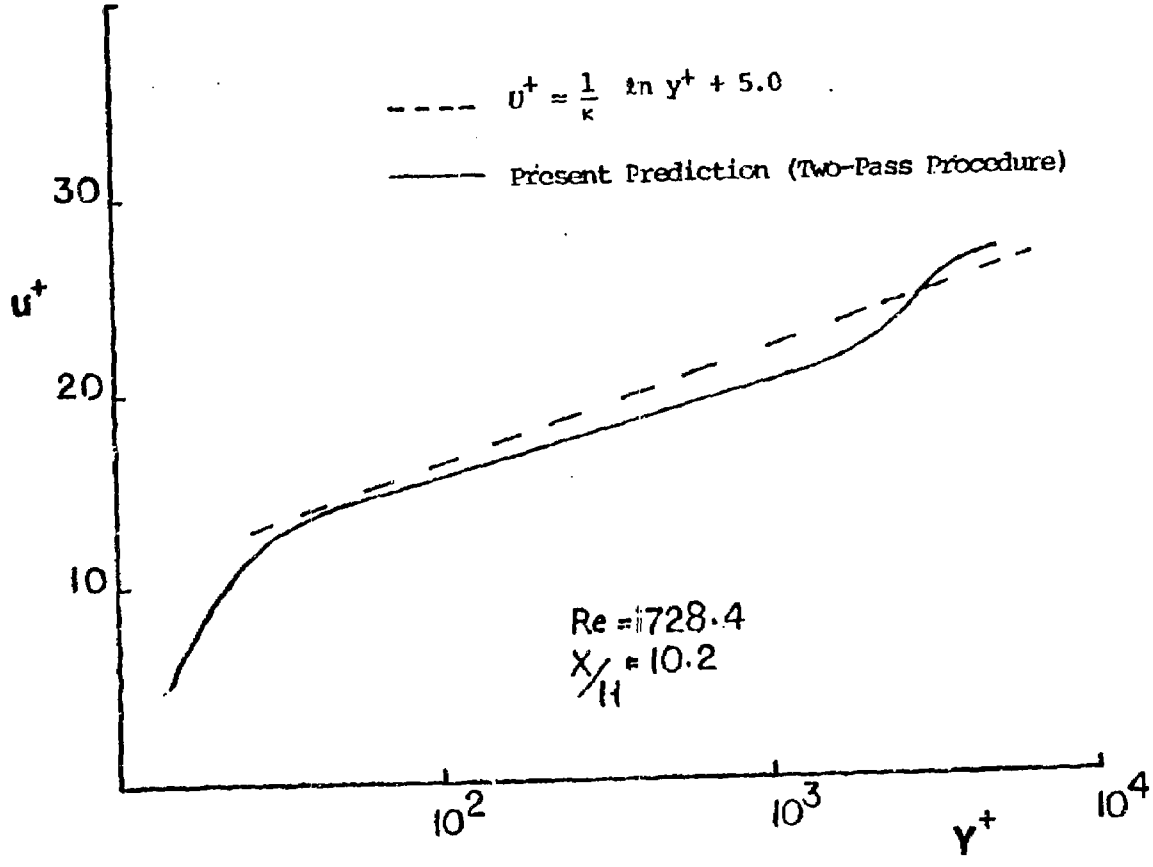

Figure 28. Mean Velocity Profile in Reattached Boundary Layer for Back-Step

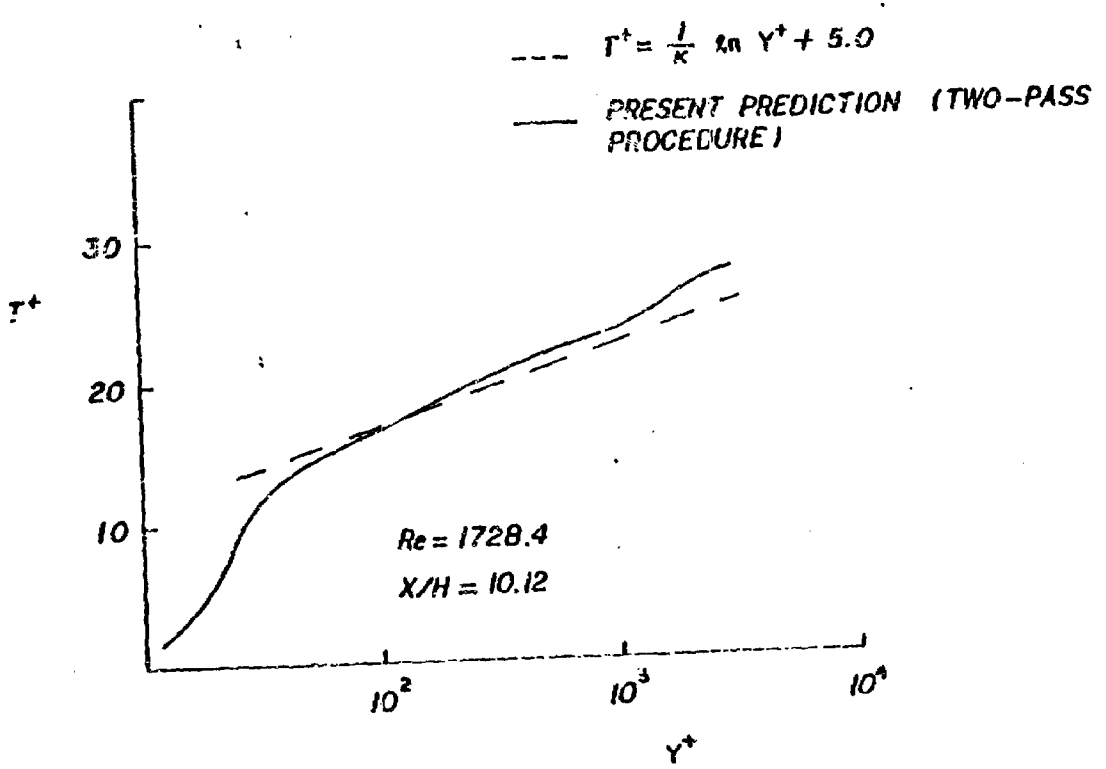

Figure 29. Mean Temperature Profile in Reattached Boundary Layer for Back-Step

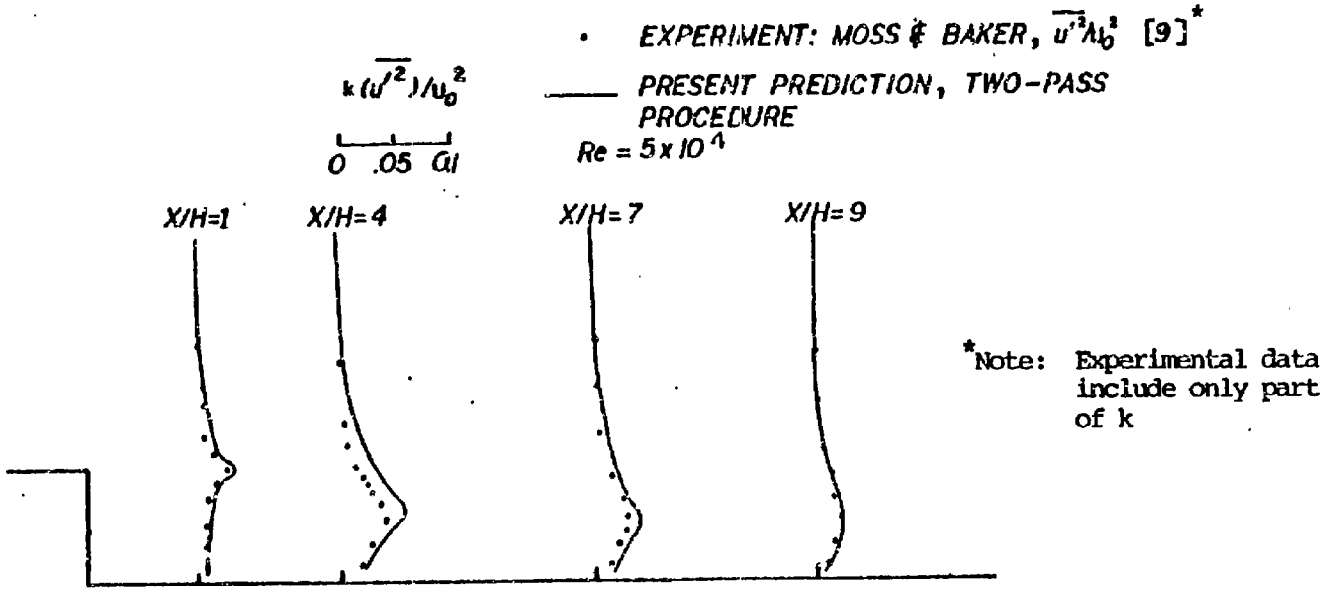

*Note: Experimental data include only part of k

Figure 30. Turbulent Kinetic Energy Downstream of Step

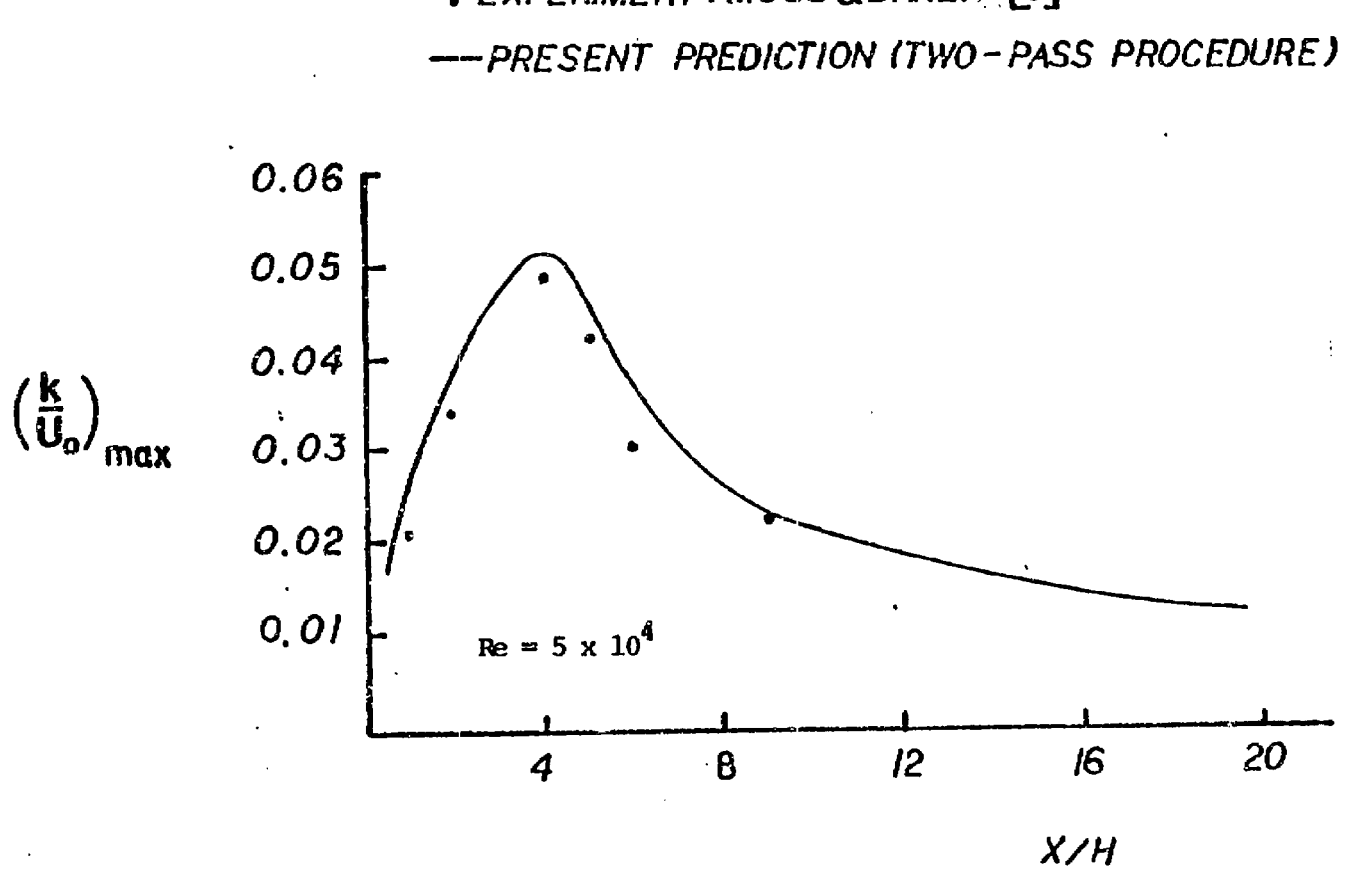

Figure 31. Peak Values of Turbulent Kinetic Energy Downstream of Step

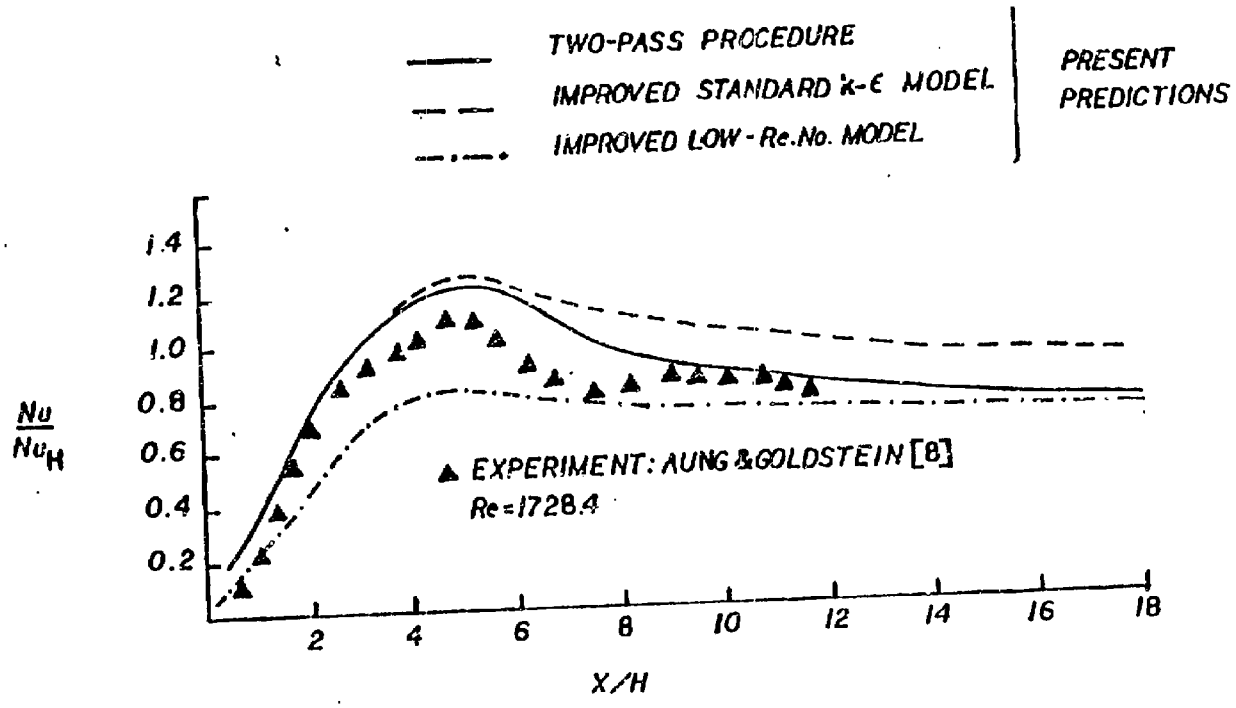

Figure 32. Streamwise Variation of Nusselt Number Downstream of Step for Single and Two-Pass Procedures

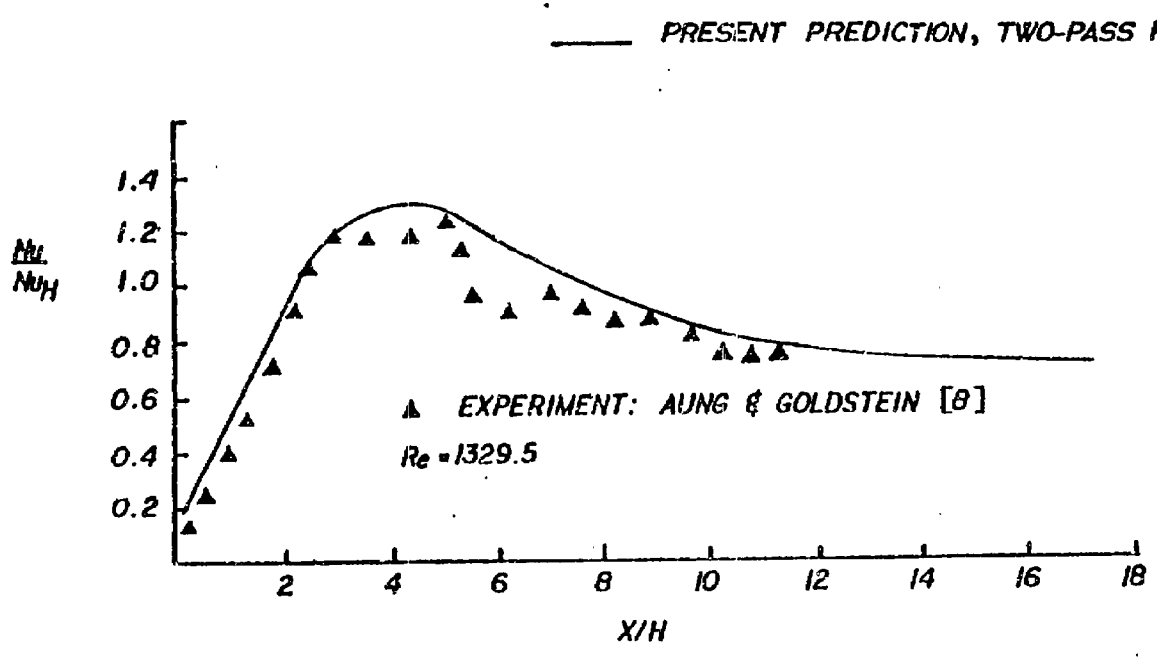

Figure 33. Streamwise Variations of Nusselt Number Downstream of Step for Two-Pass Procedure

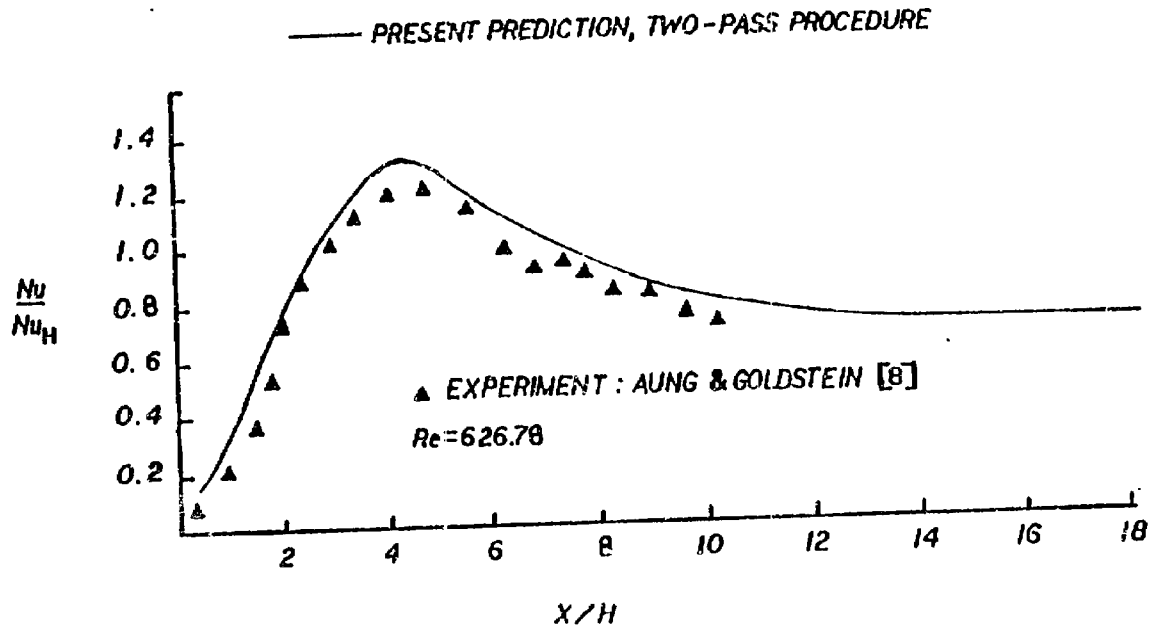

Figure 34. Streamwise Variation of Nusselt Number Downstream of Step for Two-Pass Procedure

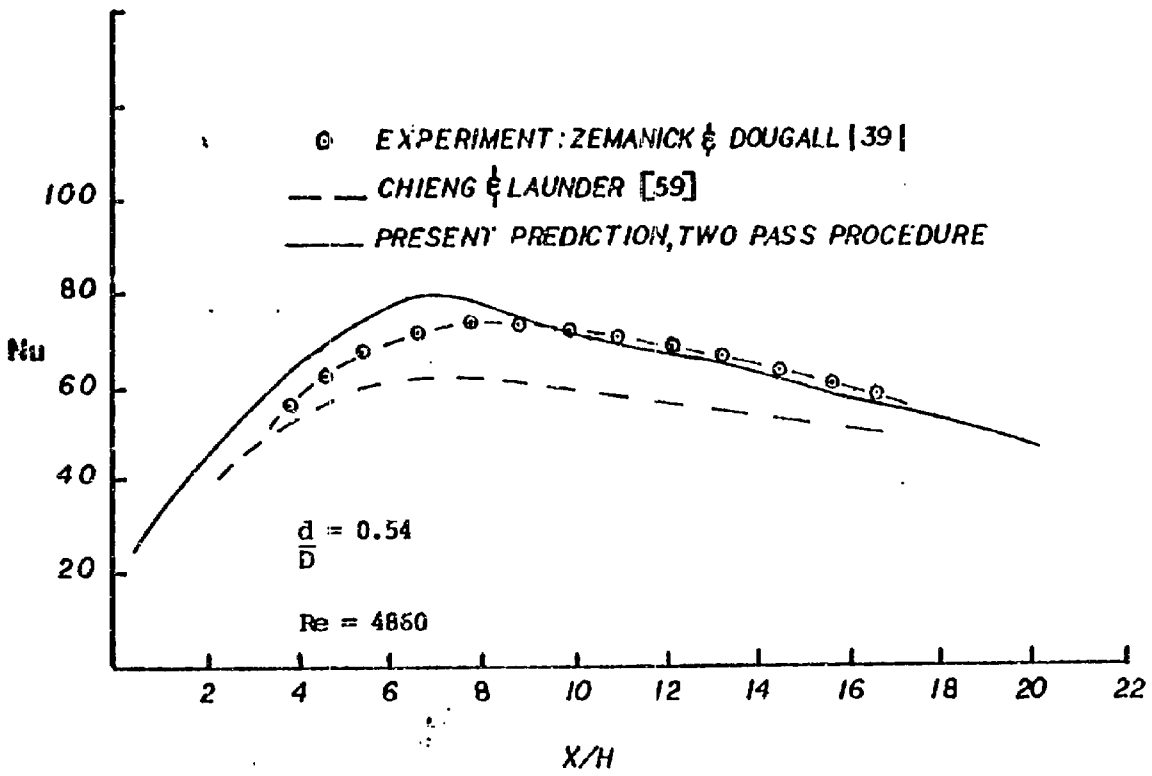

Figure 35. Streamwise Variation of Nusselt Number Downstream of Sudden Pipe Expansion for Two-Pass Procedure

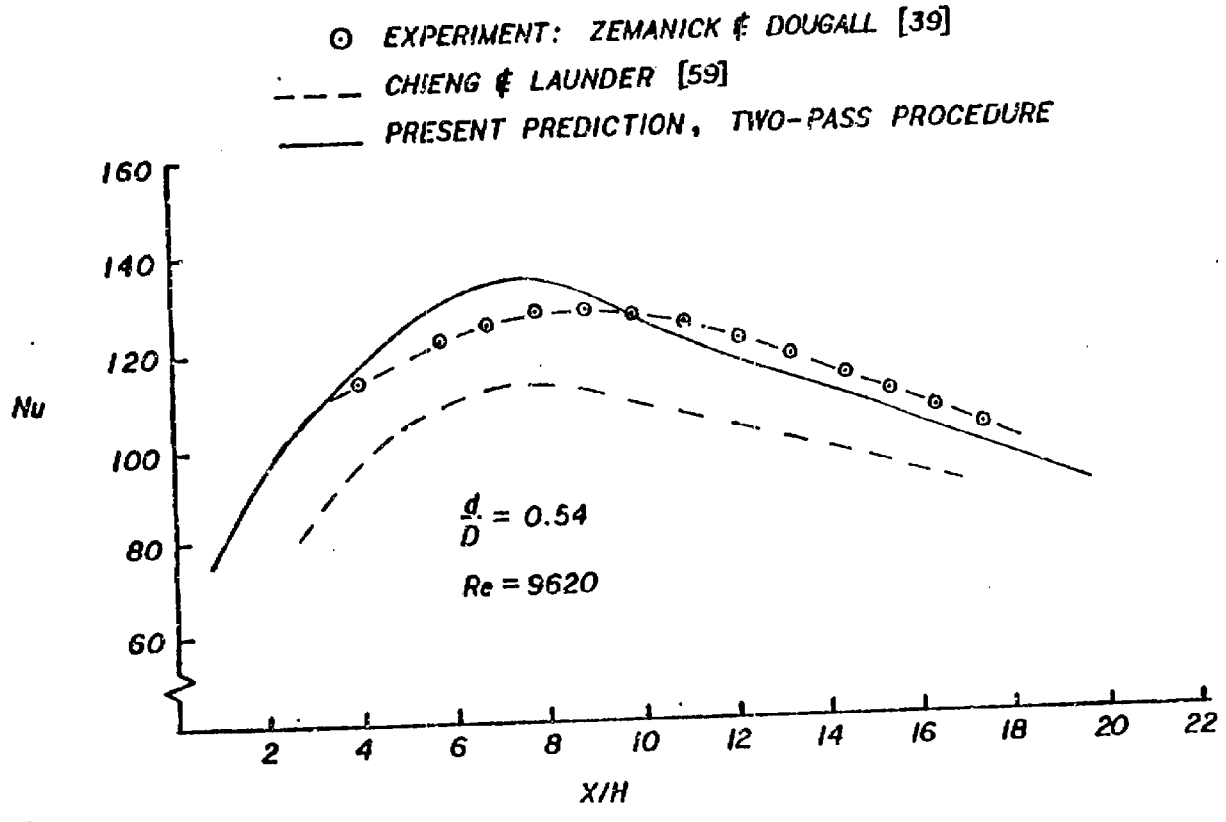

Figure 36. Streamwise Variation of Nusselt Number Downstream of Sudden Pipe Expansion for Two-Pass Procedure

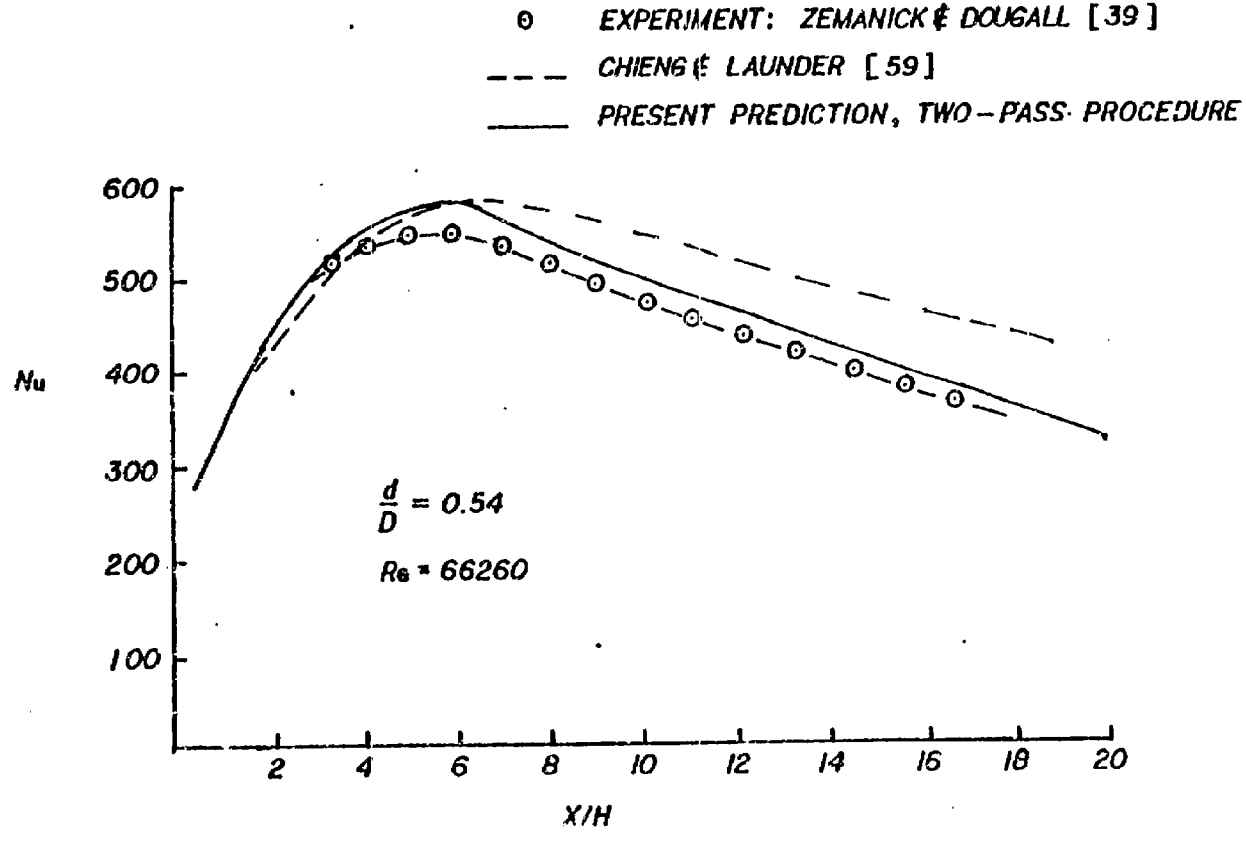

Figure 37. Streamwise Variation of Nusselt Number Downstream of Sudden Pipe Expansion for Two-Pass Procedure

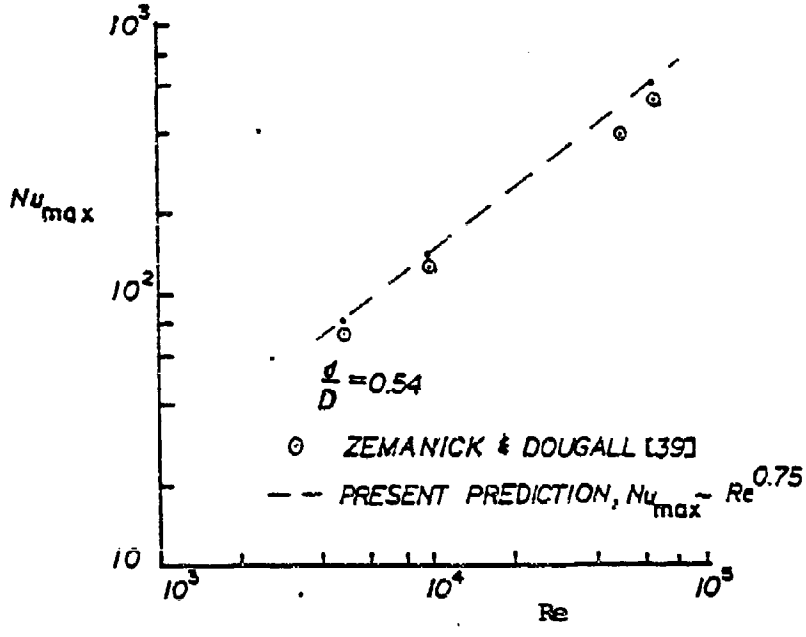

Figure 38. Variation of Maximum Nusselt Number with Reynolds Number Downstream of a Sudden Pipe Expansion

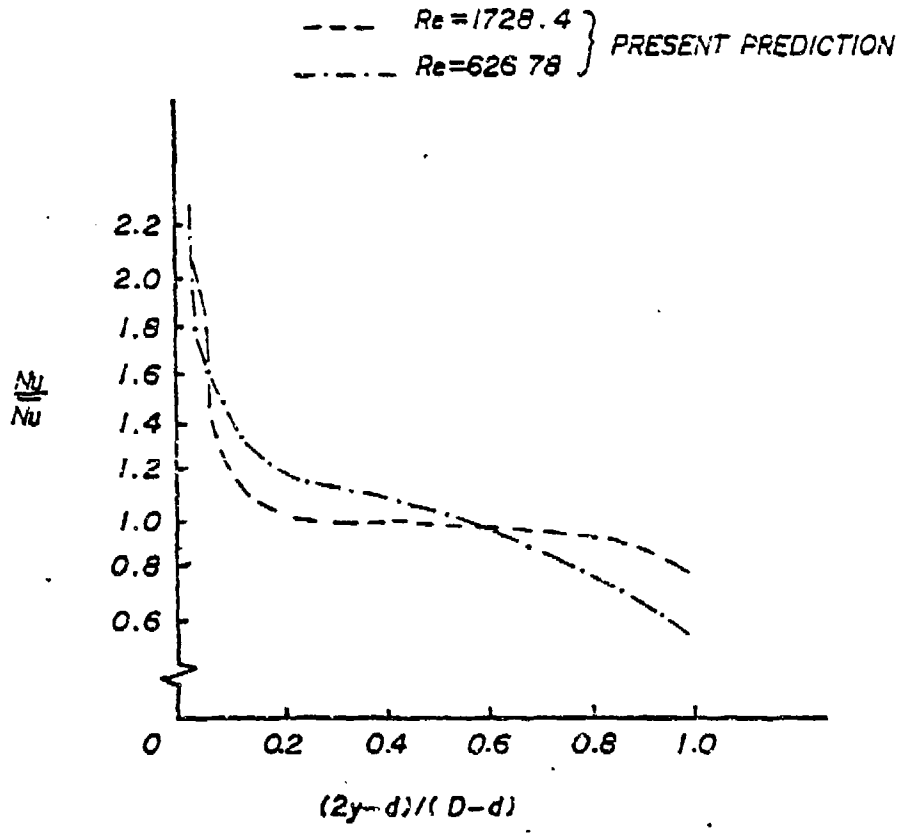

Figure 39. Cross-Stream Variation of Nusselt Number on the Downstream Face of the Back-Step

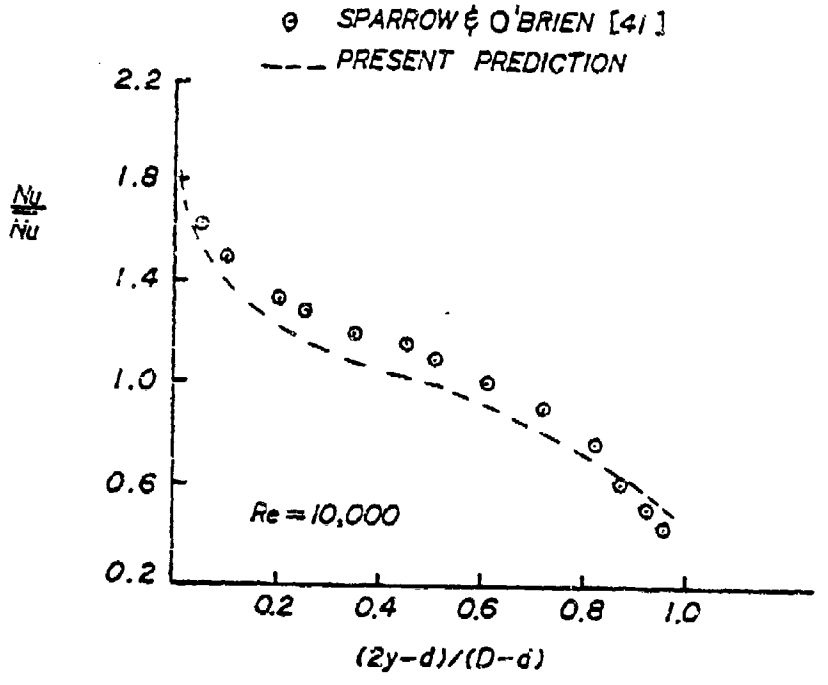

Figure 40. Cross-Stream Variation of Nusselt Number on the Downstream Face of the Pipe Expansion

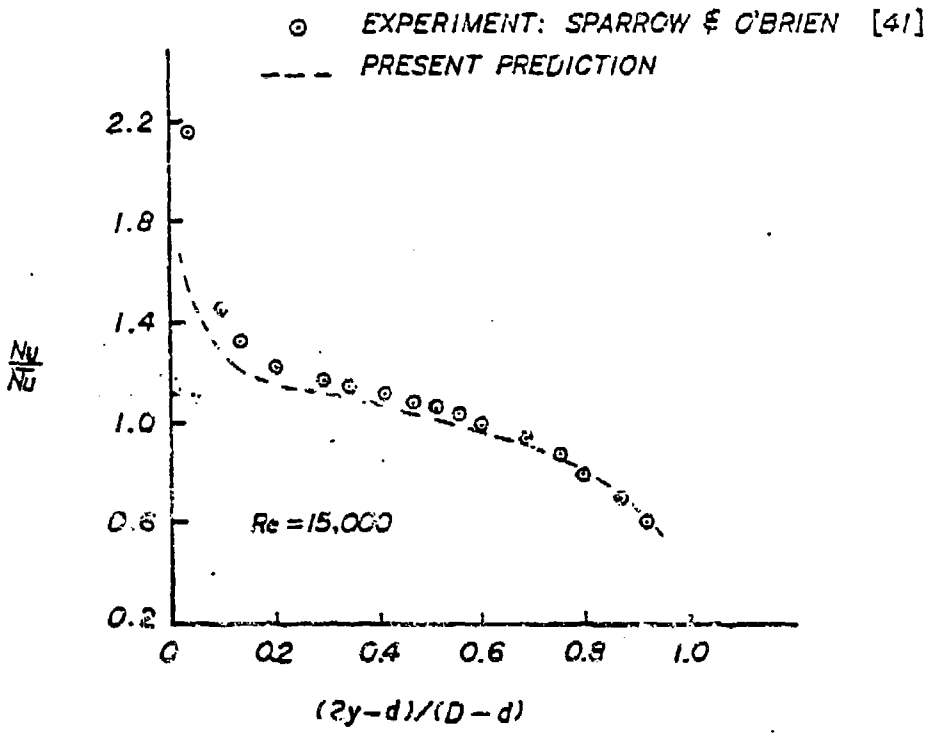

Figure 61. Cross-Stream Variation of Nusselt Number on the Downstream Face of the Pipe Expansion

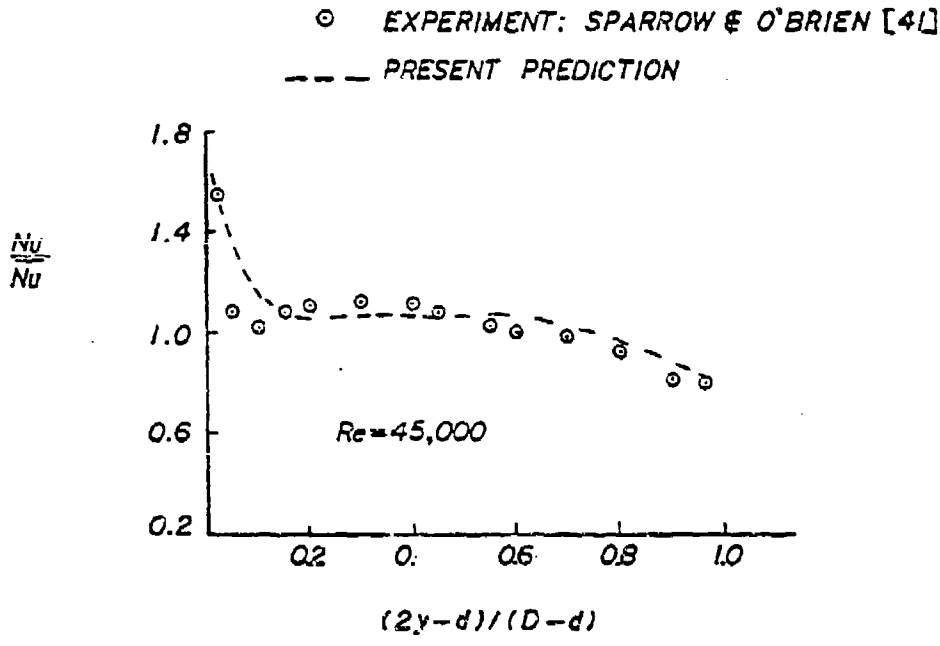

Figure 42. Cross-Stream Variation of Nusselt Number on the Downstream Face of the Pipe Expansion

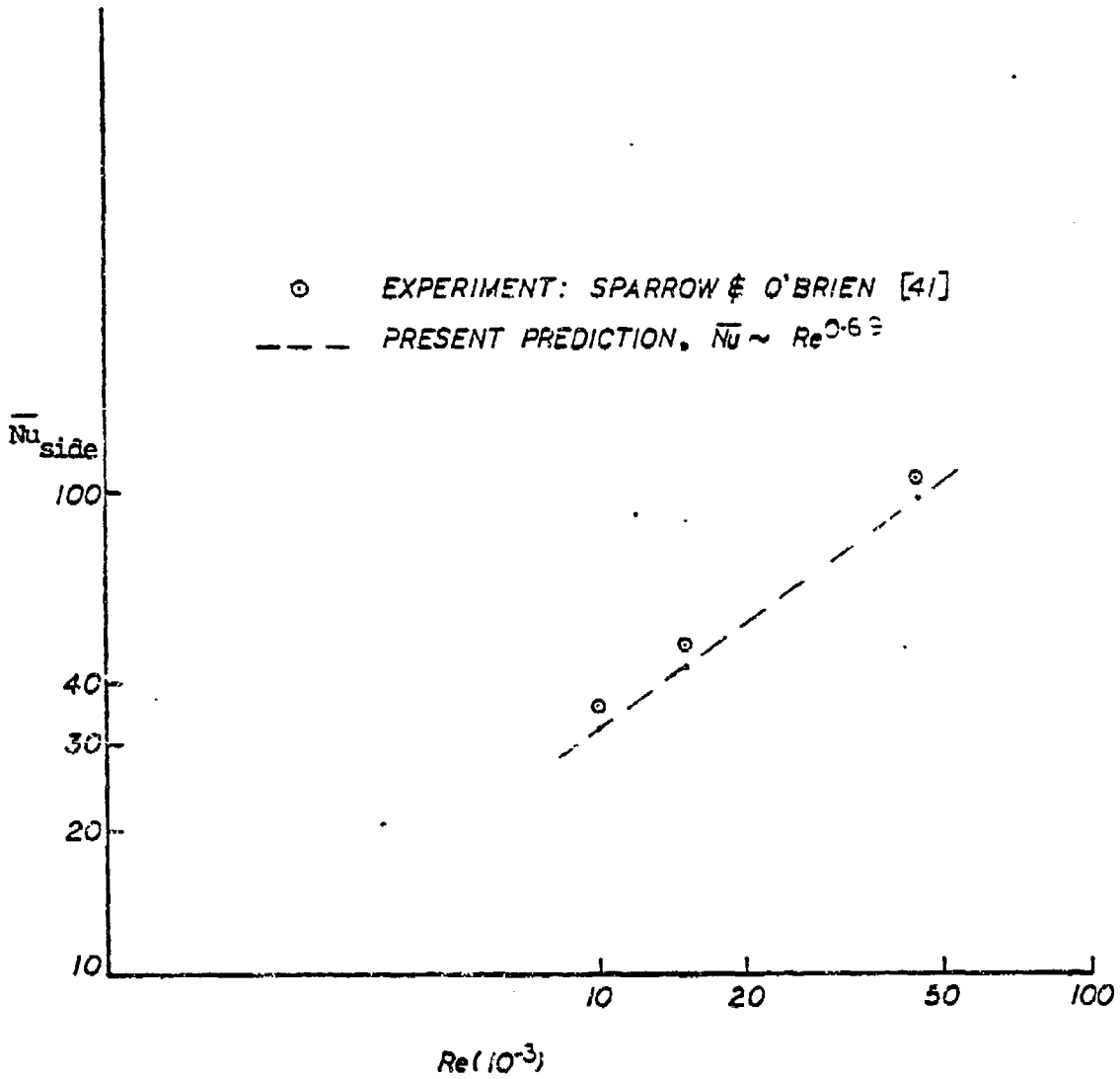

Figure 43. Variation of Average Nusselt Number with Reynolds Number for the Downstream Face of a Sudden Pipe Expansion

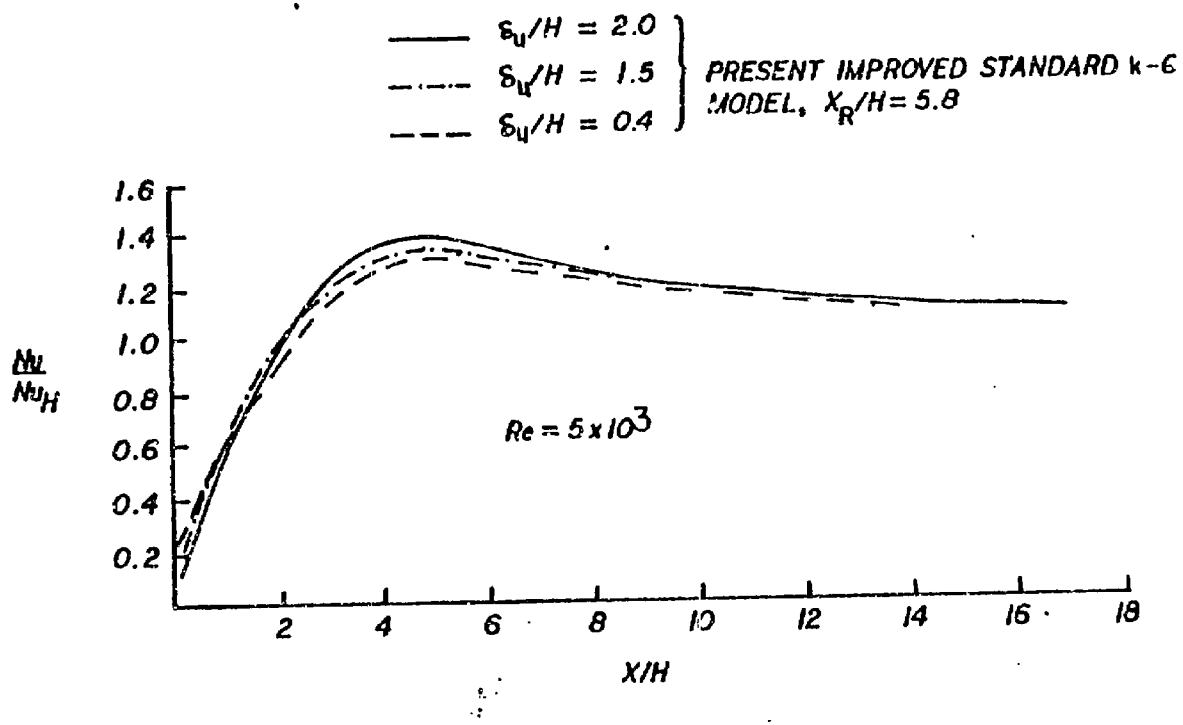

Figure 44. Effects of Approach Boundary Layer Thickness on Nusselt Number Downstream of Step

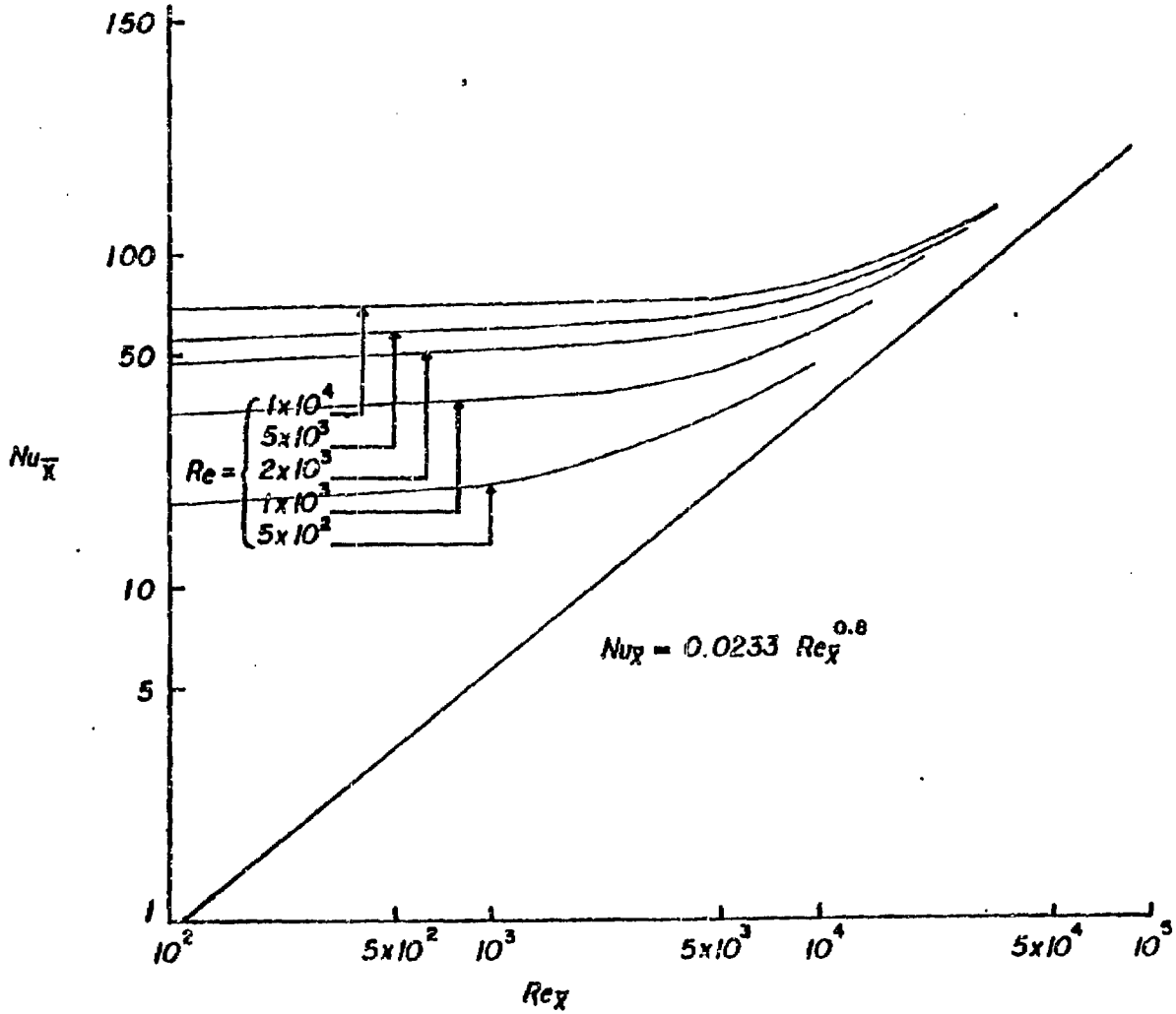

Figure 45. Boundary Layer Nusselt Number Growth Beyond Reattachment for the Back-Step

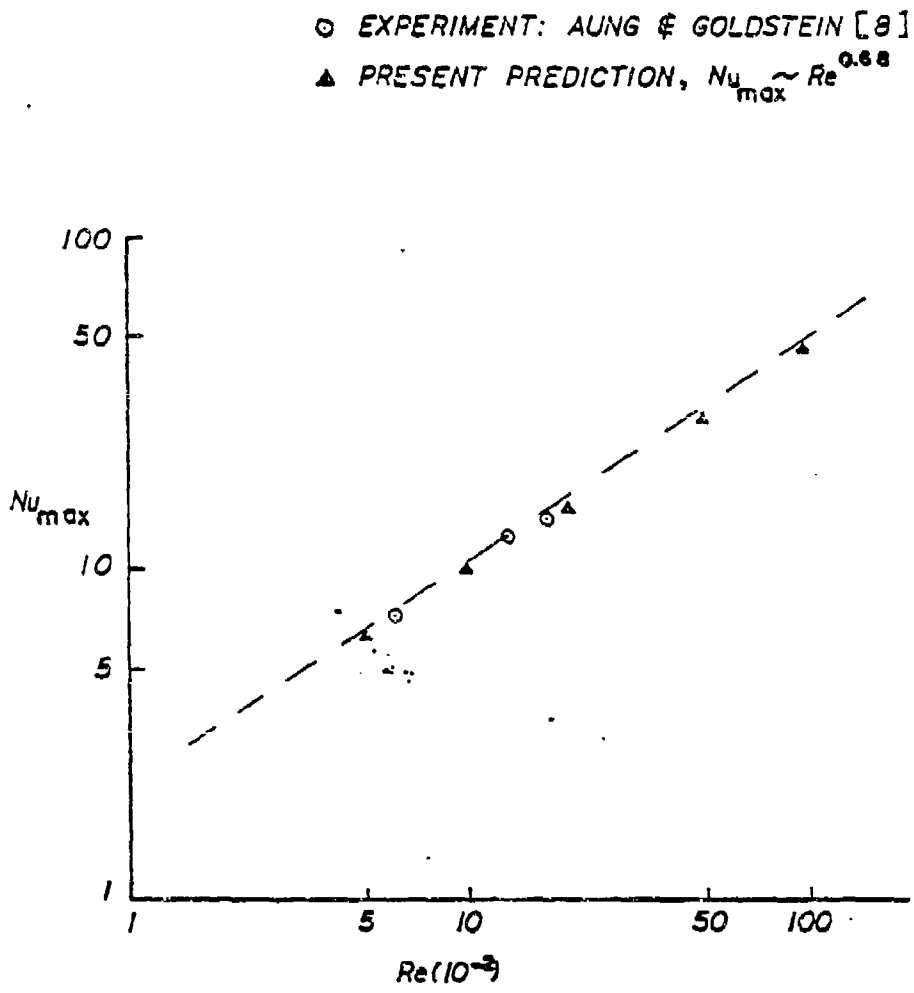

Figure 46. Variation of Maximum (Peak) Nusselt Number with Reynolds Number Downstream of Back-Step

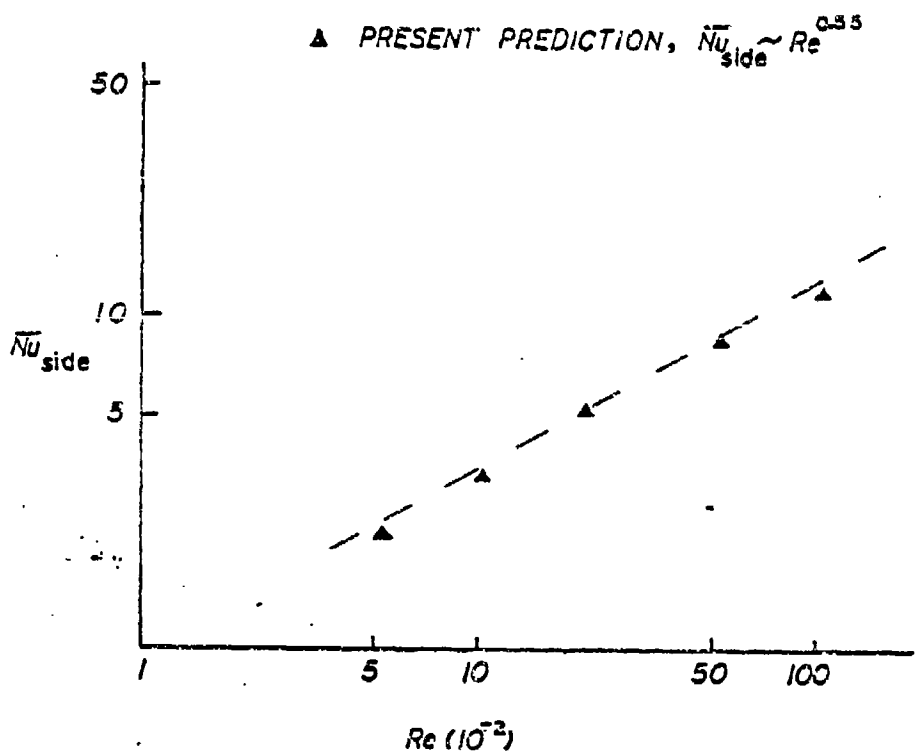

Figure 47. Variation of Average Nusselt Number with Reynolds Number for the Downstream Face of Back-Step

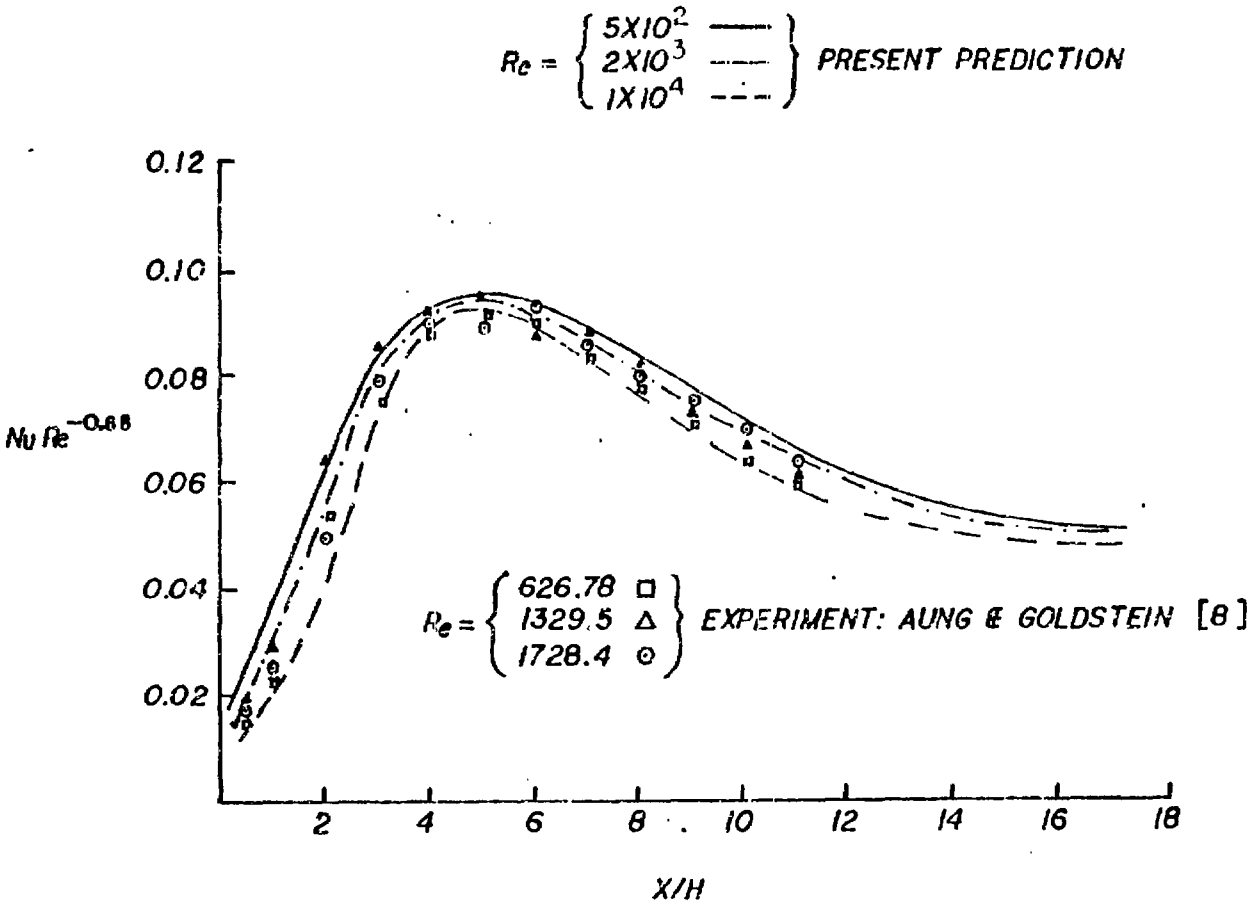

Figure 48. Streamwise Nusselt Number for Back-Step Normalized Through its Maximum Reynolds Number Dependence

DISTRIBUTION LIST

HEAT TRANSFER

	One copy except as noted
Mr. M. Keith Ellingsworth Power Program Office of Naval Research 800 N. Quincy Street Arlington, VA 22203	5
Defense Documentation Center Building 5, Cameron Station Alexandria, VA 22314	12
Technical Information Division Naval Research Laboratory 4555 Overlook Avenue SW Washington, DC 20375	6
Professor Paul Marto Department of Mechanical Engineering US Naval Post Graduate School Monterey, CA 93940	
Professor Bruce Rankin Naval Systems Engineering US Naval Academy Annapolis, MD 21402	
Office of Naval Research Eastern/ Central Regional Office Bldg 114, Section D 666 Summer Street Boston, Massachusetts 02210	
Office of Naval Research Branch Office 536 South Clark Street Chicago, Ill. 60605	
Office of Naval Research Western Regional Office 1030 East Green Street Pasadena, CA 91106	
Mr. Charles Miller, Code 05R13 Crystal Plaza #6 Naval Sea Systems Command Washinton, DC 20362	

Enclosure (2)

Steam Generators Branch, Code 5222
National Center #4
Naval Sea Systems Command
Washington, DC 20362

Heat Exchanger Branch, Code 5223
National Center #3
Naval Sea Systems Command
Washington, DC 20362

Mr. Ed Ruggiero, NAVSEA 08
National Center #2
Washington, DC 20362

Dr. Earl Quandt Jr., Code 272
David Taylor Ship R&D Center
Annapolis, MD 21402

Mr. Wayne Adamson, Code 2722
David Taylor Ship R&D Center
Annapolis, MD 21402

Dr. Win Aung
Heat Transfer Program
National Science Foundation
Washington, DC 20550

Mr. Michael Perlsweig
Department of Energy
Mail Station E-178
Washington, DC 20545

Dr. W.H. Theilbahr
Chief, Energy Conservation Branch
Dept. of Energy, Idaho Operations Office
550 Second Street
Idaho Falls, Idaho 83401

Professor Ephriam M. Sparrow
Department of Mechanical Engineering
University of Minnesota
Minneapolis, Minnesota 55455

Professor J.A.C. Humphrey
Department of Mechanical Engineering
University of California, Berkeley
Berkeley, California 94720

Professor Brian Launder
Thermodynamics and Fluid Mechanics Division
University of Manchester
Institute of Science & Technology
P088 Sackville Street
Manchester M601QD England

Professor Shi-Chune Yao
Department of Mechanical Engineering
Carnegie-Mellon University
Pittsburgh, PA 15213

Professor Charles B. Watkins
Chairman, Mechanical Engineering Department
Howard University
Washington, DC 20059

Professor Adrian Bejan
Department of Mechanical Engineering
University of Colorado
Boulder, Colorado 80309

Professor Donald M. McEligot
Department of Aerospace and Mechanical Engineering
Engineering Experiment Station
University of Arizona 85721

Professor Paul A. Libby
Department of Applied Mechanics and Engineering Sciences
University of California San Diego
Post Office Box 109
La Jolla, CA 92037

Professor C. Forbes Dewey Jr.
Fluid Mechanics Laboratory
Massachusetts Institute of Technology
Cambridge, Massachusetts 02139

Professor William G. Characklis
Dept. of Civil Engineering and Engineering Mechanics
Montana State University
Bozeman, Montana 59717

Professor Ralph Webb
Department of Mechanical Engineering
Pennsylvania State University
208 Mechanical Engineering Bldg.
University Park, PA 16802

Professor Warren Rohsenow
Mechanical Engineering Department
Massachusetts Institute of Technology
77 Massachusetts Avenue
Cambridge, Massachusetts 02139

Professor A. Louis London
Mechanical Engineering Department
Bldg. 500, Room 501B
Stanford University
Stanford, CA 94305

Professor James G. Knudsen
Associate Dean, School of Engineering
Oregon State University
219 Covell Hall
Corvallis, Oregon 97331

Professor Arthur E. Bergles
Mechanical Engineering Department
Iowa State University
Ames, Iowa 50011

Professor Kenneth J. Bell
School of Chemical Engineering
Oklahoma State University
Stillwater, Oklahoma 74074

Dr. James Lorenz
Component Technology Division
Argonne National Laboratory
9700 South Cass Avenue
Argonne, Illinois 60439

Dr. David M. Eissenberg
Oak Ridge National Laboratory
P.O. Box Y, Bldg. 9204-1, MS-0
Oak Ridge, Tennessee 37830

Dr. Jerry Taborek
Technical Director
Heat Transfer Research Institute
1000 South Fremont Avenue
Alhambra, CA 91802

Dr. Simion Kuo
Chief, Energy Systems
Energy Research Laboratory
United Technology Research Center
East Hartford, Connecticut 06108

Mr. Jack Yampolsky
General Atomic Company
P.O. Box 81608
San Diego, CA 92138

Mr. Ted Carnavos
Noranda Metal Industries, Inc.
Prospect Drive
Newtown, Connecticut 06470

Dr. Ramesh K. Shah
Harrison Radiator Division
General Motors Corporation
Lockport, New York 14094

Dr. Ravi K. Sakhuja
Manager, Advanced Programs
Thermo Electron Corporation
101 First Avenue
Waltham, Massachusetts 02154

Mr. Robert W. Perkins
Turbotec Products, Inc.
533 Downey Drive
New Britain, Connecticut 06051

Dr. Keith E. Starner
York Division, Borg-Warner Corp.
P.O. Box 1592
York, PA 17405

Mr. Peter Wishart
C-E Power Systems
Combustion Engineering, Inc.
Windsor, Connecticut 06095

Mr. Henry W. Braum
Manager, Condenser Engineering Department
Delaval
Front Street
Florence, New Jersey 08518

Dr. Thomas Rabas
Steam Turbine-Generator Technical Operations Division
Westinghouse Electric Corporation
Lester Branch
P.O. Box 9175 N2
Philadelphia, PA 19113

Professor Daryl Metzger
Chairman, Mechanical and Energy
Systems Engineering
Arizona State University
Tempe, Arizona 85281